Historic Thermal Calibration of Landsat 4 TM through an
Improved Physics Based Approach

By

Jonathan M. Miller

Bachelor of Science, Astronautical Engineering

United States Air Force Academy, 2005

A thesis submitted in partial fulfillment of the

requirements for the degree of Master of Science

in the Chester F. Carlson Center for Imaging Science

Rochester Institute of Technology

June 2010

Signature of the Author_____

Accepted by_____
             Coordinator, M.S. Degree Program   Date

CHESTER F. CARLSON CENTER FOR IMAGING SCIENCE

ROCHESTER INSTITUTE OF TECHNOLOGY

ROCHESTER, NEW YORK

CERTIFICATE OF APPROVAL

M.S. DEGREE THESIS

The M.S. Degree Thesis of Jonathan M. Miller
has been examined and approved by the
thesis committee as satisfactory for the
thesis required for the
M.S. degree in Imaging Science

Dr. John R. Schott, Thesis Advisor

Dr. Carl Salvaggio

Dr. Anthony Vodacek

30 June 2010
Date

1 Abstract

This work is intended to establish the calibration of the Thematic Mapper (TM) sensor, thermal band (band 6) aboard the Landsat 4 Spacecraft. Due to multiple organizations having operational control of the spacecraft and a lack of historical calibration data, a physics based approach will be used to calibrate the thermal data recorded over water during the operational lifetime of the spacecraft, which spanned 1983-1993. Using historical data from weather station observations, Radiosonde instruments, and moored weather buoys owned and operated by the National Data Buoy Center (NDBC), a ground truth comparison can be calculated and propagated through the atmosphere using a physics based model. The ground truth measurements are then compared to archived Landsat 4 data to determine how well the instrument is calibrated. This comparison over many data points allows construction of an overall calibration curve for the Landsat 4 data over the lifetime of the spacecraft. In addition to calibrating the Landsat 4 TM, this research will also include investigation into a possible transition period of negative to positive bias on the Landsat 5 TM, somewhere in the 1996-1999 timeframe. The same technique will be used in both calibration attempts.

Results indicate that the Landsat 4 data was well calibrated in the timeframe before storage (1983-1984), however after the storage period (1987-1993) the sensor had a negative bias of -3.3 K. It is suggested to bias post 1987 Landsat 4 data by adding 0.4533 [W/m^2 sr μm] to the sensor reaching radiance. Results from this correction radiometrically correct Landsat 4 data to ±0.48 K verified through an error analysis of the

calibration procedure. The results from this study are consistent with the results from previous work performed on Landsat 5 TM in 2008.

Results from the Landsat 5 study were inconclusive in finding a precise date for the bias shift in the 1996-1999 timeframe of Landsat 5 data. Twenty one additional data points were added to previous work completed in 2008, but no obvious shift was observed.

This procedure for calibrating the Landsat 4 TM sensor tested the limits of the physics based calibration approach and proved that multiple buoys, multiple locations of the buoys (different bodies of water), unfavorable wind conditions, and Radiosonde data from larger distances away from the target can still produce valid results when calibrating a thermal sensor. Testing the robustness of the physics based calibration process opens the door to more available data, resulting in more extensive calibration curves for past work and future systems.

2   Acknowledgments

I would like to thank the following individuals for their help throughout the thesis process:

Dr. Schott – Thank you for keeping me on track and for all of your insight into Landsat. You helped me tremendously with analysis of the data, and with contacts in NASA for getting additional information.

Dr. Vodacek and Dr. Salvaggio – Thank you for your guidance and inputs for making my research a better. I appreciate your help throughout the writing and defending process.

Cindy Schultz – Thank you for taking care of us AF guys. Thank you for scheduling the defense, making sure my announcement was in on time, keeping me on track to finish in time, and of course not having a piano to move.

Nina Raqueno – Thank you for all of your help with gathering Landsat data, and familiarizing me with the software required to perform this calibration.

Mom and Dad – Thanks for all of your support over the years. I know the last two years were busy for me, so thanks for your support and patience during this time. Also thank you for coming to RIT for the defense, hopefully you weren't too bored.

The Bastian Family – Thank you for your support over the past two years. It has been very nice having a family here in Rochester to spend time with. I look forward to many more family gatherings in the future.

Lindsay – The best part of coming to Rochester was the fact that I am leaving with you. Thank you for all the support over the past two years. We both know it was a busy two years, but somehow we did it. I can't wait to start our future together, Thank You so much I love you!!

3   Table of Contents

4   Table of Figures

11

5   Introduction

The purpose of this research is to establish a calibration record for the National Aeronautics and Space Administrations Landsat 4 spacecraft. The nine-year history of Landsat 4 data is possibly un-calibrated due to a lack of verification of the calibration of the sensor. This research will utilize a physics based approach to evaluate the calibration of the Thematic Mapper (TM) channel 6.

This physics based approach will use the historical data collected by the Landsat 4 spacecraft and compare it to ground truth data collected on the same date as the historical data.   The physics based model is a four-step approach using critical environmental data to characterize the scene in question. Because the concentration is on the thermal sensor, the temperature of large bodies of water, rather than targets on the landmass, will be used to create a calibration curve. A large body of water is considered a homogeneous surface, therefore an ideal choice for a target background. A land target background would contain many fluctuations in temperature over a small unit area due to: reflection of different objects, material properties of the objects, and shadow/shade regions. These fluctuations would not give us an accurate temperature reading over the ground sample distance (GSD) of the TM sensor.

The first step of the process will determine the water temperature of the target. To complete this task the fleet of moored weather buoys owned and operated by the National Oceanic and Atmospheric Administration will be utilized. These weather buoys can provide the air temperature, wind speed, and most importantly to our research: water

temperature (which will be converted to a surface leaving radiance value). The second step of the process will uses a physics based model to characterize the atmosphere on the day of Landsat 4 data acquisition. The preferred physics model to perform this step is the MODerate resolution atmospheric TRANsmision (MODTRAN) code. MODTRAN is a physics based model created by the US Air Force and is the industry leader on characterizing the atmosphere on any given day, under any given solar conditions (Schott, 2007). The third step involves calculating the sensor reaching radiance of the known water temperature using the atmospherics parameters computed by the physics based model. The final step compares the ground truth sensor reaching radiance to the radiance value in the Landsat 4 data archive. Any difference between the radiances characterizes a bias shift needed to correct the data. This process will then be repeated over multiple scenes throughout the lifespan of the Landsat 4 spacecraft, resulting in an overall calibration curve.

This physics based model approach has been used and proven in the past. A calibration curve for the time periods of 1985-2001 has been created for Landsat 5 through the research done by RIT's Frank Padula (Padula, 2008). Findings from his research lead us to the second part of this paper.

An odd bias shift from a warm bias (positive values) to a cold bias (negative values) occurred somewhere in the 1996-1999 timeframe. This apparent shift is seen in Figure 1, results produced by Padula. (Padula, 2008)
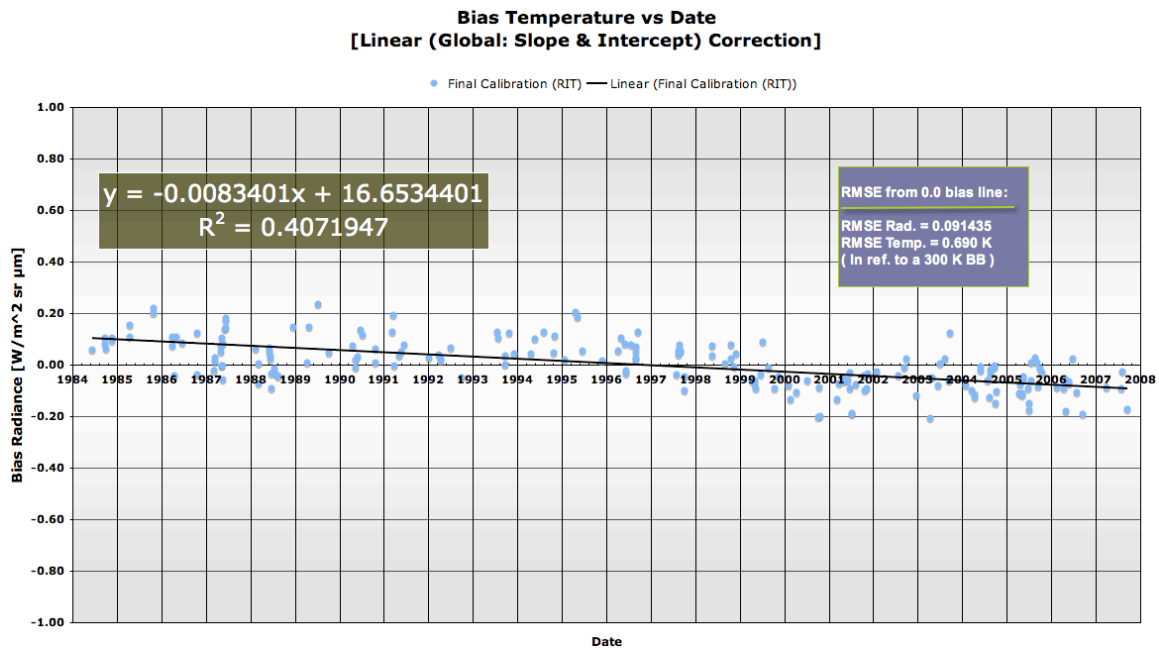
Figure 1. Calibration Curve for Landsat 5. The circled area shows an apparent bias shift from warm bias (positive) to the data having a cold bias (negative) (Padula, 2008)

The second part of this research project consists of running more Landsat 5 data during the time frame of 1996-1999 to pin-point the exact date of the bias shift. By determining the exact date of the bias shift, NASA engineers may be able to understand what event caused the TM sensor change from a warm bias to a cold bias.

15

6 Background

6.1 Landsat Program History

In 1972 the Landsat program began its 30+ year career with the launch of Landsat 1. The Landsat program is the longest running program for space-based acquisition of land remote sensing data. The program is a collaboration between the National Aeronautical and Space Association (NASA) and the United States Geological Survey (USGS). Landsat collects worldwide land data including vegetation, water, land use, and thermal information. The spacecraft are tasked to collect data of the US each time they pass over. Because of this enormous tasking, USGS has an archive of over 30 years worth of land data of the United States. This data is important to many users such as the farming industry, environmentalists, developers, and even in the political arena. In addition to US collects, Landsat 4,5, and 7 have collected data on nearly every continent since 1986. (USGS, Landsat Mission, 2009)
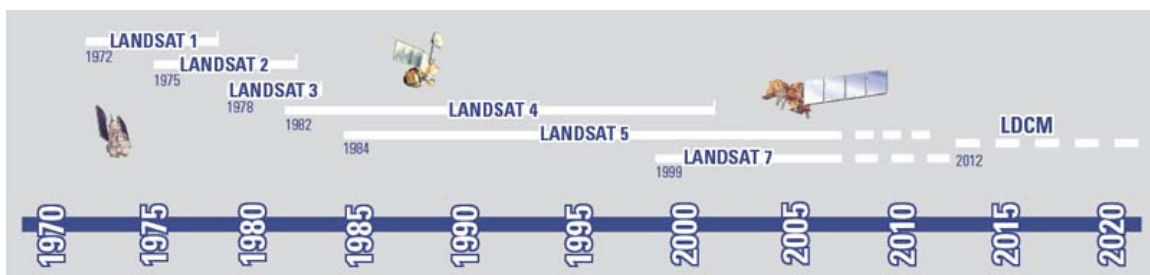
Figure 2. History of the Landsat Program. The Landsat Program was started with the launch of Landsat 1 in 1972 and has been providing land data for over 37 years now. (USGS, The Landsat Program-History, 2009)

As seen in Figure 2 the Landsat program consists of seven satellites, six of them successfully making orbit. NASA was contracted to build and launch the Landsat satellites into a sun-synchronous polar orbit, allowing the satellite to view the same location on earth with the sun being in approximately the same position in the sky at each viewing.

Each satellite was designed for a 3-5 year lifespan and contained either or both of two primary sensor packages. The first sensor is the Multispectral Scanning Sensor (MSS), which operated on six bands or channels ranging from the visible to the near IR regions. The second sensor on the spacecraft, the Thematic Mapper (TM) that can be seen in Figure 3, is the sensor calibration effort of this research. Table 1 describes the 7 bands that the TM detects and this calibration effort will concentrate on channel six, the thermal band. (USGS, The Landsat Program-History, 2009)
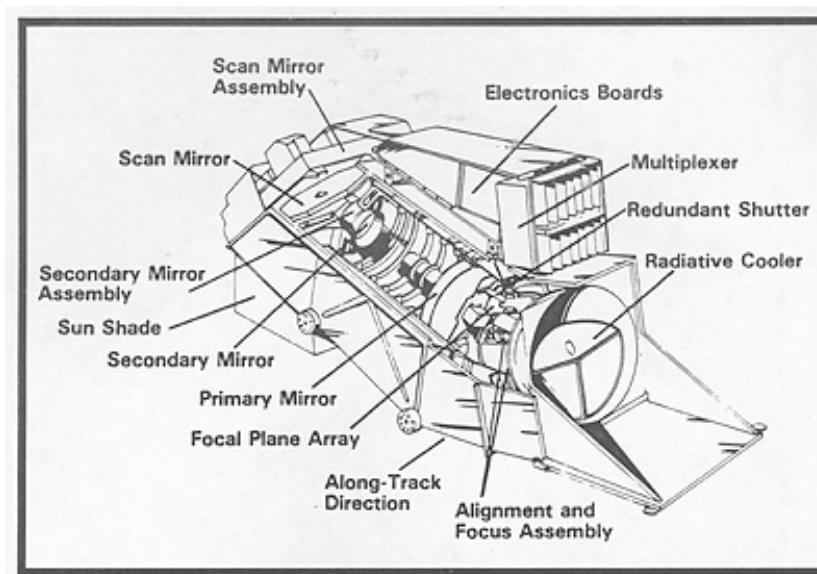
Figure 3. Cut away view of the Landsat 4 Thematic Mapper (TM). (USGS, Landsat Mission, 2009)

MSS	Bandwidth [μm]	Resolution [m]	TM	Bandwidth [μm]	Resolution [m]
N/A	N/A	N/A	Band 1	Visible (0.45 – 0.52)	30
N/A	N/A	N/A	Band 2	Visible (0.52 – 0.60)	30
N/A	N/A	N/A	Band 3	Visible (0.63 – 0.69)	30
Band 4	Visible (0.5 - 0.6)	57 x 79	Band 4	Near IR (0.76 – 0.90)	30
Band 5	Visible (0.6 – 0.7)	57 x 79	Band 5	Near IR (1.55 – 1.75)	30
Band 6	Near IR (0.7 – 0.8)	57 x 79	Band 6	Thermal (10.40 – 12.50)	120
Band 7	Near IR(0.8 – 0.9)	57 x 79	Band 7	Mid-IR (2.08 – 2.35)	30

Table 1: Spectrum and wavelength of MSS and TM sensors on Landsat 4 (USGS, The Landsat Program-History, 2009)

Like most earth observing satellites, Landsat 4 does have an on orbit calibration device for the TM, which is shown in Figure 4. This device is in the form of a wand containing a surface of known temperature and a mirror to reflect a blackbody at a different temperature. The wand is waived in front of the sensor after each line of data is collected. The recording of the known temperatures of the wand and the blackbody produces a baseline measurement of the sensor, and a gain or bias can be adjusted as needed. Ignoring the fore optics and changes in fore optics result in the most likely sources of calibration error.
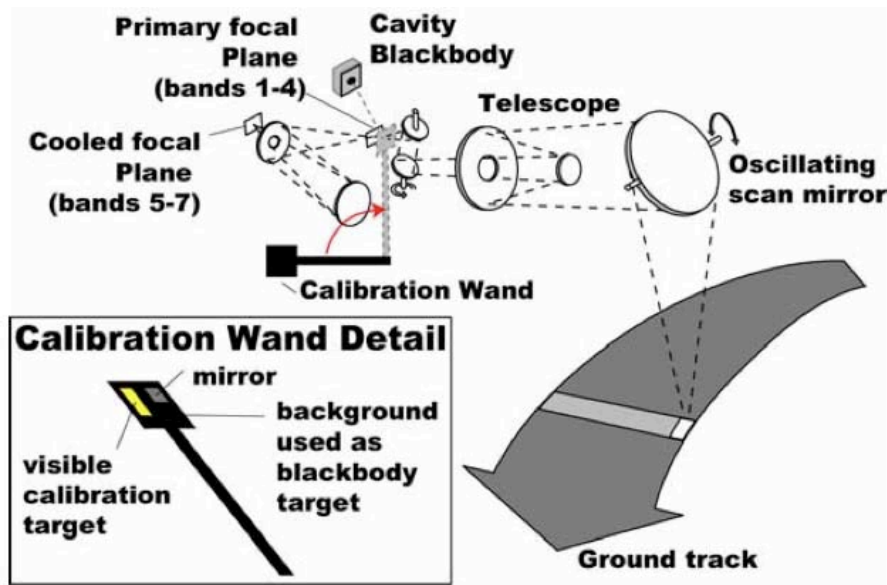
Figure 4. Schematic of the Landsat 4 scanning satellite. The sensor is calibrated on orbit using a calibration wand that is waived in front of the sensor at a given interval. This gives the sensor a known data point in between taking actual tracks of data. (USGS, Landsat Mission, 2009)

6.1.1 Landsat 4

Landsat 4, shown in Figure 5, was launched in 1982 but unfortunately shortly after early

orbit checkout, 50% of the solar array panels failed. Due to the dangerous situation

where the satellite was only working on half of the power needed, NASA decided to

accelerate the launch schedule for Landsat 5 (an identical satellite). Landsat 5 was then

launched in 1984 and after early orbit checkout became the primary satellite to collect

data. In 1984 Landsat 4 was placed into "storage" and returned to operational status in

1987 primarily collecting overseas data until 1993. In 1993 Landsat 4 was plagued with

communications system failures, which made the transmission of data nearly impossible

(could only be done through a system of relay satellites called TDRSS). The

communication failures made the spacecraft unusable and Landsat 4 collected no further

data until it was finally decommissioned in 2001. (USGS, The Landsat Program-History, 2009)

The ownership of the Landsat program brings questions to the calibration history/record. When Landsat 4 was launched, NASA was the organization in charge of the day-to-day operations of the satellite. In 1985, under a new government contract, a private organization called Earth Observation Satellite Company (EOSAT) gained control of the operations. In 1997 the Landsat program went through a re-organization and the program was then passed from NASA to the USGS (United States Geological Survey). Although the program changed between government agencies, EOSAT remained in control of the daily operations. Another contract change in 2001 placed control of the daily operations into the hands of the USGS (Barsi, 2000). One would believe that by using an on orbit calibration technique the TM sensor would be in calibration throughout the spacecrafts lifetime, however the calibration records for the Landsat program from 1982 until 2001 were either poorly documented, not collected, or not completed. The research conducted here is aimed at going back and verifying the calibration of the TM sensor on Landsat 4 from 1982 until the end of its operational life in 1993.
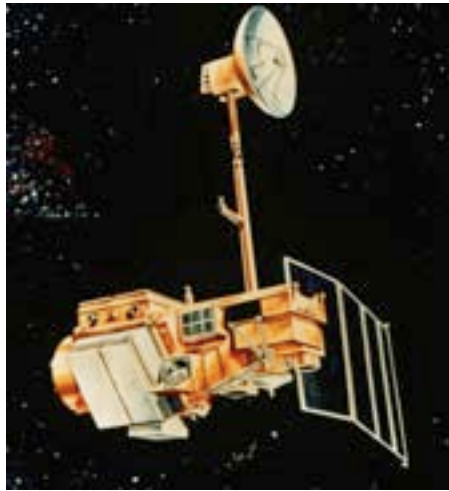
Figure 5. Artist rendition of the Landsat 4 spacecraft. (USGS, The Landsat Program-History, 2009)

6.2   Calibration Efforts

Multiple techniques have been used to calibrate similar Landsat spacecraft, particularly

Landsat 5 and 7, which give us confidence that the archive of Landsat 4 data can be

calibrated. The techniques previously used included using lakes as targets (Tonooka,

2005), and using a physics based model approach to calibrate the on orbit sensor (Padula,

2008).

6.3   Ideal Targets

In order to successfully calibrate the TM on both Landsat 4 and Landsat 5 it is imperative

to select targets that will give us the most accurate results. A non-ideal target would be an

object that has a large amount of variability in either temperature or emissivity such as

landmasses and urban areas. A good ideal target is a relatively large homogeneous object

such as a dry lakebed or a large body of water. Large targets are preferred for the TM so

that multiple pixels of data can be collected at a time. Recall that the ground sample

distance (GSD) of the TM is 120m.

A second consideration to an ideal target is the atmospheric conditions during the collection of the data. Dry atmospheric conditions are preferred (cloud free scenes) because the radiative transfer computation is directly related to the total water vapor column above the calibration site (Tonooka, 2005). Less water vapor over the target area results in less variability in the atmosphere, which in turn will lead to a more accurate radiative transfer function.

In order to fulfill the prescribed criteria of an ideal target, water bodies with moored weather buoys have been selected as the targets for Landsat 4 calibrations. The weather buoys are located in large bodies of water, and stringent scene selections requiring cloud free collections will occur. The weather buoys are capable of providing ground truth data using a thermister in the water below the surface. The buoys selected for this research have been in place during the lifetime of Landsat 4 (1982-1993) as well as during the possible transition period of Landsat 5 (1996-1999), therefore are the primary targets for this calibration effort.

6.4   Radiance to Temperature Conversions

In most cases, when measuring the temperature of an object, simply touching the sensor to the object in question will result in a reading indicating how hot or cold the object is. In the remote sensing world the sensor will never make contact with the object in question, making reading the temperature of an object much more difficult.

The TM sensor aboard Landsat 4 records the radiance of a scene, not the temperature of the scene. Radiance is the flux per unit projected area, per unit solid angle, and can be used to characterize the flux from or onto a surface (Schott, 2007). In

22

order to determine the temperature of an object far below the sensor a conversion from the radiance measurement into a temperature value must occur. This conversion is accomplished using the Planck equation for blackbody radiators. Inverting Planck's equation allows a radiance measurement to be calculated as an apparent temperature using:

$$T_{app} = \frac{hc}{\lambda k}\left[\ln\left(\frac{2h^2}{L\lambda^5}\right)+1\right]^{-1} \quad [K] \tag{6.1}$$

Previous authors have simplified the equation to a more general form (Sospedra, 1998):

$$T_{app} = \frac{K_2}{\ln\left(\dfrac{K_1}{L+1}\right)} \quad [K] \tag{6.2}$$

where L is the radiance recorded at the sensor [mWcm^{-2}sr^{-1}μm^{-1}], and according to Schott and Volchok (Schott J. R., 1985) the parameters vary for K_1 and K_2 , but without correcting for the atmosphere the TM sensor on Landsat 4 the K values are:

$$K_1 = 67.172[mWcm^{-2}sr^{-1}\mu m^{-1}]$$
$$K_2 = 1284.3[K]$$

and for Landsat 5 the K values are:

$$K_1 = 60.776[mWcm^{-2}sr^{-1}\mu m^{-1}]$$
$$K_2 = 1260.56[K]$$

where the K values incorporate the sensor spectral response effects.

6.5   Bulk to Skin Water Temperature Models

The bulk temperature (T_b) of a water body is defined as the temperature measured by ships or buoys at a depth of a few centimeters or meters below the surface, rather than the

23

sea surface skin temperature (Zeng, 1999). The bulk temperature is what the moored

buoys thermister will be measuring. Unfortunately this will not be the temperature that

the sensor on the spacecraft will be seeing (Figure 6). The temperature the spacecraft

sensor will observe is the radiance of the surface of the water, or the skin temperature.

Skin temperature (T_s) is defined as the temperature of a molecular sub-layer of thickness

on the order of 1 μm at the surface of the water (Zeng, 1999).
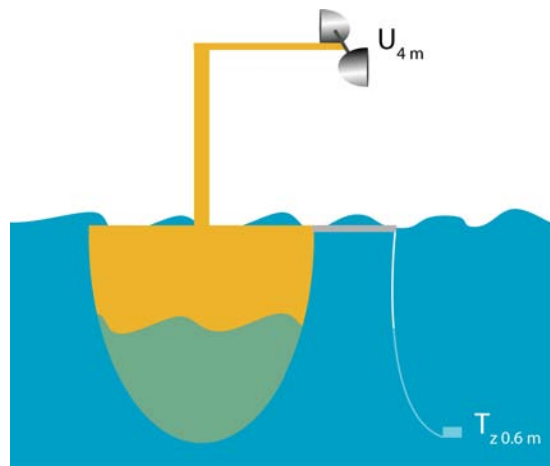
Figure 6. NOAA moored buoys have a thermister at a depth of 0.6 [m]. This will record the bulk water temperature, not the temperature observed by the satellite (skin temperature).

The skin temperature of a body of water is affected by time of day, wind speed,

and sky conditions. The illustration in Figure 7 displays how the skin temperature can

vary due to the parameters listed above.
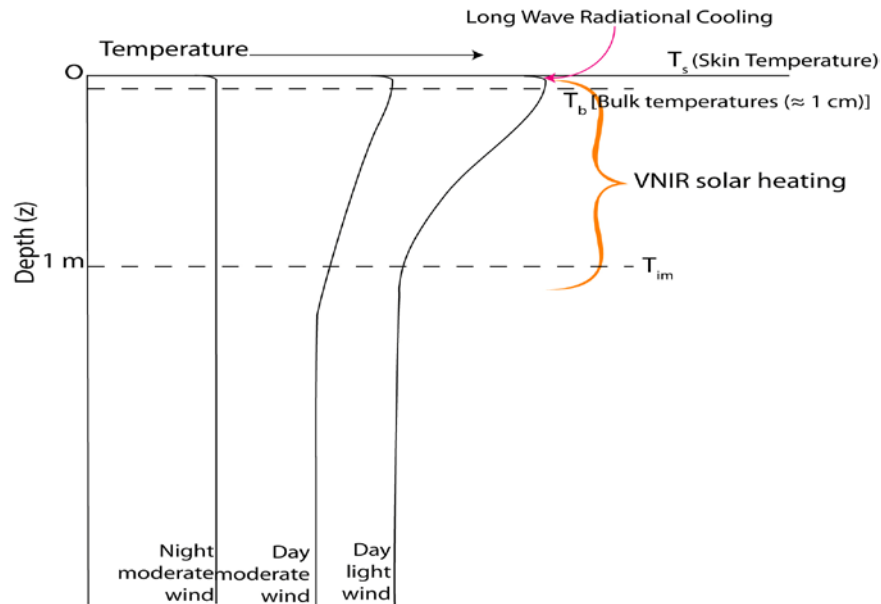
Figure 7. Illustration of the temperature variation in the bulk and skin temperatures with respect to varying wind speeds

Heating during the day or cooling during the night can vary the bulk to skin temperature difference by as much as 0.1-0.3 K (Zeng, 1999). In order to calculate the potential difference between the measured bulk temperature and the skin temperature, the buoy data is extrapolated from the depth of the thermister to the surface of the body of water.

The method used to extrapolate the skin temperature from the bulk temperature was developed by Zeng et al (Zeng, 1999) and validated on Landsat 5 calibration efforts by Padula (Padula, 2008). The technique takes into account the wind speed, net surface heat flux, and the depth of the thermister. The first step to the extrapolation process is to find the average skin temperature over a 24-hour period. Mathematically the average skin temperature is calculated using:

$$\langle T_s \rangle = \langle T_z \rangle - az - d \quad [\text{K}] \tag{6.3}$$

where $\langle T_z \rangle$ is the average bulk temperature over a 24 hour period in Kelvin [K], $\langle T_s \rangle$ is

the average skin temperature over a 24 hour period [K], z is the depth of the bulk

temperature measurement [m] (the buoy thermister in our case), d is surface cool skin

effect [K] (this value averaged to be 0.22 K, however the value of 0.17 K from (Donlon,

2002) may be more consistent and is therefore used in this research), and a is the thermal

gradient represented by:

$$a = 0.05 - \frac{0.6}{u_m} + 0.03\ln(u_m) \quad [\text{K/m}] \tag{6.4}$$

where u_m is the 24 hour average wind speed at a height of 10 m above sea level [m/s].

Figure 8 is an illustration of equations 6.3 and 6.4.
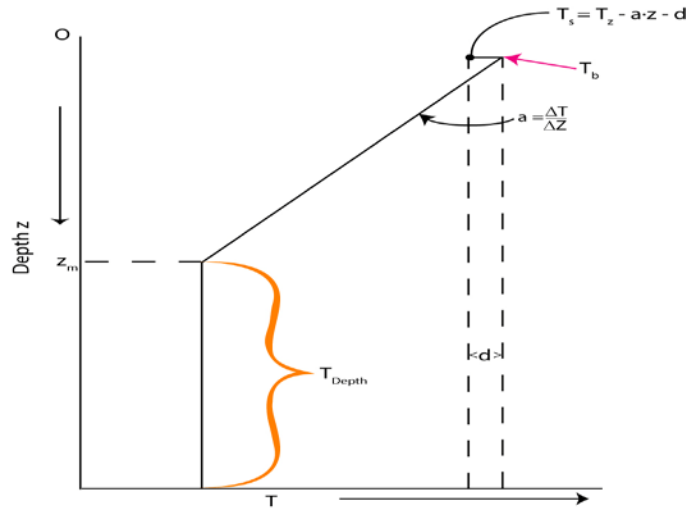
Figure 8. Pictorial representation of the first part of Zeng approach to skin temperature correction (equations 6.3 and 6.4)

The second part of the extrapolation process acknowledges the fact that the surface temperature will vary with time (diurnal variation), therefore can be solved empirically using Equation 6.5.

$$f(t - cz) = \frac{T(z,t) - \langle T_z \rangle}{e^{-bz}} \qquad (6.5)$$

$T(z,t)$ is the buoy temperature at depth z and time t, $\langle T_z \rangle$ is the average bulk temperature over a 24 hour period, cz is a phase term, and e^{-bz} is the diurnal amplitude. This second step is accomplished by solving for f(t) through the interpolation of f(t-cz) around the specific hour of interest (t). The phase constant (c) was empirically derived by (Zeng, 1999) to be:

$$c = 1.32 - 0.64 \ln(u_m) \quad [\text{hr/m}] \qquad (6.6)$$

and the damping constant with depth as:

$$b = 0.35 + 0.018 e^{(0.4 u_m)} \quad [\text{m}] \qquad (6.7)$$

Graphically this step can be seen in Figure 9. This can be viewed as first correcting the diurnal temperature variation for the dampening effect of depth and then correcting for the temporal phase shift between the peak temperature at the surface and the peak temperature at depth.
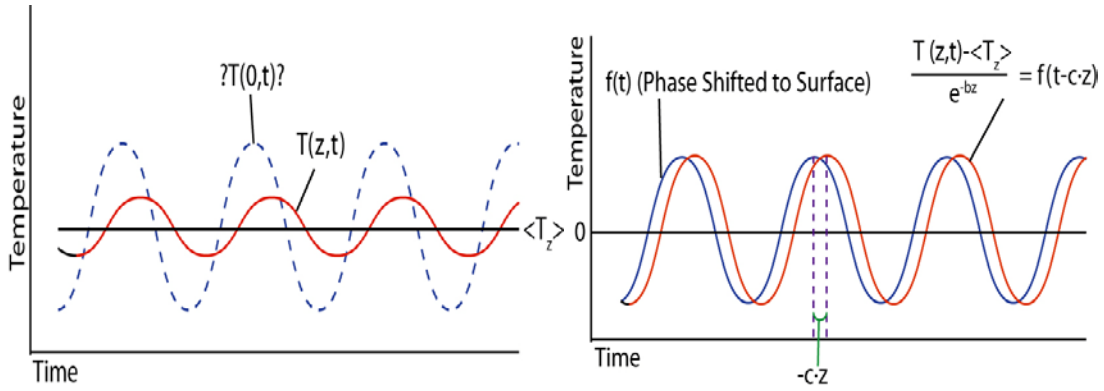
Figure 9. Graphic representation of the unknown diurnal surface temperature at time t (left), and the Zeng empirical correction method (right)

The final step in extrapolating the skin temperature is completed using the 24 hour average skin temperature ($\langle T_s \rangle$) and f(t); both solved above.

$$T_s = T(0,t) = \langle T_s \rangle + f(t) \tag{6.8}$$

$T(0,t)$ represents the skin temperature at the hour of interest, or in other words the skin temperature at the time of the spacecraft collection. This process, including the parameters for the variables defined above, were developed and tested by (Zeng, 1999) using data from the Tropical Ocean-Global Atmosphere (TOGA) Coupled Ocean-Atmosphere Response Experience (COARE) in the south Pacific Ocean under clear sky conditions.

The Zeng technique of skin temperature calculation is optimal for the Landsat 4 calibration because it is ideal for analysis of fixed location temperature measurements (buoy data rather than moving ship data), can be used universally over many types of bodies of water (not just the South Pacific Ocean), and valid under clear sky conditions; all the same criteria used in the Landsat 4 study.

28

6.6   Summary

This chapter discussed the history of the Landsat program, the configuration of Landsat 4, and the calibration history of Landsat 4. Also in this chapter an ideal target was defined, and the specific types of targets best suited for this research were introduced. The discussion of converting the ground truth water temperature data into a radiance value that the Landsat TM sensor will receive was introduced. Finally how to extrapolate the skin temperature (temperature at the molecular level of the water) from the measured bulk water temperature recorded by the weather buoy thermister was introduced. The skin temperature, or surface leaving radiance, propagated to the sensor is the value recorded by the TM sensor on Landsat 4.

7   Theory

7.1   Radiation Propagation

7.1.1   Thermal Energy Paths

To calibrate the Thematic Mapper sensor on Landsat 4, the important piece of the puzzle

is the temperature of the target, but that is not easy to find in a typical scene.

Unfortunately any object that is above absolute zero will radiate energy, meaning that

objects in the scene will be giving off energy, not just our target. In order to isolate the

target's energy, and eventually temperature, an understanding of where other sources of

energy are coming from is important. Figure 10 depicts the different types of thermal

energy in a scene.
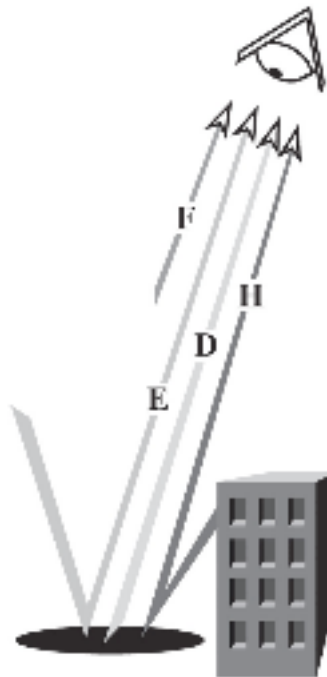
Figure 10. Self-emitted thermal energy paths. (Schott, 2007)

The most important photons for this research are depicted in Figure 10 as the D path photons. These photons are the radiation caused by the temperature of the target, propagated through the atmosphere. The atmosphere is at some temperature above zero, meaning that it too will emit photons, which will reflect off the target and propagate back up to the sensor, and can also be referred to as down-welled radiance (Figure 10, E path photons). Some of the photons emitted by the atmosphere will scatter upward directly toward the sensor without reflecting off the target. These photons are called upwelled radiance or path radiance and are represented in Figure 10 as F path photons. The final path or sources of photons to consider in a scene are those that are emitted by background objects, reflected by the target, and then propagated through the atmosphere. (Figure 10, H path photons) The H path photons are a function of the emissivity and temperature of the background object and in most cases, such as large exposed surfaces like water bodies, are negligible (Schott, 2007).

7.1.2 Blackbody Radiance

A blackbody, as defined by (Schott, 2007), is an ideal surface or cavity where all electromagnetic energy is perfectly absorbed and then completely re-radiated, resulting in the object having an absorptivity of one and a reflectivity of zero. Using the idea of a blackbody radiator, Planck derived an equation using vibrational energy states between atoms (Planck, 1901):

$$M_\lambda = \frac{2\pi hc^2}{\lambda^5\left(e^{\frac{hc}{\lambda kT}} - 1\right)}$$

(7.1)

where T is the temperature [K], h is the Planck constant [6.6260755e-34 J/s], c is the

speed of light [2.998e8 m/s], k is Boltzmann's gas constant [1.3806e-23 J/K], and λ is

wavelength. Planck's equation shows that the exitance of radiance from a body of

interest is dependent on the temperature of the body and the wavelength of interest.

(Schott, 2007)

Ideal blackbodies can only be approximated by perfect absorbers. In order to

describe less than perfect absorbers or emiters we use a term called emissivity.

Emissivity ($\varepsilon(\lambda)$) is defined as the ratio of spectral exitance ($M_\lambda(T)$) from an object at

temperature T, with a blackbody at that same temperature ($M_\lambda BB(T)$).

$$\varepsilon(\lambda) = \frac{M_\lambda(T)}{M_{\lambda BB}(T)}$$

(7.2)

Emissivity describes how well an object radiates energy compared to a blackbody

radiator and has a value that ranges from 0 to 1, with 1 being a perfect blackbody

radiator. (Schott, 2007)

7.1.3 Transmission, Reflection, and Absorption

Along with emissivity there are other fundamental properties of matter to introduce.

These properties come in the form of transmission, reflection, and absorption.

Transmission (τ) is the ability of a material to allow the flux to propagate through it.

Transmission can be represented as a ratio between the exitance from the back of the

sample (M_τ) to the irradiance of the front of the sample (E_i):

$$\tau = \frac{M_\tau}{E_i}$$

(7.3)

Reflectivity (r) is the ability of the material to turn incident flux back into the hemisphere

above the material. Reflectivity can be expressed as the ratio between the exitance from

the front of the sample (M_r) to the irradiance of the front of the sample (E_i):

$$r = \frac{M_r}{E_i}$$

(7.4)

Absorptivity (α) is the ability of the material to remove electromagnetic flux from a

system by converting it to another form of energy. It can also be represented by the ratio

of flux per unit area incident on the surface that is converted into another from of energy

(M_α) to the irradiance onto the surface (E_i):

$$\alpha = \frac{M_\alpha}{E_i}$$

(7.5)

Because of conservation of energy, all energy must be absorbed, transmitted or reflected

resulting in:

$$\alpha + \tau + r = 1$$

(7.6)

or in the case where we have an opaque material:

$$\alpha + r = 1 \qquad (7.7)$$

According to Wallace and Hobbs (Wallace, 1977), Kirchoff's law states that materials that are strong absorbers at a specific wavelength are also strong emitters at that wavelength giving the relationship of:

$$a_\lambda = \varepsilon_\lambda \qquad (7.8)$$

Using Kirchoff's law the conservation of energy for an opaque material can be substituted and re-written as:

$$r = 1 - \varepsilon \qquad (7.9)$$

7.2   Governing Radiometry

As seen earlier in this section, using the Planck equation and the idea of a blackbody radiator, the amount of radiance given off by the target will depend on the wavelength at which the target is being viewed, and the temperature of the target. The amount of radiance from the target reaching the sensor will also be a factor based on how much upwelled radiance from the atmosphere, downwelled radiance from the atmosphere, and finally radiance from background objects is also reaching the sensor. Mathematically these forms of radiation can be expressed in one large equation, commonly known as the big equation and can be defined as:

$$L_\lambda = \left[\varepsilon L_{BB} + \left(F(1-\varepsilon)L_d + (1-F)(1-\varepsilon)L_b\right)\right]\tau + L_u \qquad (7.10)$$

with the terms defined in table 2.

ε	target emissivity
L_{BB}	blackbody radiance at temperature T [w/m^{-2}srμm]
$1-\varepsilon$	reflectivity of the target using Kirchoff's law
τ	transmission through the atmosphere
F	fraction of the sky dome seen by the target (F=1 for large exposed surfaces)
L_d	downwelled radiance from sky onto target [w/m^{-2}srμm]
L_b	self emitted background radiance onto target [w/m^{-2}srμm]
L_u	self emitted upwelled radiance [w/m^{-2}srμm]

Table 2: Definition of terms in the big equation (Eq. 3.10)

As previously discussed in section 7.1.1, for this study the background radiation (L_b) is negligible (particularly true for water surfaces), therefore the big equation can be re-written as:

$$L_\lambda = \left[\varepsilon L_{BB} + (1-\varepsilon)L_d\right]\tau + L_u \qquad (7.11)$$

7.2.1 Effective Radiance

The big equation (Eq. 7.10) sums up the multiple types of radiation that are reaching the sensor, but what is the sensor actually seeing? To understand what the sensor is registering the idea of responsivity is introduced. Responsivity at each wavelength is defined as the signal out (S) per unit flux incident (Φ) on the detector at the wavelength

of interest. (Schott, 2007) This gives us the spectral response, which can be expressed as:

$$R(\lambda) = \frac{dS}{d\Phi(\lambda)}$$

(7.12)

with units of [amps/W] or [volts/W]. The unitless peak normalized spectral response function is expressed as:

$$R'(\lambda) = \frac{R(\lambda)}{R(\lambda)_{max}}$$

(7.13)

where $R(\lambda)_{max}$ is the maximum value of the $R(\lambda)$ function (Eq. 7.12). The peak normalized effective value over the bandpass of interest is obtained by weighting the radiometric term (Eq. 7.11) by the normalized response value (Eq. 7.13)

$$L_{\lambda eff} = \frac{\int L_\lambda R'(\lambda) d\lambda}{\int R'(\lambda) d\lambda}$$

(7.14)

The effective radiance ($L_{\lambda eff}$) is the ground truth derived radiance within the bandpass of interest (for this research the thermal band) and can be compared to the effective radiance values in the Landsat 4 archive.

7.3   Atmospheric Propagation

A key factor in interpreting the ground truth data lies in understanding the effects the atmosphere has on radiation. In general the atmosphere is viewed as a harsh environment and must be eliminated or characterized before remotely sensed data can be analyzed

36

(Schott, 2007). Characterizing the atmosphere can be broken into two main categories; absorption and scattering.

7.3.1 Atmospheric Absorption

Absorption is defined as the process of removal of energy (photons) from the beam by conversion of the electromagnetic energy into another form (usually thermal). This absorption occurs when a photon induces a molecular vibration, rotation, or electron orbital transmission to another energy state. (Schott, 2007) A typical atmospheric absorption spectrum can be seen in figure 11:
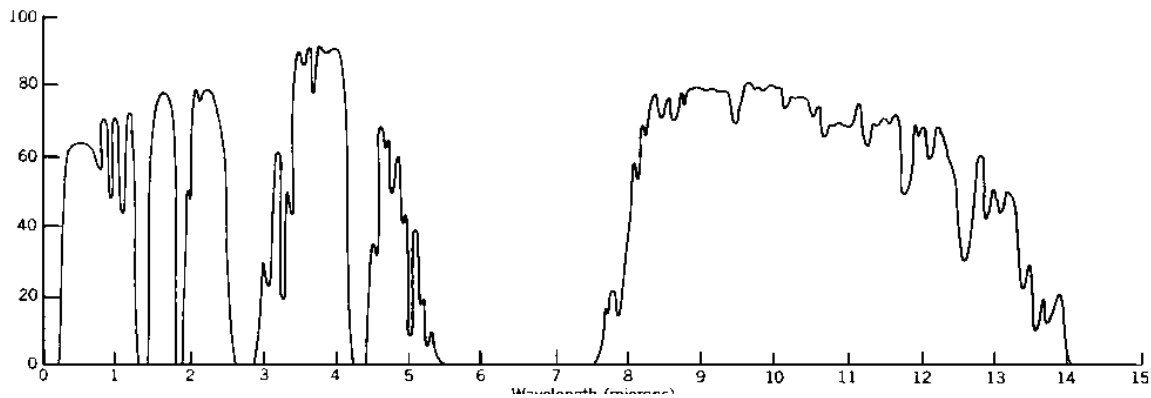
Figure 11. Atmospheric absorption spectrum. The percentage of transmission is on the left and the wavelength is the scale across the bottom. In our study we are interested in the 10.4-12.5 μm range(EOI, 2009)

According to (Schott, 2007), the transmission along a beam can be characterized using three inputs: the number density of each constituent molecule along the path, the absorption cross section as a function of wavelength for each constituent, and how that cross section varies with environmental parameters such as temperature and pressure along the path. Mathematically the transmission can be calculated using (Schott, 2007):

37

$$\tau = e^{-C_\alpha m z} \tag{7.15}$$

where C_α is the absorption cross section, m is the number density or number of molecules per unit volume, and z is the path length.

7.3.2 Atmospheric Scattering

The second major loss for a beam of energy traveling through the atmosphere is scattering. Scattering can be defined as a change in direction and spectral distribution of the energy in a beam. (Schott, 2007) Scattering can be characterized by three scattering approximations: Rayleigh, Mie, and Non-selective.

Rayleigh scattering results from the electromagnetic wave interacting with very small particles, particles so small that they make up the atmosphere. Rayleigh scattering occurs when the particles are much smaller that the wavelength of the incident flux.

Mie scattering occurs when the wavelength is approximately the same size as the particles it is interacting with. Some particles responsible for Mie scattering include aerosols, fossil fuel combustion products, and very small dust particles.

The final category of scattering, Non-selective scattering, occurs when the particles are much larger than the wavelength. Examples of particles that can cause Non-selective scattering are: water droplets and ice crystals. Mathematically the transmission loss due to absorption and scattering sources can be represented by:

$$\tau = e^{-(\beta_\alpha + \beta_r + \beta_a + \beta_{ns})z} = e^{-\beta_{ext} z} \tag{7.16}$$

where β_{ext} is the sum of all the extinction characteristics (absorption (β_α), Rayleigh(β_r),

Mie($\beta_\cdot$), Non-selective(β_{ns})), and z is the path length.

7.3.3 MODTRAN

Understanding atmospheric conditions helps figure out exactly what the sensor reaching

radiance of a particular target would be. The only way to fully understand the

atmospheric conditions on a specific day is to accurately model the atmosphere. To

calibrate Landsat 4, the most widely used and readily available tools to propagate

radiation through the atmosphere will be utilized. The model of choice MODerate

resolution atmospheric TRANsmision (MODTRAN) (Berk A., 1999), assumes that the

atmosphere is divided into multiple homogeneous layers as depicted in Figure 12 (Schott,

2007).
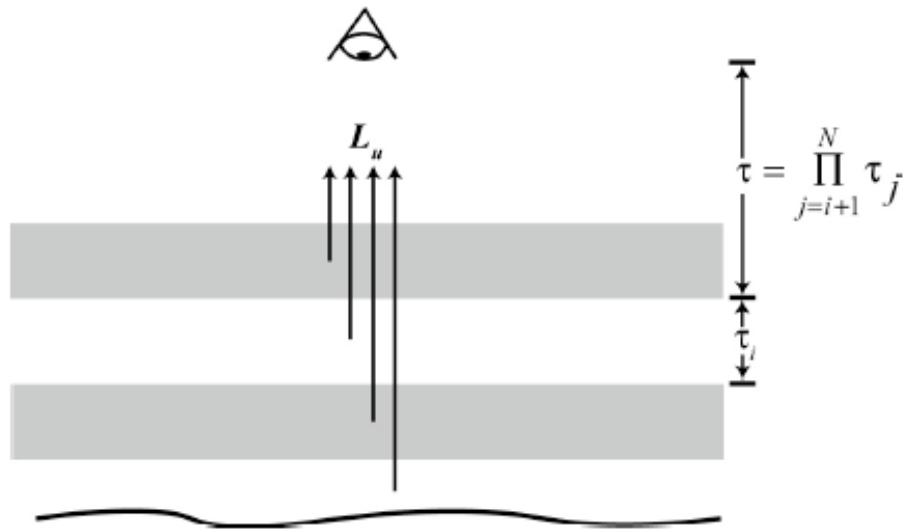
Figure 12. MODTRAN models the atmosphere as a series of homogeneous layers. (Schott, 2007)

Summing up the layers of the atmosphere, MODTRAN can calculate the transmission of the radiance from the surface to the top of the ith layer. In regions where solar reflection effects are negligible, including the thermal regions, MODTRAN uses a propagation equation that can be approximated as:

$$L_\lambda = \varepsilon L_{T\lambda} \prod_{i=1}^{N} \tau_{i\lambda} + \sum_{i=1}^{N} \left[(1 - \tau_{i\lambda}) L_{Ti\lambda} \prod_{j=i+1}^{N} \tau_{j\lambda} \right] = \varepsilon L_{T\lambda} \tau_\lambda(h,\theta) + L_{u\lambda}(h,\theta) \qquad (7.17)$$

where $L_{T\lambda}$ is the blackbody equivalent spectral radiance associated with the temperature of the ith layer, $\tau_\lambda(h,\theta)$ is the effective bandpass transmission, and $L_u(h,\theta)$ is the upwelled radiance (Schott, 2007).

The MODTRAN output will only be as accurate as the accuracy of the inputs. Radiosonde data, which includes temperature and pressure, will be recorded at multiple layers throughout the atmosphere and will be the main input into characterizing the atmosphere for MODTRAN. MODTRAN allows the user to input a target surface temperature and emissivity in order to generate the surface leaving spectral radiance, ($\varepsilon L_{T\lambda}$). Using that information MODTRAN will solve equations in the form of Equation 7.17 for the sensor reaching radiance (Schott, 2007).

7.4   Sampling of Environmental Parameters

7.4.1   Upper-Air Data

Upper air data is needed to characterize the column of atmosphere above our intended ground truth target. Characterizing this part of the atmosphere will utilize the National Weather Services (NWS) Radiosonde data.

Over the past sixty years the NWS has been launching Radiosonde instruments to measure the atmosphere. A Radiosonde is an instrument package that is suspended below a two-meter wide balloon that is filled with helium. As the helium gas expands the balloon carries the Radiosonde to an altitude of about 30 km before the balloon bursts and the Radiosonde floats back to the earth with the help of a small parachute (see Figure 13). During the ascent phase of the Radiosonde's journey, it constantly measures the pressure, temperature, and relative humidity. (ENWS, 2001)

Figure 13. Radiosonde device during ascent phase (left) (Radiosonde, 2009) and descent phase (right)(Radiosonde2, 2009)

The NWS has 92 stations located within the United States, Alaska, the Pacific, and Puerto Rico which all launch Radiosonde balloons twice a day at 00:00 UTC and 12:00 UTC (Figure 14). The large availability of Radiosonde launch sites and archived

data, result in a sufficient amount of data available to characterize the upper air

atmosphere near a ground truth target. (ENWS, 2001)
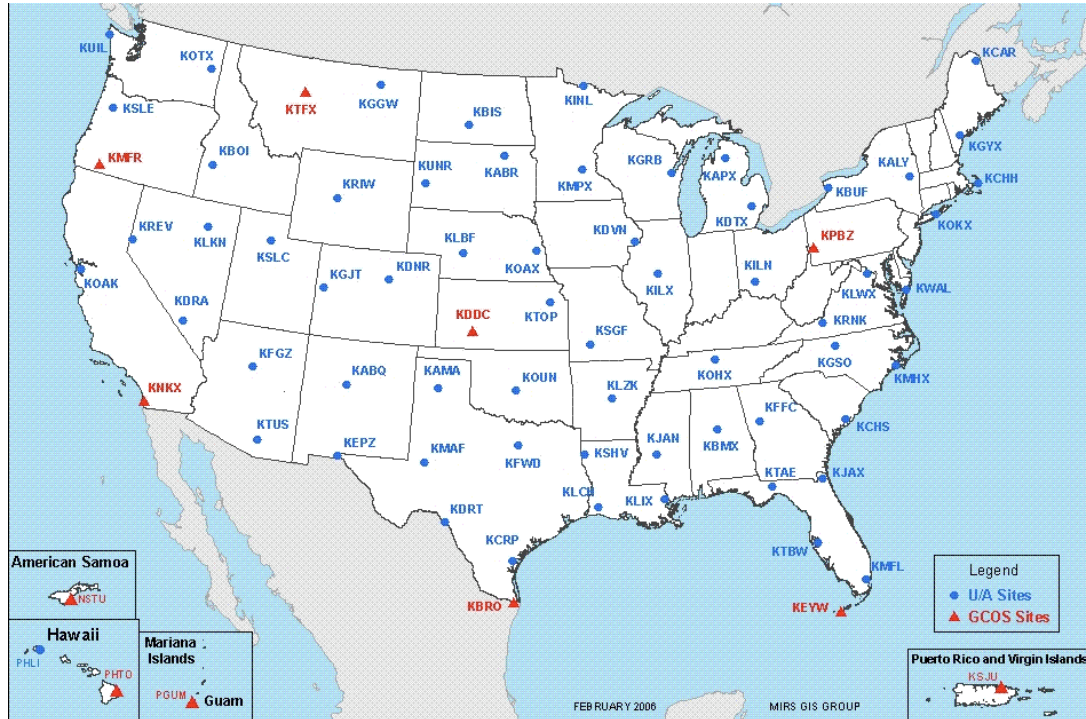
Figure 14. US map of Radiosonde Launch sites. (NWS, 2009)

7.4.2 Buoy Data

Taking advantage of moored weather buoys owned and operated by National Oceanic

and Atmospheric Administration's (NOAA) National Data Buoy Center (NDBC), the

ground truth water temperature can be determined. The NDBC is a collection of moored

buoys in the Great Lakes, Atlantic Ocean, Pacific Ocean, and Gulf of Mexico. Although

NOAA operates most buoys, a small number of buoys are operated by colleges,

universities, and in some cases commercial companies (NDBC, 2008). This research

will be limited to the buoys operated by NOAA for buoy calibration and maintenance purposes.

As seen in Figure 15 the buoys come in different sizes and shapes, but collect relatively the same information. All of the buoy types contain the same basic meteorological instruments including a thermister (used to record water temperature at depth) and an anemometer (measures wind speed).

Moored Buoy Program
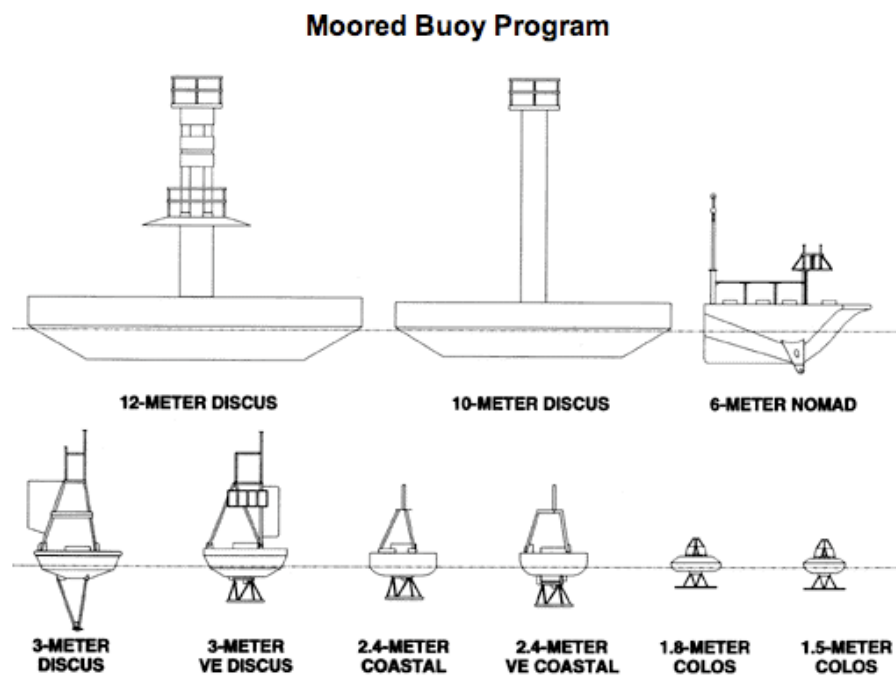
Figure 15. Buoy types owned and operated by the NDBC (NDBC, 2008)

Buoys located in the Great Lakes are deployed to a specific location in the springtime and retrieved in the fall. During the winter season the buoy is calibrated and serviced by NOAA. Buoys moored in the ocean and Gulf of Mexico are left in the water year-round and calibrated/serviced on a regular basis (once a year).

Buoys record the air pressure, wind speed, air temperature, and water temperature every hour. The NDBC keeps this data on record where it is available for users to download and for this research can be utilized as a ground truth measurement of the water temperature at a location of interest on a specific day/time. An example of a NOAA weather buoy is shown in Figure 16.

Buoy 42040	
Elevation [m]	0
Anemometer height [m]	5
Thermister depth [m]	-0.6
Water Depth [m]	274.3

Figure 16. Buoy 42040 located off the coast of Louisiana in the Gulf of Mexico. (NDBC, 2008)

7.5   Summary

This chapter discussed the history of the Landsat program and the reasoning behind why the calibration of Landsat 4 is necessary. The radiometry needed to compute the sensor reaching radiance of the target has been described, and the effects of how the atmosphere interacts with the radiance has also been introduced. The chapter wrapped up with an

overview of the environmental measurement tools needed to gain a ground truth

measurement (NOAA buoys), and to characterize the column of atmosphere above the

target (NWS Radiosonde).

8   Approach

Performing the calibration effort introduced earlier in this paper requires the use of a multi-step process. The first part of the process involves collecting an image over a specified location, as shown in Figure 17. Once the image is collected the radiance of the image at a particular region of interest (the buoy location in the scene) can be extracted. This part of the process will result in the image-derived radiance (averaged over the bandpass of the TM band 6 sensor) reaching the sensor on that particular date.
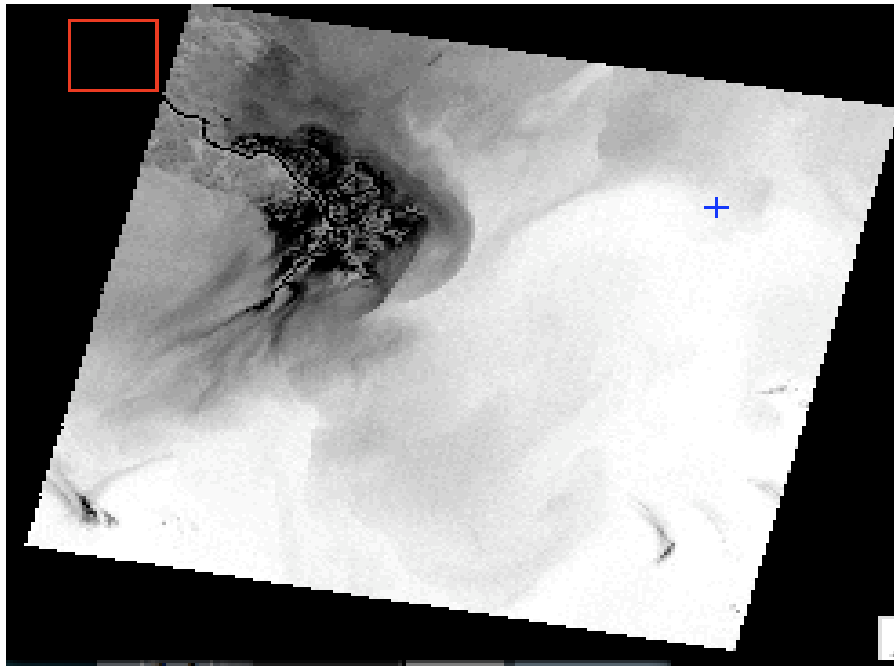
Figure 17. Landsat 5 scene with Region of Interest identified

The second part of the calibration process consists of obtaining ground truth data from the buoy, and computing the sensor reaching radiance. This part of the calibration process involves first calculating the skin temperature of the water from the buoy

thermister, then modeling the column of atmosphere above the buoy using Radiosonde and weather data. Performing these two steps predicts the sensor reaching radiance.

The final part of the calibration process compares the actual sensor reaching radiance (ground truth) to the image derived radiance. This comparison of radiance values reveals if a temperature bias correction is needed for the data. Completing multiple scenes throughout Landsat 4's operational life results in an overall calibration curve.

8.1   Proposed Calibration Sites

Unfortunately Landsat 4 did not have a long history of operational life; therefore the numbers of images available are limited. The ideal scenario when performing this type of calibration is to find one single buoy to use as the ground truth source over the entire lifetime of the sensor. This is not the case for Landsat 4 where many buoys are needed to produce enough data to create a calibration curve. This research will use a combination of buoys used in previous work by Frank Padula (Padula, 2008) along with other buoys in U.S. waters.

Successfully selecting a buoy fit for the calibration process requires fulfilling a couple of factors. The first criteria when selecting a buoy is making sure that a Radiosonde launch site is relatively close by. Without Radiosonde data the atmospheric column cannot be properly characterized.

The second criterion when selecting a buoy relies on the availability of surface weather data in the proximity of the buoy. The surface weather data is needed for wind speed and dew point calculations taken into account for calculating the skin temperature of the body of water.

The third and final criterion when selecting a buoy location is available buoy data. The calibration period of Landsat 4 ranges from 1983-1992 and the period of interest for this study in Landsat 5 is 1996-1999. Some of the buoys considered for use were not operational during the Landsat 4 or Landsat 5 calibration periods of interest or were removed from the body of water seasonally due to rough water conditions and/or annual maintenance. An eligible buoy must fill all three criteria to be used in the calibration effort.

8.1.1   Great Lakes

The first buoy location is the Great Lakes (Figure 18). Multiple buoys from this region were utilized in previous Landsat calibrations; therefore they have been validated as good sources of ground truth data and will be used again for the Landsat 4 calibration.
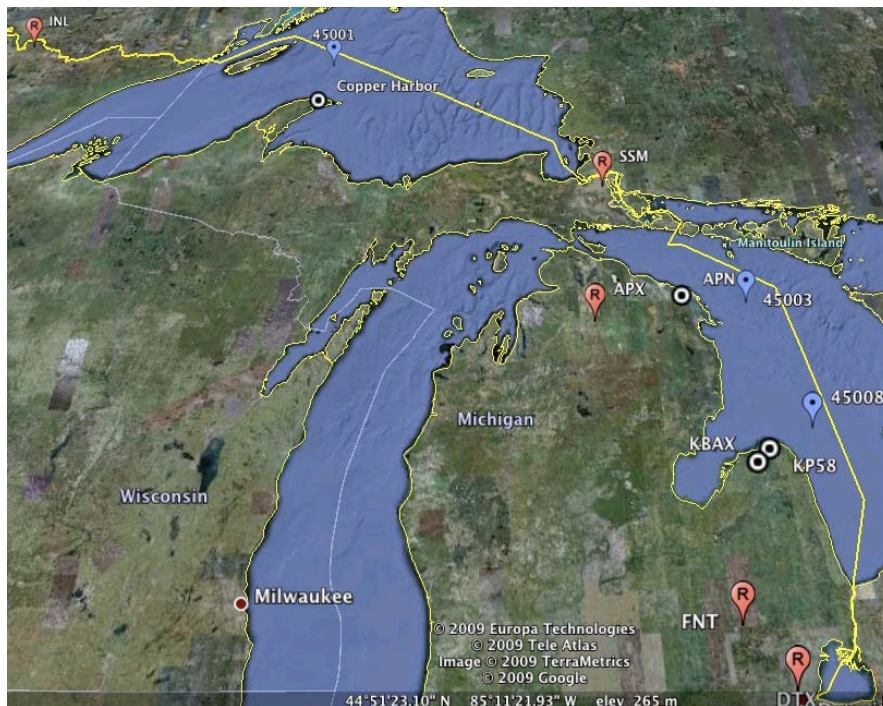
Figure 18. Great Lakes region buoys (blue), Radiosonde sites (red) and weather stations (white)

Lake Huron has two available buoys (45003 & 45008) shown in Figure 19. Both

of these buoys can be seen in one Landsat image, resulting in two potential ground truth

readings per image. The buoys are not in the water year-round so the dates of collection

are seasonal (typically May to October). The depth where buoy 45003 is located is 134.7

[m] and buoy 45008 is in 54 [m] of water. Both buoys are located in deep enough water

to eliminate water-mixing factors (which is a potential for a large thermal gradient over a

small area). Both buoys have a history of data dating back to 1980 and 1981, which is

sufficient for Landsat 4's calibration timeline.
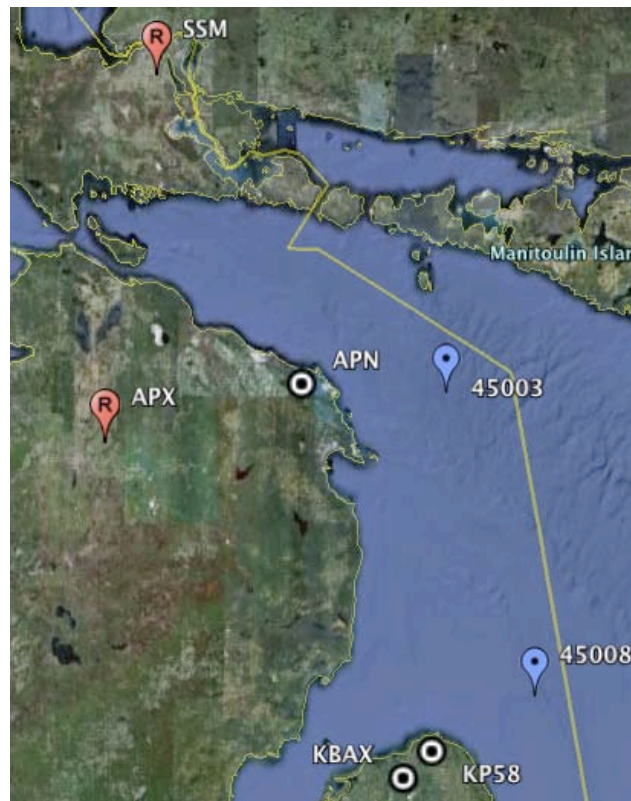
Figure 19. Lake Huron buoys (blue), Radiosonde sites (red) and weather stations (white)

The Lake Huron buoy location has Radiosonde data available from two locations, Sault Saint Marie Michigan (SSM) and Gaylord/Alpena Michigan (APX). Prevailing wind direction over the buoys produces plenty of useable weather data. Weather station data is also available in the area from Alpena County Airport (APN), Bad Axe (KBAX), and Port Harbor (KP58).

Lake Superior has one buoy location that is useable for Landsat 4 calibration effort. This buoy is 45001, which is located in 261 [m] of water, has historical data dating back to 1979, and its location can be seen in Figure 20.

Figure 20. Lake Superior buoys (blue), Radiosonde sites (red) and weather stations (white)

The site has access to two Radiosonde locations, and depending on prevailing winds can use either site. In previous research (Padula, 2008) SSM was the preferred site, although Radiosonde data from International Falls Minnesota (INL) can also be considered. Surface weather data is available from a ground station in Copper Harbor, which is directly due south of the buoy.

8.1.2   North-Eastern Seaboard

The second region used for calibrating Landsat 4 is the North-Eastern Seaboard. This location that can be seen in Figure 21 consists of three buoys, one located off of Cape Cod Massachusetts (44008) and two buoys off of the coast of Maine (44007 & 44005).

Figure 21. Eastern Seaboard buoys (blue), Radiosonde sites (red) and weather stations (white)

The buoys are in water with depths of 65.8 [m] (44008), 201.2 [m] (44005), and 23.7 [m] with historical data ranging back to 1988, 1978, and 1982 respectively. Because the buoys are located in the Atlantic Ocean they are deployed year-round providing more opportunities for data.

Radiosonde data and weather data is available for buoy 44008 from Chatham, MA (CHH), and for buoys 44005 and 44007 the Radiosonde and weather data comes from Portland, ME (PWM).

8.1.3 Gulf of Mexico

Collecting more data for Landsat 5 in the 1996-1999 timeframe requires locating new buoys to add to the fleet of available locations. Two buoys in the Gulf of Mexico were identified to continue this calibration effort and can be seen in Figure 22. The location was chosen because the buoys are in the water year-round, producing more data in the timeframe of interest.
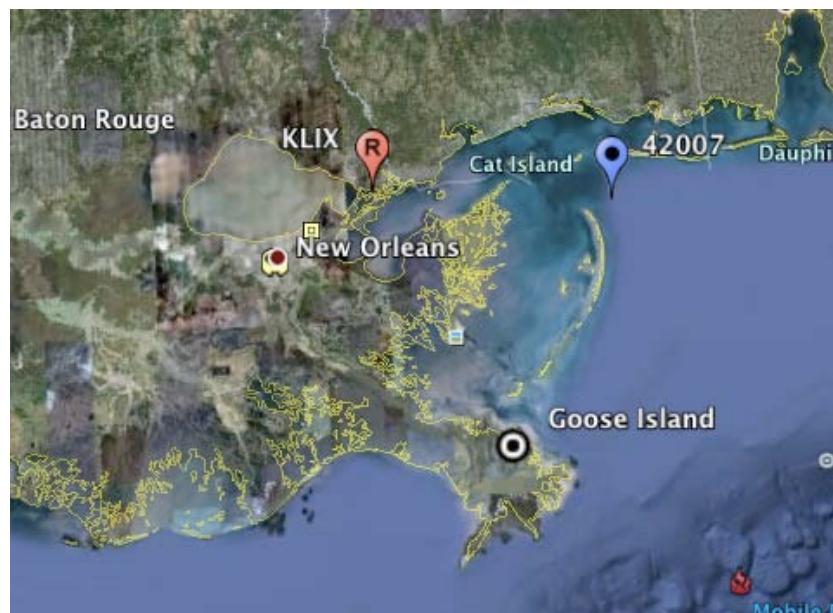

Figure 22. Gulf of Mexico buoys (blue), Radiosonde sites (red) and weather stations (white)

Buoy 42040 is located off of New Orleans where the Mississippi River empties into the Gulf of Mexico. It is located in 60 [m] of water and has data ranging from 1995 to present. Radiosonde data is available for the New Orleans site out of the New Orleans

Airport (KLIX) and weather data was available from a nearby weather station on Goose Island.

Buoy 42036 is located west of Tampa Bay FL, in 54 [m] of water. The historical data ranges from 1994 to present. The Florida buoy has Radiosonde data available from Tampa Bay Florida (TWB), and fortunately the prevailing winds blow west out of Tampa, allowing the Radiosonde to collect data in the general direction of the buoy. The final criterion, surface weather, is also available out of Tampa International Airport (KTWB).

As for Landsat 4, both buoys used in the Landsat 5 calibration (42040 and 42036) did not have any buoy data during Landsat 4's timeline, or did not have any cloud free images. One additional buoy in the Gulf of Mexico was discovered and this buoy can be seen in Figure 23.

Figure 23. Gulf of Mexico buoys (blue), Radiosonde sites (red) and weather stations (white) for Landsat 4 data

Buoy 42007 is located above a depth of 23 [m] of water and uses the same source of Radiosonde data and weather data as one of the previous buoy used in Landsat 5 (44040). This Radiosonde data was from New Orleans (KLIX) and the weather data was from Goose Island. Fortunately this buoy is located North of the Mississippi delta, therefore there were no apparent mixing layers around the buoy causing surface temperature gradients, as was seen in the other New Orleans buoys.
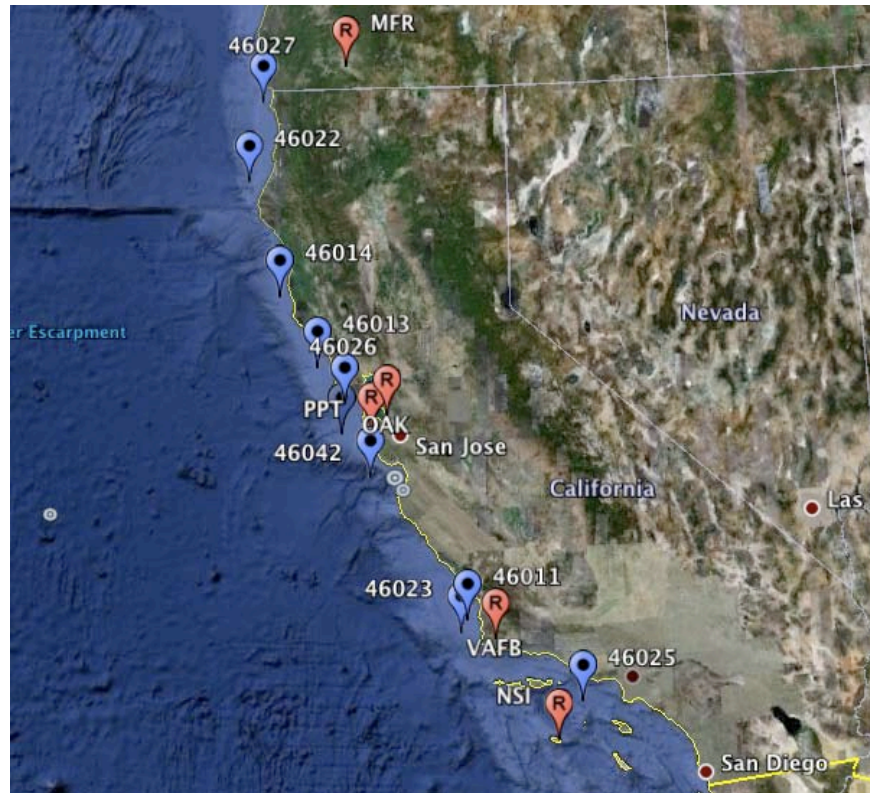
8.1.4 West Coast

A further search of available buoy data from the U.S. ultimately led to the West Coast. NOAA has an abundance of buoys up and down the west coast, but one issue occured whenever the prevailing winds were on-shore not off-shore, causing the Radiosonde data to not fly directly over the buoy. These are not ideal buoys to use based on the historic use of the physics based approach to calibration, but if successful this can open up the amount of available data for future calibration efforts.

Because of the prevailing wind direction, the scenes selected for processing were limited to clear days with stable air masses. This criteria allows us to assume that the sounding data should be indicative of the upper air over a relatively large area. This assumption allows us to use the Radiosonde data even though it is not collected directly over the buoy. Remember that the lower layers of the atmosphere are extrapolated in the Radiosonde data using inputs from local surface weather conditions, therefore the combination of local surface conditions, and a stable air mass results in accurate Radiosonde data for the west coast buoys.

Another possible issue using the west coast buoys is the marine layer. Fortunately the majority of marine layer is not present during the collection time (around noon local time) and any images showing the marine layer in the visible channels were removed.

Due to the small amount of useable data from the North-Eastern Seaboard, Great Lakes, and Gulf of Mexico buoys, the West Coast buoys were used in spite of the on-shore wind pattern. Figure 24 displays the buoys that were used for the calibration curve of Landsat 4, containing data ranging from 1983 until 1992.

Figure 24. West Coast buoys (blue) and Radiosonde sites (red) used for Landsat 4 calibration

NOAA buoy 46025 is located off of Santa Monica, CA and is located in water with a depth of 905 [m]. Radiosonde and weather data is closely available from San Nicholas Island (NSI) and is the only west coast buoy where the prevailing wind will bring the Radiosonde over the buoy.

Further up the coast, off of Vandenberg AFB CA, buoys numbered 46011 and 46023 lies in 204 [m] and 384 [m] water respectively. Radiosonde and weather data are available from Vandenberg AFB and the prevailing winds in the winter months will bring the Radiosonde data directly above the buoys.

In the Bay Area of California buoy numbers 46042, 46012, and 46026 lie in water with a depth of 1574 [m], 213 [m], and 54.6 [m]. Radiosonde and weather data for buoy 46042 is available from Pillar Point, CA (PPT) and for buoys 46012 and 46026 the data is provided by Oakland, CA. (OAK)

North of San Francisco, CA buoy 46013 lies off the coast of Bodega Bay and is sitting in water with a depth of 116.4 [m]. The Radiosonde data is provided by Oakland, CA (OAK) and the weather data is provided by San Rafael, CA. The other buoy in this area is buoy 46014, which is located off of Point Arena, CA. This buoy lies in 274 [m] deep water and also uses Oakland for the Radiosonde data and Point Arena for the weather data. These two northern California buoys have the greatest distance between the buoy and the Radiosonde launch site, but as can be seen in the Results section they still give results in line with the other buoys used in the calibration process.

The final two buoys used from the West Coast are buoy 46022, located off the coast of Eureka, CA and in 630 [m] deep water, and buoy 46027 which is located off of

Crescent City, CA and in 47 [m] deep water. Both buoys used the closest Radiosonde data from Medford, OR (MFR) and used weather data from Eureka and Crescent City. Buoy 46022 had the second largest distance from the Radiosonde data, but like buoy 46014 the resulting data was again similar to buoys with closer Radiosonde data.

Two of the West Coast buoys were also used in the Landsat 5 calibration. Those two buoys were 46012 and 46042 (San Francisco Bay Area).

8.1.5 International Sites

Landsat 4 did not have an extensive lifespan like its successor Landsat 5. The shorter lifespan results in a lack of data, compared to Landsat 5. Researching all of the possible sites in the Great Lakes, Eastern-seaboard, Gulf of Mexico, and West Coast produces only a handful of Landsat 4 scenes available for processing. Records from NASA indicate that Landsat 4 was used on many international collections while it was acting as the backup to Landsat 5 from 1987-1993. Coverage maps of Landsat 4 (like the example shown in Figure 25) show areas in the Mediterranean Sea, Hawaii, and Japan, which may have data available. Further research into moored buoys, ships, or other forms of sea surface temperature measurements resulted in no viable ground truth data available at this time to calibrate Landsat 4. Future research into this area may be able to expand on the calibration curve created by this study.
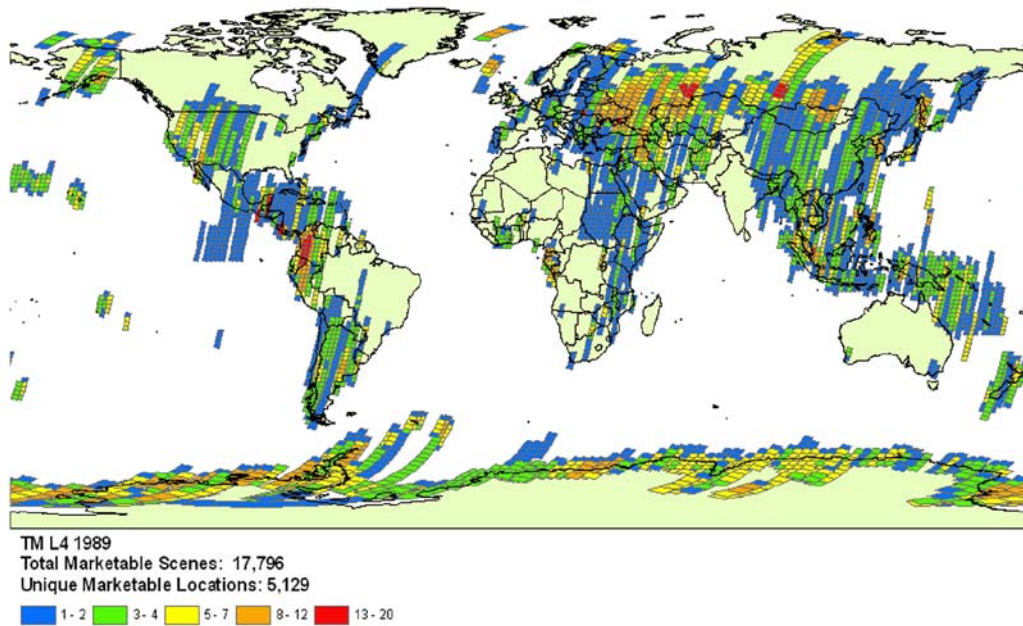
Figure 25. Landsat 4 coverage map of 1989 [NASA]

8.2 Good vs. Bad scenes

Not all Landsat data is useable for the physics based model of calibrating the TM sensor.

A preferred image has to meet a few strict criteria. The first criterion is that the scene

must be a cloud free image. Using a cloud free image allows better characterization of

the atmosphere, which allows us to consider the atmosphere as a homogeneous medium.

The second criterion is having available buoy and weather data for the date the scene was

collected. In some cases, primarily the Great Lakes, the moored buoys are not in the

water year-round, which means that for a portion of the year buoy data is missing.

Similarly the weather station could have problems with their equipment resulting in a

lack of temperature and pressure data needed to characterize the atmosphere, or

determine the skin temperature of the water. The third and final criterion is having data

that does not contain large thermal variations around the buoy. The TM has a GSD of

120 m, meaning a large homogeneous target area is critical in calculating an accurate

calibration data point. As you can see in Figure 26 the scene on the left would not be

used due to large thermal variations, where the scene on the right with low thermal

variations would be used.
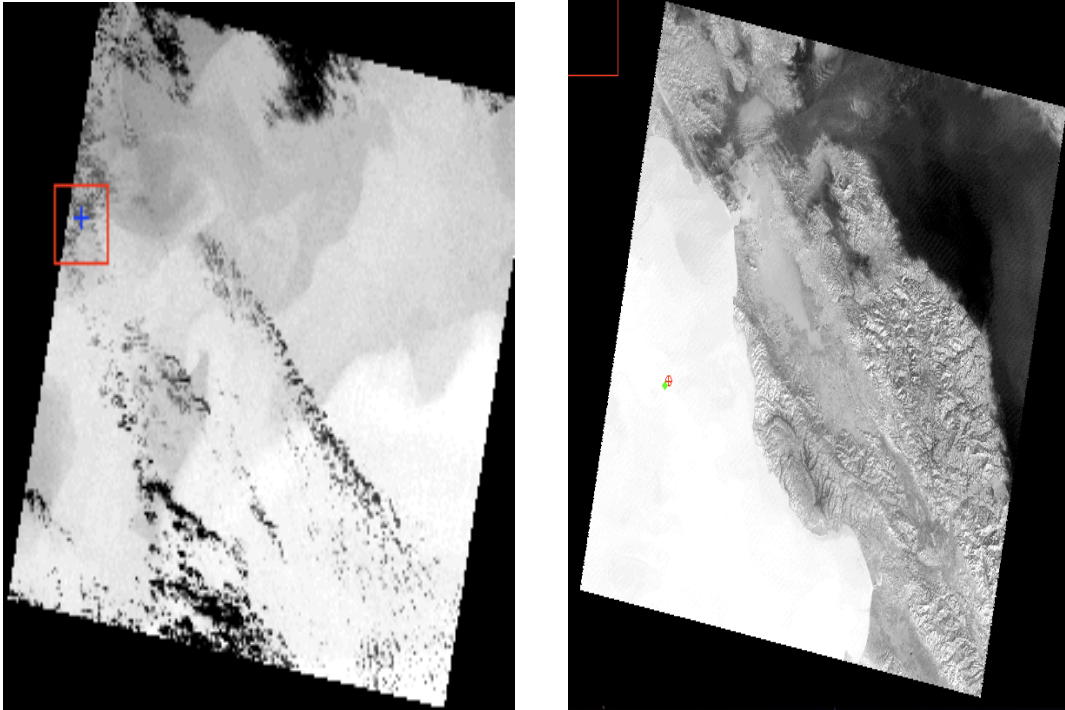
Figure 26. The left image is a Landsat scene with large thermal variations around the buoy (blue marker), and the right scene has a small thermal variation around the buoy (blue marker)

8.3   Calibration Process

When a good Landsat 4 scene has been selected, calibrating the TM sensor will follow a

four-step process as shown in Figure 27. The first step involves obtaining the water

temperature from a moored buoy and calculating the surface temperature (T_s) using the

Zeng approach [Section 6.4]. Using T_s, the emissivity of water ($\varepsilon = 0.986$), and the

spectral band locations of TM band 6, the surface leaving radiance due to temperature is calculated using the Planck equation. [Eq. 7.1]

The second step involves characterizing the column of atmosphere above the buoy. This is accomplished by inputting the weather data (temperature, pressure, and dew point) along with the Radiosonde data (temperature, pressure, and dew point at altitude) into MODTRAN. The output from MODTRAN is used to calculate the atmospheric parameters of upwelled radiance, downwelled radiance, and atmospheric transmission. Using the surface leaving radiance and MODTRAN calculated atmospheric parameters; the sensor reaching radiance can be predicted.

The third step involves calculating the radiance from the Landsat 4 scene. This step is accomplished by creating a region of interest consisting of 3 pixels by 3 pixels around the moored buoy location, computing the average digital count and standard deviation, then converting that digital count into radiance.

The fourth and final step compares the radiance values. The image derived radiance is compared to the ground truth predicted sensor reaching radiance, and the difference between the radiances indicates a bias for the sensor.
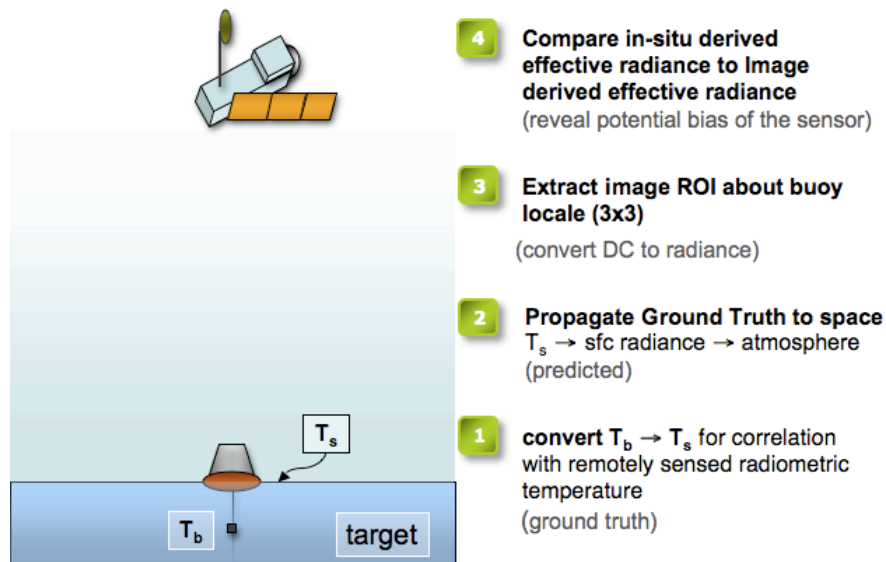
Figure 27. Pictorial overview of the four-step calibration process (Padula, 2008)

8.4   Computation of Skin Temperature

Previous Landsat calibration efforts (Padula, 2008) conducted a study to determine which method was best for calculating the skin temperature (T_s) of the surface of a body of water using recorded submerged water temperature readings. Through this study it was found that the Zeng method [Section 6.4] was the preferred choice.

Calculating the T_s includes using the bulk water temperature from a moored buoy, wind speed, and the depth of the bulk temperature measurement being run through the Zeng program. The bulk water temperature is measured using a thermistor, which is submerged below the moored buoy.   The depth of the thermister depends on the size/type of NDBC buoy, which is an input into the Zeng program.

Wind speed is a driving factor in calculating T_s, therefore at the time of image capture (information contained in the header file) a wind speed measurement is required

for an accurate T_s calculation. When a high wind speed value is present the Donlon correction will be used. (This is a 0.17K correction to the bulk temperature) (Donlon, 2002)

8.5   Recreation of Atmospheric Column

The second part of the four-step calibration technique characterizes the column of air above the buoy, which helps determine the sensor reaching radiance. [Section 7.4] Creating the column of air above the buoy involves using multiple meteorological tools. The column of air to be modeled extends from the surface of the earth up to 100 km.

Using an IDL program, the raw data from a Radiosonde can be graphed as a sounding typically from altitudes of a few meters up to 30 km. Two Radiosondes are launched per day, producing two opportunities to characterize the atmosphere per day. Both soundings are compared and selected based on which one has less water vapor present. One way to determine how much water vapor is present is to look at the dew point depression (DD). DD is defined as the difference between the dew point and the temperature. As a rule if the DD is ≤ 3 C a saturated layer, or cloud, is present (Padula, 2008). Recalling back to Section 6.3 cloud free data is a must. When a good Landsat scene is selected for use, the Radiosonde data soundings are plotted using IDL and the best one (one with less saturation) is selected.
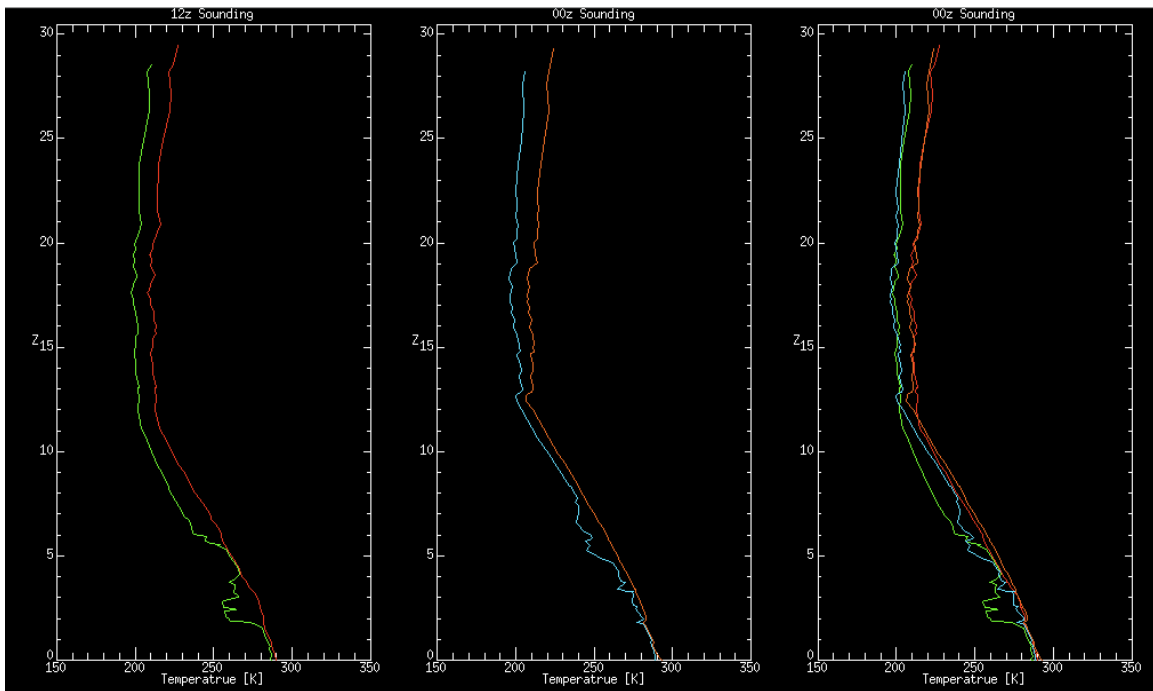
Figure 28. 12z, 00z, and the combined soundings from 24 Mar 1996. The 12z sounding has a saturated layer from 4 to 5 km . The 00z sounding has a saturation zone between 0 and 5 km. The 12z sounding would be chosen for further processing.

Figure 28 is a sample of the 12z, 00z, and the combination of the two Radiosonde soundings on 24 Mar 1996 from New Orleans, LA. The line on the left of the sounding is the dew point temperature, and the line on the right is the air temperature at that specific altitude. The 12z sounding has a moisture layer between 4 km and 5 km, but appears to not have any other saturation layers outside of that area. The 00z sounding has a saturation layer from 0 km to 5 km and another layer from 7 km to 13 km is close to being a saturation layer. In this case the 12z sounding would be used for further processing and eventually input into MODTRAN.

8.5.1 Surface Correction

The Radiosonde data is the primary source of atmospheric conditions input into MODTRAN for the process of characterizing the atmosphere. Surface weather data is the next most important piece of information needed for MODTRAN. In addition to the Radiosonde data, surface weather data is used for two main reasons. The first reason is based on the fact that the chance of getting Radiosonde data within about 30 miles of the buoy is essentially zero. (Schott, 2007) Surface weather data on the other hand is available in many weather stations around the country and even on the buoys themselves. The second reason that surface weather data is important comes from the fact that most Radiosonde launch sites are above sea level. The lower, warmer layers of the atmosphere contain more horizontal variation resulting in the atmosphere being less homogeneous. Understanding what is happening at the lowest levels of the atmosphere is crucial in eliminating any unknown variations in the atmosphere.

Radiosonde data will be extrapolated using surface temperature, pressure, and dew point measurements from a selected inversion point to the surface of the earth. Surface measurements are collected on an hourly basis, unlike the Radiosonde data, which is collected twice a day. The surface correction is done in the same IDL program used in Section 8.5 and can be seen in Figure 29.
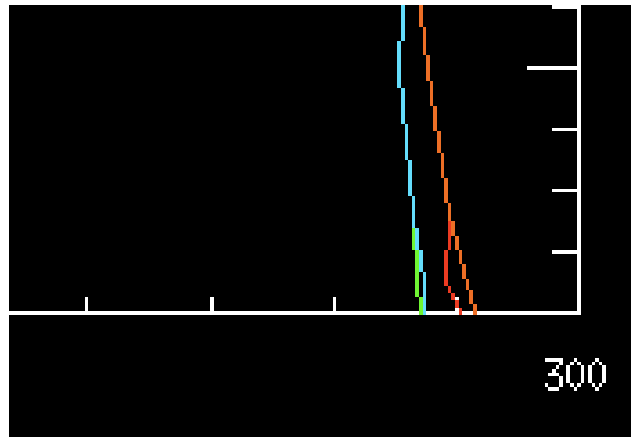
Figure 29. Surface correction applied to the Radiosonde sounding. A line is extrapolated from the Radiosonde data (right line in both temperature and dew point measurements) using surface weather data (temp, pressure, and dew point)

8.5.2 Upper-Air Interpolation

As discussed in Section 7.4.1 the average Radiosonde balloon will collect data up to ~30 km in altitude. To accurately calculate the sensor reaching radiance the atmosphere is characterized up to the effective top of the atmosphere (100 km). The final step when creating the atmospheric column inputs for MODTRAN is interpolating the atmosphere up to 100 km by use of a MODTRAN standardized atmosphere. At higher altitudes the atmosphere is more homogenous, therefore it is acceptable to use a standard MODTRAN atmosphere to interpolate the column of air above the buoy.
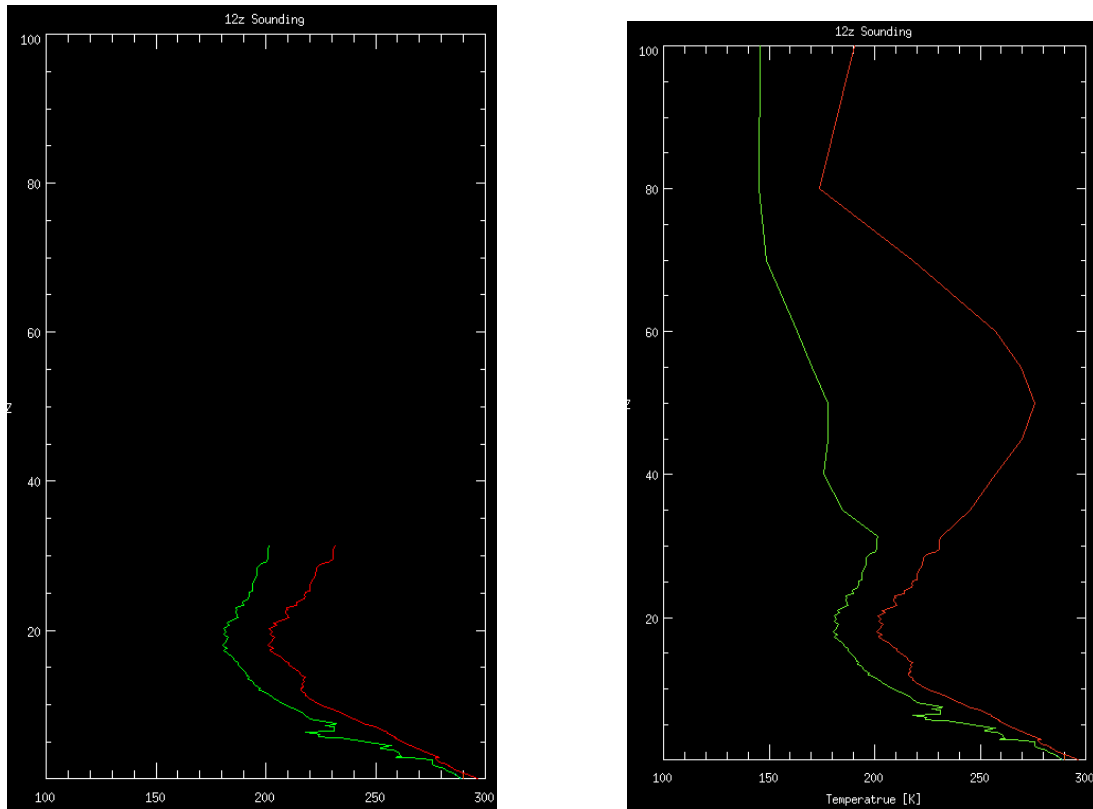
Figure 30. Typical Radiosonde sounding with max altitude of 30 km (left) and the upper atmosphere interpolated using a mid latitude summer day profile in MODTRAN (right)

As seen in Figure 30 applying the Mid-Latitude summer day profile from MODTRAN, extends the Radiosonde data up to the sensor altitude of 100 km.

8.6   Extracting Atmospheric Terms

MODTRAN is the radiative transfer model used to compute the upwelled radiance, downwelled radianace, and transmission of the atmosphere over each buoy on the day of interest. This process is completed by assembling the column of air above the buoy as described in Section 8.5 and inputting those values into MODTRAN using a tape 5 card deck.

The MODTRAN output file, tape6, will contain the wavelength [μm], transmission, and upwelled radiance [W/cm^{2}srμm] terms. To obtain the downwelled radiance term a second program called DIRSIG will be utilized. DIRSIG provides an atmospheric database (ADB) file, which contains the downwelled radiance [W/cm^{2}srμm] term.

Using the Zeng approach [Section 6.4] the skin temperature (T_s) can be found from the buoy thermister. This skin temperature will then be converted into a surface leaving radiance by using the Planck equation (Eq. 7.1) and the known emissivity of water (ε=0.986). Finally a predicted sensor reaching radiance (L_{eff}) is found using Eq. 7.14.

8.7   Obtaining Image Derived Radiance

The third part of the four-step calibration technique obtains the image derived radiance. This is accomplished using a good quality Landsat 4 scene. [Section 6.3] Knowing the geographic location of the buoy, a shapefile is created in a computer program called ENVI and geographically placed on the Landsat image.   Figure 31 is an example of he shapefile determining the exact location of the buoy in the scene (blue crosshair).
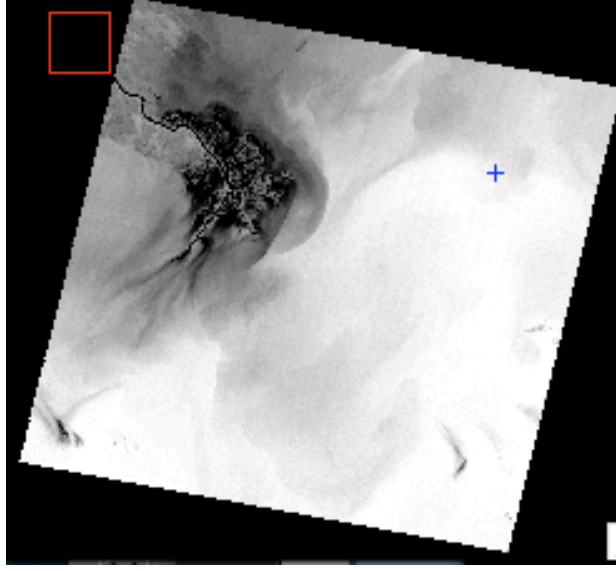
Figure 31. ENVI is used to display a Landsat scene and a shapefile is created from the geographic location of the buoy. ENVI will geometrically place the buoy on the scene (blue crosshair)

Once the buoy location is identified in the scene, a region of interest around the buoy is selected. To achieve a factor of three in reduction of noise a 3 x 3 region or 9 pixels will be selected to calculate an average DC value of the region. Equation 8.1 converts the DC value to a radiance value:

$$L = (DC_{avg} * gain) + bias \qquad (8.1)$$

where gain and bias are taken from the Landsat header file.

8.8   Comparison of Radiance Values

The fourth and final step in the calibration technique compares the image derived radiance (L) to the ground truth predicted sensor reaching radiance. (L_{eff}):

$$\Delta L = L - L_{eff} \qquad (8.2)$$

Based on Equation 8.2, a positive ΔL indicates a warm bias, and a negative ΔL indicates the sensor has a cold bias. This ΔL is input into a look up table, which is created using the Planck equation and a blackbody curve relating temperature to radiance, producing a ΔT. This ΔT is one data point, and after collecting multiple data points over a period of time a temporal calibration curve is built.

8.9   Validation of Approach

The four-step calibration technique was originally put to the test in work accomplished by Padula in 2008. Padula processed 186 scenes, resulting in 214 data points in an effort to calibrate Landsat 5/7 TM band 6. Padula's research reached the conclusion that Landsat 5's TM sensor had fluctuated 1.064 K over a twenty-year period. Through his research Padula discovered that the technique would confidently be accurate to within 0.5 K. According to the results from previous research performed by Padula, the four-step technique appears to be a solid approach to calibrating band 6 of the TM on Landsat 4.

8.10   Summary

This section discussed the approach proposed for use in calibrating the TM sensor on Landsat 4. It included an overview of the proposed buoy locations, Radiosonde collection points, and weather stations utilized to gather all the data needed for the calibration technique. The section wrapped up by explaining the criteria needed for a good scene, and a step by step overview of the calibration technique.

9   Results

9.1   Landsat 5

Before diving into the Landsat 4 archive, a continuation of the Landsat 5 TM calibration was completed. As mentioned in Section 5, previous work by Padula suggested a bias shift sometime in early 1999 in the TM sensor on Landsat 5 (Padula, 2008). In order to pinpoint an exact date of when the shift occurred more data points from that timeframe were needed. After a thorough review of previous results, the bias shift was believed to be anywhere from Jan 1996 to Dec 1999, expanding the area of further research from one to four years. Using this expanded timeframe forty scenes were selected for processing where 21 of the scenes resulted in calibration points. Figure 32 displays the distribution of how many scenes came from each year group in the 1996-1999 range.
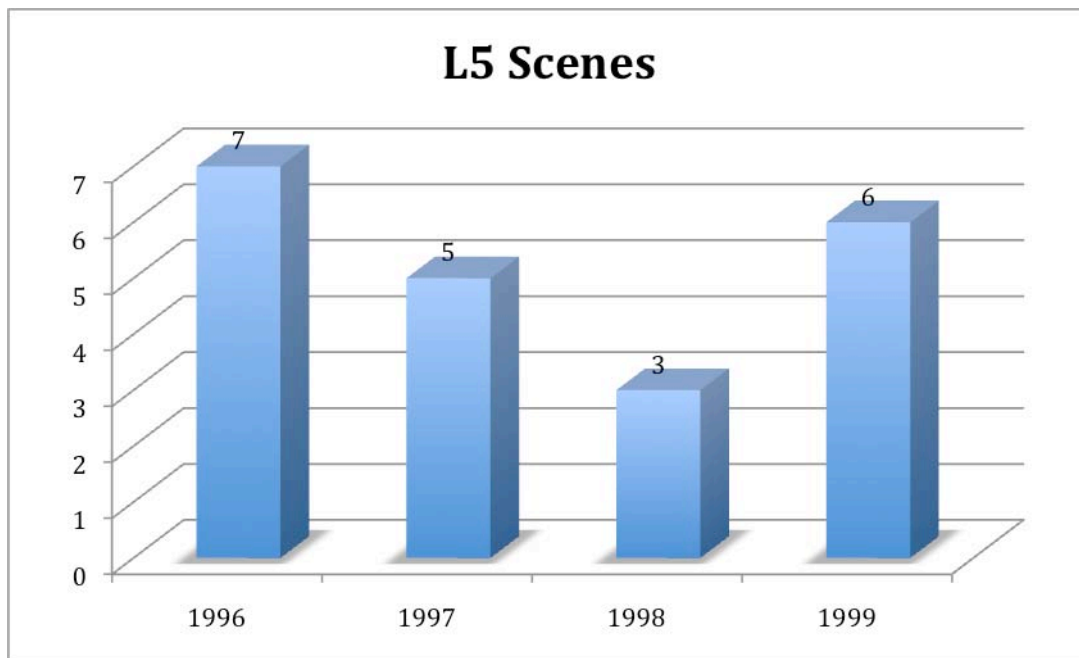
Figure 32. The twenty-one usable data points were well spread out over the 1996-1999 timeframe

9.1.1 New Orleans site

The goal of the research was to gather as much data in the 1996-1999 timeframe as possible. The idea was to look for buoys that would be in the water year-round just in case the bias shift occurred during the winter. This eliminated any buoys not located in the ocean. In the Gulf of Mexico NDBC buoy 42040 had buoy, Radiosonde, and weather data readily available, making it an ideal candidate for Landsat 5 calibration processing. Twenty plus scenes from the area were considered, but due to a large thermal variation in the scenes many of them could not be used. This large thermal fluctuation was due to the Mississippi River emptying into the Gulf of Mexico at this location.
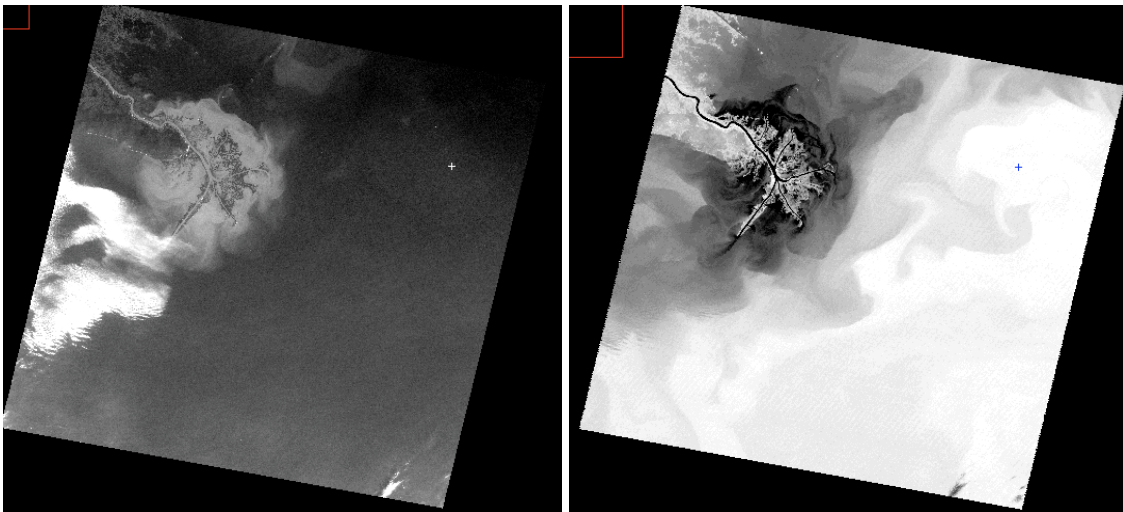
Figure 33. Visual spectrum of scene with the buoy marked white (left) and same scene with buoy marked (blue)

As seen in Figure 33 the water temperature in the thermal image (right) does not look homogeneous at all. This mixing in the water is mostly likely a result of the Mississippi delta in the scene. This scene was not used for fear that the thermal gradients could produce a false temperature due to imperfect knowledge of the buoy location, which in turn creates an erroneous calibration point.

9.1.2   Florida Site

Due to the small number of usable scenes from the New Orleans site, NDBC buoy 42036 was also used for Landsat 5. This buoy, while still located in the Gulf of Mexico, was close to the Florida coast. Like the New Orleans buoy it had buoy, Radiosonde, and weather data available. Unlike the New Orleans scene the Florida scene had no thermal mixing effects, but had less cloud free days.

9.1.3   California Site

A third site was chosen to once again add more data points to the 1996-1999 dataset. Although the prevailing winds would not directly carry the Radiosonde instrument directly over the buoy, two west coast buoys were chosen. In an attempt to reduce errors only two buoys within the same scene were chosen from the west coast, rather than a handful of buoys up and down the coast. Those two scenes were in the San Francisco bay area, and had available weather and Radiosonde data nearby. Using the west coast buoys we were able to add an additional ten scenes to the calibration curve.

9.1.4   Results

After processing the available scenes for Landsat 5 in the 1996-1999 timeframe, the data did not show any more information than previously reported. The 21 data points

contained both positive and negative biases in the same time period, but no definite break from a positive trending bias to a negative one.
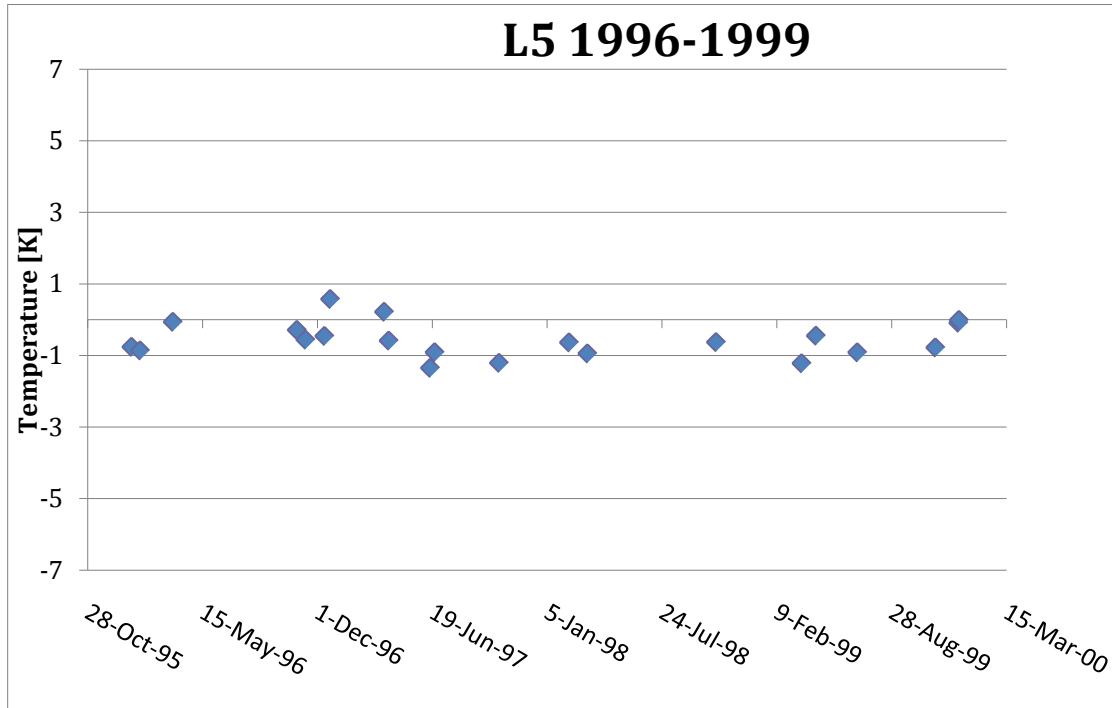
Figure 34. After processing all of the acceptable scenes from the Gulf of Mexico, a specific bias shift is still not clear

One could arguable break this data into two sets and claim that the bias shift occurred between Aug 97 and Mar 98, but when compared to Padula's results creating this break is not acceptable. Figure 35 is an expanded view of Padula's Landsat 5 calibration results and it shows that in 1996 and 1998 there are both positive and negative biases, a pattern that was repeated in this study.

The pattern of Landsat 5 bias points appears to have some scale of seasonal oscillation occurring. Averaging all the Landsat 5 data from 1984 -2007 on a 3-4 month average and a 4-5 year average (Appendix C) fails to show a true seasonal oscillation.
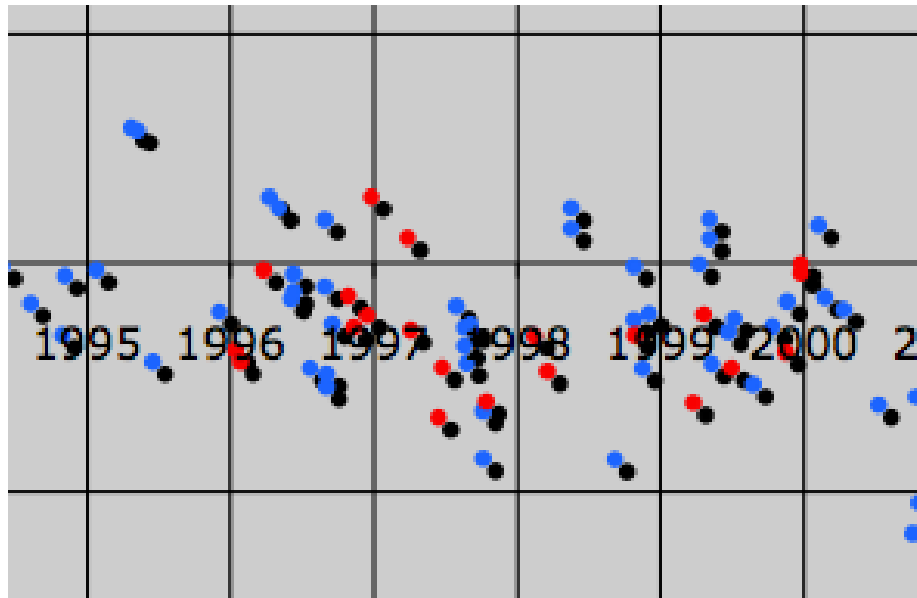
Figure 35. Results from Padula (blue and black dots) exhibited the same characteristics as the 1996-1999 Landsat 5 study (red dots)

As a final check to make sure that the calibration curve for Landsat 5 data in the 1996-1999 was consistent with previous data, a plot was created that compared the predicted top-of-atmosphere radiance to the image derived radiance. As seen in Figure 36 the slope of the best fit line is 0.966 (compares to 1.0 calculated by Padula 2008) and the correlation value (R^2) is 0.98309 (compares to 0.984 calculated by Padula 2008). This gives us high confidence that the physics based approach using different buoys in this research has produced data that is statistically similar to the slope, intercept, and bias found by Padula 2008 and can therefore be included into the previous calibration curve for Landsat 5.
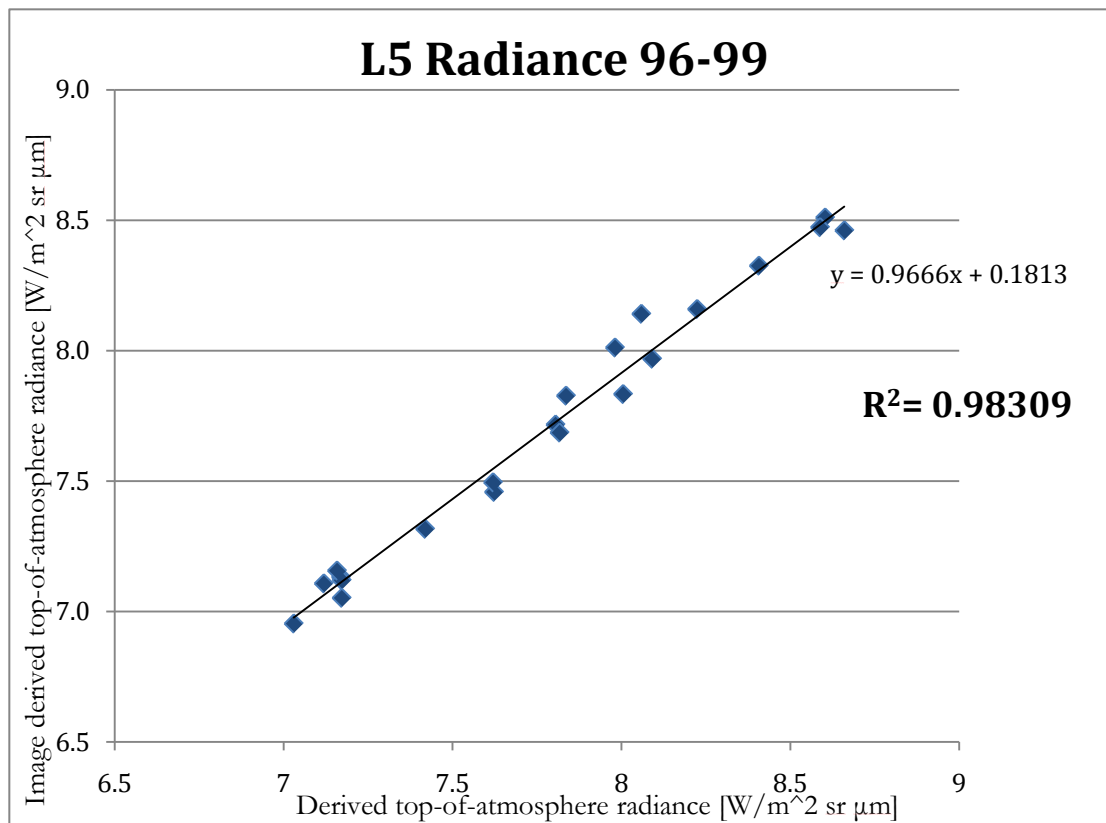
Figure 36. Predicted at sensor radiance and imaged derived top-of-atmosphere radiance for Landsat 5 data collected from 1996-1999 NOAA weather buoys in the Gulf of Mexico and West Coast USA

9.2   Landsat 4

9.2.1   NOAA Buoys

Unlike Landsat 5 the ability to find useable Landsat 4 data was quite challenging. The majority of data used in Padula's (2008) calibration of Landsat 5 came from primarily two buoys in the Great Lakes. Unfortunately in order to calibrate Landsat 4 all 118 NOAA buoys in the east coast U.S., west coast U.S., Gulf of Mexico, Alaska, Hawaii, and Caribbean were evaluated for useable data and a final total of seventeen buoys were used. Using multiple buoys is a good test to see if the physics based approach will still

produce reasonable results using data from so many different sources and locations.

Figure 37 displays the distribution of scenes collected from each buoy.
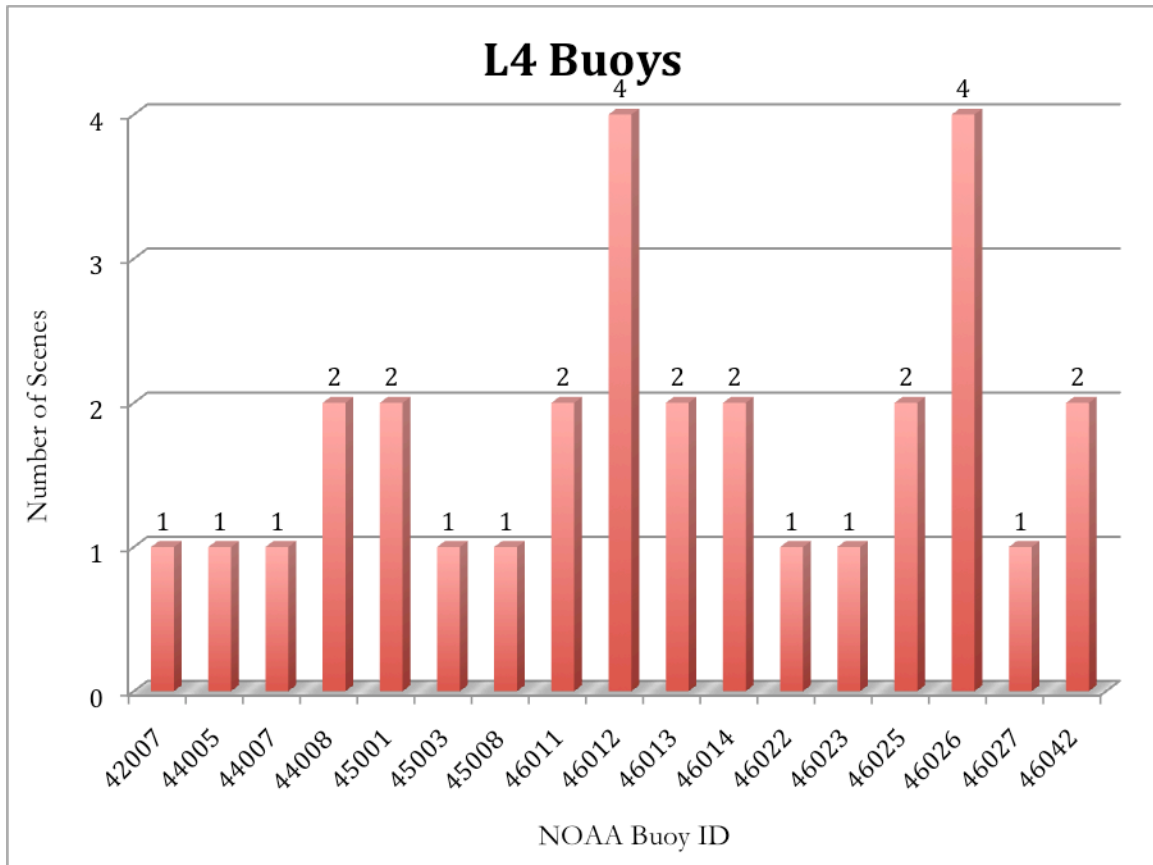
Figure 37. Breakdown of the number of NOAA buoys used for Landsat 4 calibration and the number of scenes that came from each buoy location.

9.2.2 Useable Landsat 4 Scenes

Using the seventeen buoys previously mentioned above, Landsat 4 scenes from 1982-1992 were used to create the calibration curve. Due to the constraints mentioned earlier in the paper of cloudless scene, available buoy data, and available surface meteorological data, a total of 41 scenes were evaluated and processed resulting in 30 usable data points.

The data points were distributed over the operating period of the sensor, remembering that the sensor was placed into a "storage" mode from 1984 until 1987. As you see in Figure 38 there is a period of no data from 1984 – 1987 and also there were no data points in the final operating year of the sensor (1993).
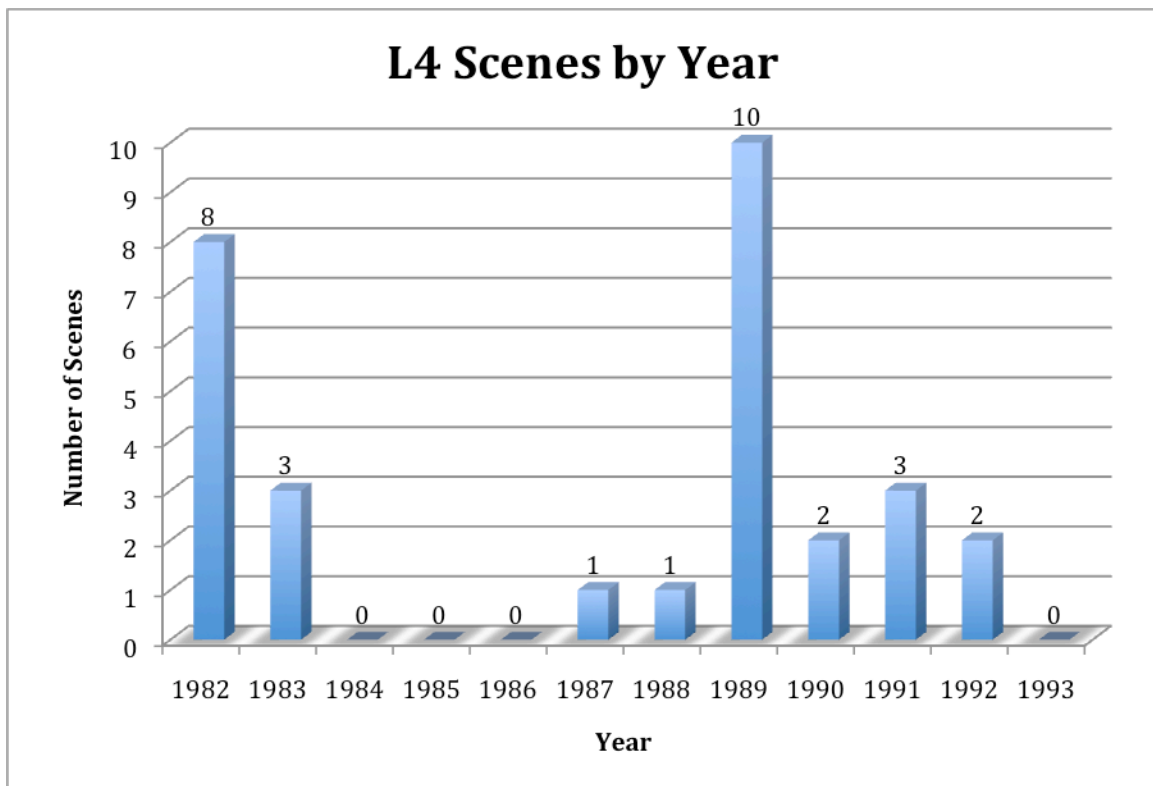
Figure 38. Distribution of number of used scenes per year during lifetime of Landsat 4

9.2.3   Results

After processing all 30 scenes for Landsat 4 a temporal bias history was created. The bias history, which can be seen in Figure 39, displays the difference in temperature between the image derived temperature, and the ground truth temperature from the

NOAA buoys. The large gap in data in the figure is again due to the fact that Landsat 4 was placed in a "storage" status from 1984-1987.
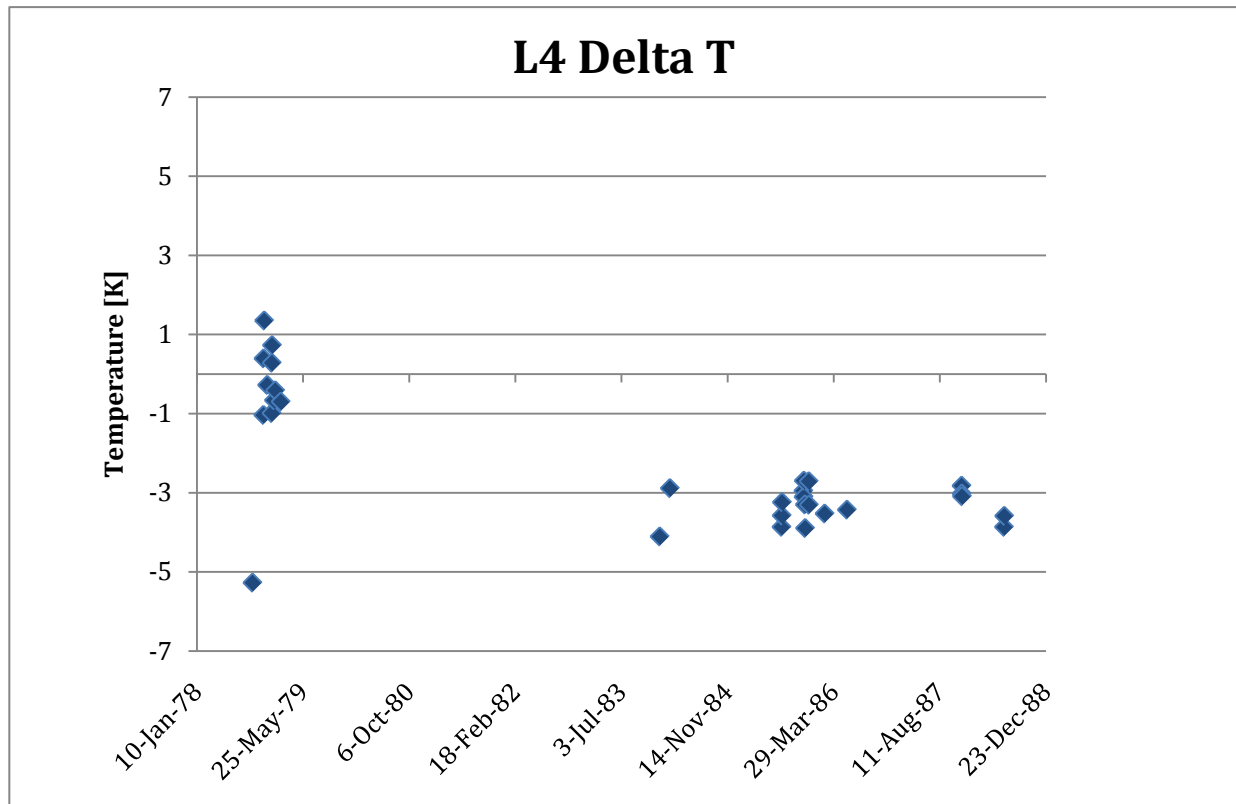
Figure 39. Calibration curve for Landsat 4 TM sensor band 6. This chart is the difference from the image derived temperature recorded by the spacecraft and the ground truth temperature recorded by the NOAA buoy.

According to Figure 39, the very first Landsat 4 scene that was processed seems to be an outlier. This scene was taken on 30 September 1982, which is approximately 75 days after the launch of Landsat 4. After further investigation into this timeframe it has been concluded that the sensor was still in its early orbit stabilization period (Barsi NASA). During the early orbit period the sensor may have erroneous readings therefore

this point has been included in the Figure, but not used for any actual calibration

calculations or errors.

9.2.3.1   Pre-1987

Unlike the Landsat 5 curve created by Padula in 2008 and the Landsat 5 curve created

from 1996-1999 in Section 9.1.4, the Landsat 4 curve does not have all of its points

centered around 0 K. One can see by Figure 39 that the data sets look completely

different before the spacecraft went into storage and after it came out of storage. In the

time before the spacecraft went into storage the difference between the temperature

recorded by the spacecraft and the actual temperature varied from -1 K to 1.8 K. Table 3

represents the average temperature difference and the standard deviation of the pre-

storage or pre 1987 time frame of Landsat 4 TM.

| Date	μ	σ
Pre-1987 (with outlier)	-0.59 K	1.72 K
Pre-1987 (without outlier)	-0.13 K	0.79 K

Table 3: Pre-1987 average temperature difference (μ) and standard deviation (σ) between image
derived temperature recorded by the spacecraft and the ground truth temperature recorded by
NOAA buoys.

When removing the outlier (the data point that was collected during early orbit

calibration) the average temperature difference (μ) is -0.13 K meaning that the sensor

appears to be well calibrated. The issue with the pre-1987 data is the standard deviation

(σ) value of 0.72 K is higher than anticipated. In previous research (Padula, 2008) the

sensor was calibrated to about 0.5 K meaning that the pre-1987 data has more fluctuations than expected. This fluctuation could be due to one of many factors including the overall process, instrument noise, or operating temperature of the sensor. After further research it was discovered that the operating temperature of the sensor has varied over the lifespan of the spacecraft. Figure 40a and Figure 40b display the variation of the temperature in the relay optics and the calibration shutter.

(a)   (b)
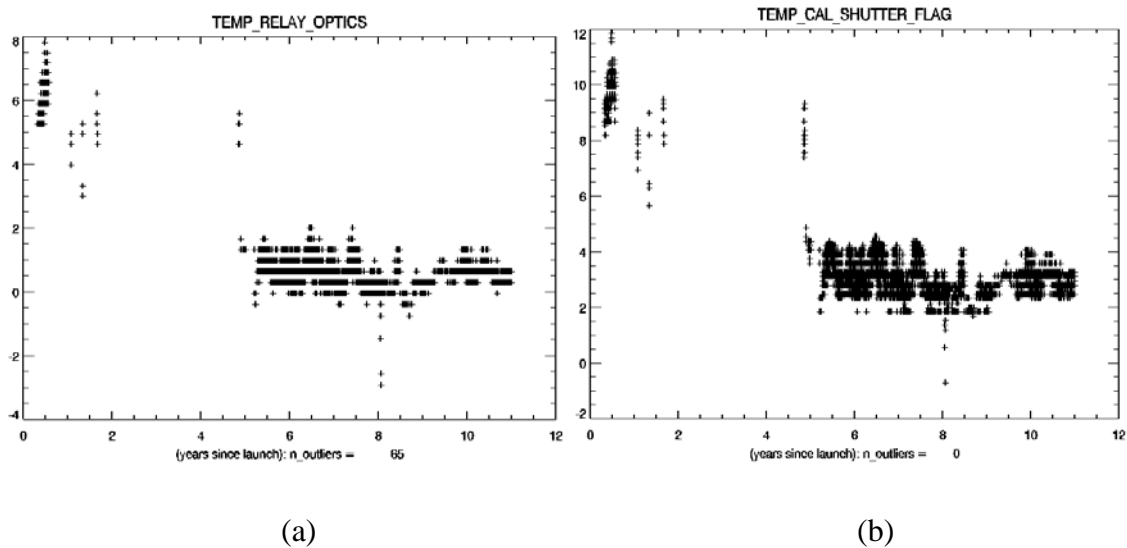
Figure 40. Temperature variations in the Relay Optics (a) and the Calibration Shutter (b) during Landsat 4 TM. July 1987 is the 5 year mark on the scale. (Barsi NASA)

The average temperature for the pre-1987 relay optics was 6.14 K and had a standard deviation of 0.62 K. This variation in temperature is potentially a source of the variation in the calibration points seen in Figure 39.

9.2.3.2   Post-1987

When the spacecraft was once again operational, after its 3-year storage period, the

calibration curve in Figure 39 looks dramatically different. Instead of the temperatures

varying around zero Kelvin, the temperatures are now varying from -4.6 K to -2.7 K.

This can be explained when comparing the data in Figure 39 to the temperature data in

Figure 40. As seen in Figure 40 the operating temperature of the sensor appears to be

much lower averaging at 3.15 K compared to the 6.14 K temperature before storage.

This shift in operating temperature accounts for post-1987 average and standard deviation

as seen in Table 4.

Date	μ	σ
Post-1987	-3.31 K	0.42 K
Post -1987 (with bias)	0.17 K	0.38 K

Table 4: Post-1987 average temperature difference (μ) and standard deviation (σ) between image derived temperature recorded by the spacecraft and the ground truth temperature recorded by NOAA buoys.

The Post-1987 data had an average temperature difference (μ) of -3.31 K and a

standard deviation (σ) of 0.42 K.   The standard deviation is more in line with previous

Landsat 5 results and can be attributed to a more stable operating temperature (smaller

standard deviation than the pre-1987 standard deviation). Adding a 0.4533 [W/m^2 sr μm]

bias to the imaged derived radiance brought the average temperature difference (μ) to

0.17 K and the standard deviation (σ) to 0.38 K. This 0.4533 [W/m^2 sr μm] bias will be

discussed further in Section 9.3.

9.3   Calibration Corrections

The results from analyzing the Landsat 4 data suggest that the data needs a correction

during one timeframe.   In the pre-1987 timeframe the data does not really need an

adjustment added to it because the average temperature difference between the image

derived temperature and the ground truth temperature were much smaller than the

measurement error. The standard deviation of the pre-1987 data looked higher than

Landsat 5 data, but could be accounted for due to temperature variations in the sensor.

Looking further into the post-1987 data, an apparent bias correction would be needed. In

order to further understand what size of correction would be needed Figure 41 was

created to display the image derived radiance vs. derived top of atmosphere radiance.
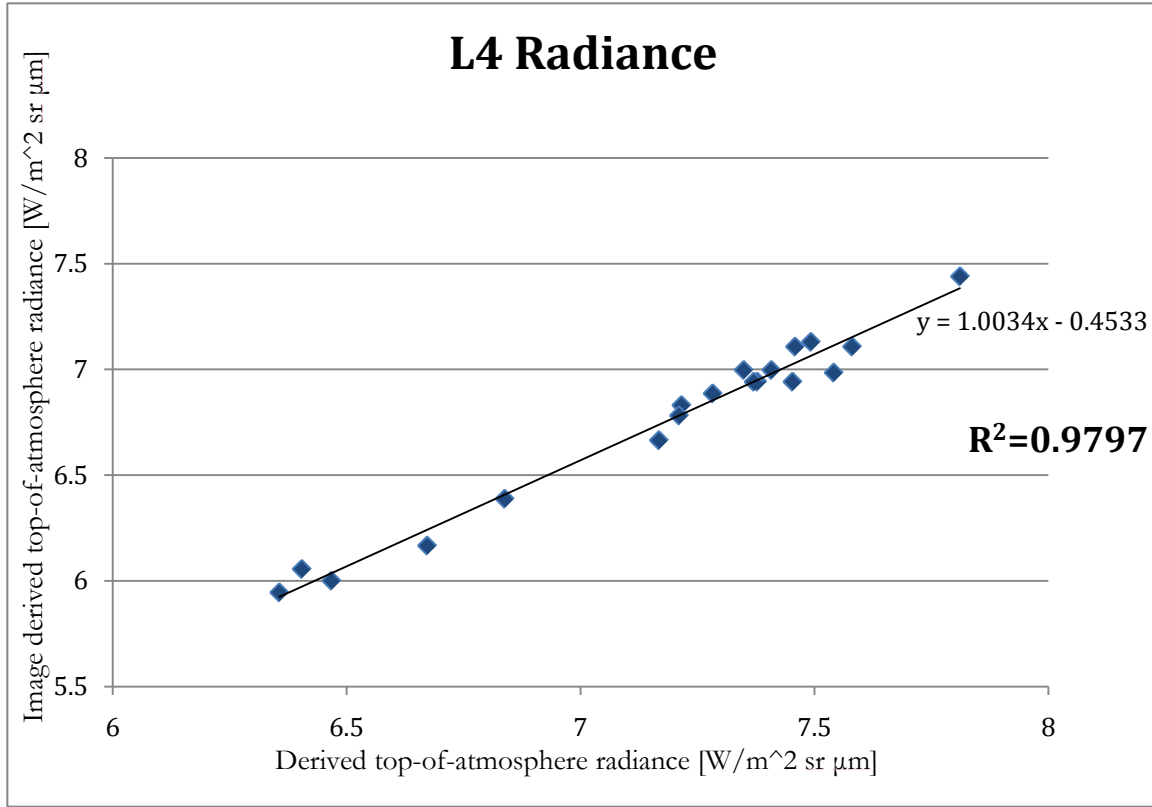
Figure 41. Predicted at sensor radiance and imaged derived top-of-atmosphere radiance

As seen in Figure 41 the slope of the best fit line is close to one (1.0034), which is expected, and there is a high correlation (0.9797) between the data which is also expected. The intercept value of -0.4533 gives us an idea of the amount of bias needed to minimize the error in the data. The uncorrected data in Figure 39 resulted in a Root Mean Squared Error (RMSE) of 0.4330 [W/m^2 sr μm] using Equation 9.1:

$$RMSE = \left(\frac{\sum (T_{act} - T_{predicted})^2}{N} \right)^{\frac{1}{2}}$$

(9.1)

where N is the total number of samples, or data points.
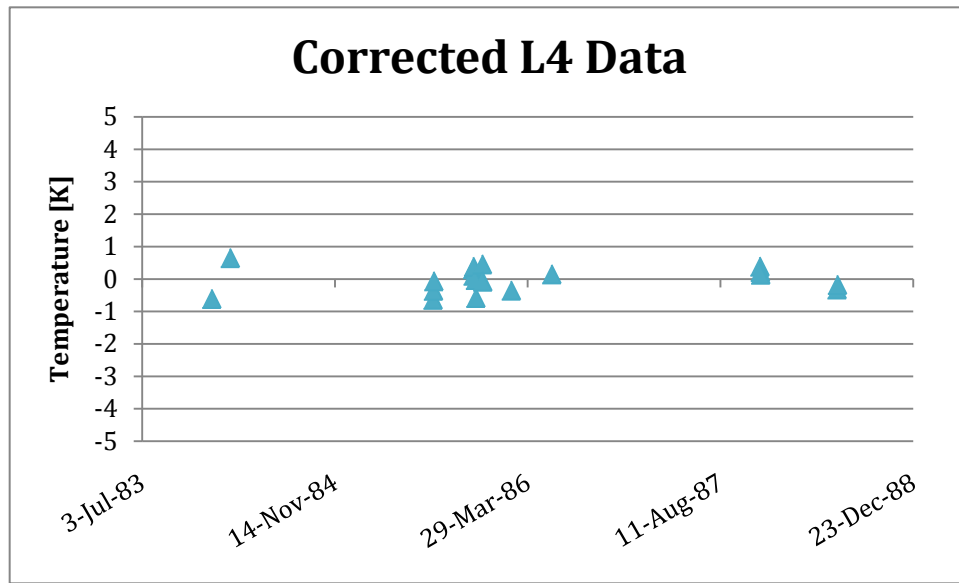
Figure 42. Calibration curve for Landsat 4 TM band 6 post-1987 data after introducing a radiance bias of 0.3935 [W/m^2 sr μm]

As displayed in Figure 42 the new average temperature difference (μ) is 0.17 K and the standard deviation (σ) is 0.38 (See Table 4). Figure 43 shows that the slope of the best-fit line when plotting the predicted at sensor radiance and the imaged derived at sensor radiance is still 1.003, the correlation value (R^2) is 0.97963, and the intercept is 0.0005. This is good evidence that introducing a bias shift to the data has not altered the distribution of the data while driving the RMSE error down to 0.412 K.

84
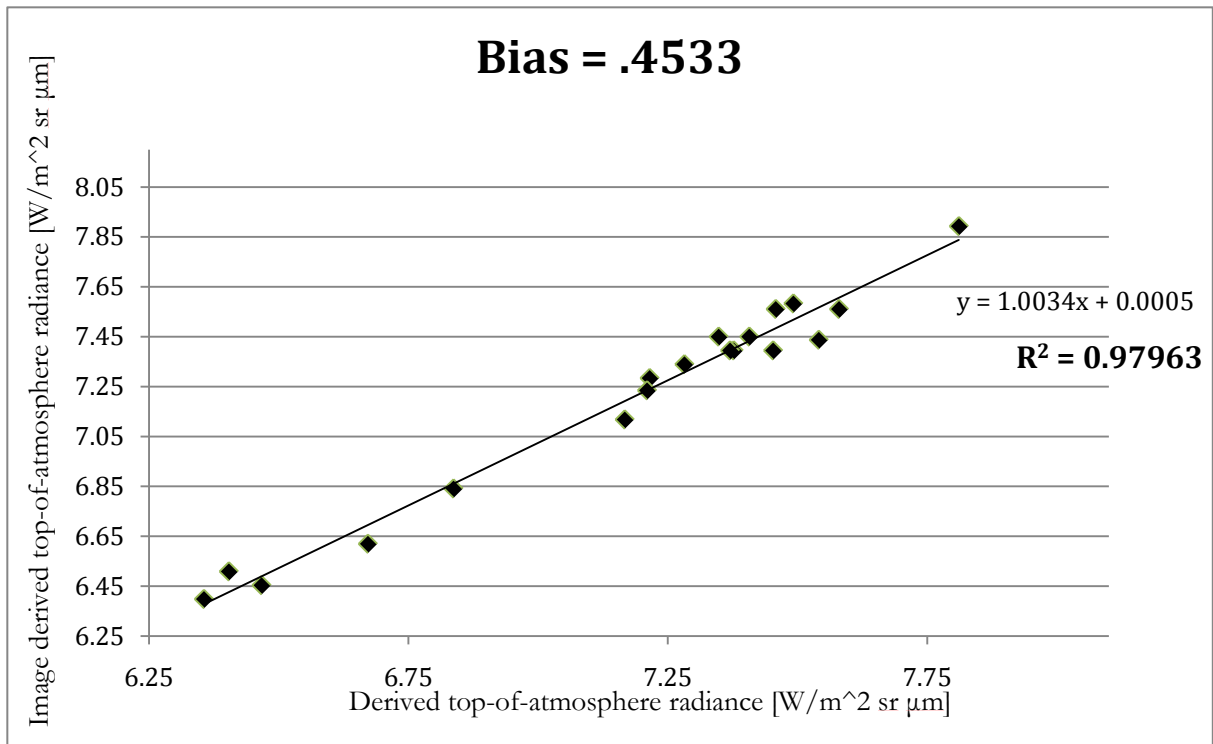
Figure 43. Predicted at sensor radiance and imaged derived top-of-atmosphere radiance with a bias shift of 0.4 [W/m^2 sr μm]

9.4   Correlation

The Landsat 4 post 1987 data was also evaluated to determine if there was a correlation between the air temperature and the bias (difference between sensor reaching and image derived radiance), or the water temperature and the bias. The air temperature had no correlation, but the water temperature did have a small amount of correlation. This slight correlation could be a slight gain issue on the sensor (higher radiance value results in less difference between sensor reaching and image derived radiance values) or could be caused by the skin temperature calculation. Because the same technique for calculating

85

the skin temperature has been proven in the past, a slight gain issue in the sensor is the probable cause for a slight correlation between water temperature and bias. (Appendix D)

9.5   Error Analysis

A complete error analysis drawing on the analysis done by Padula in 2008 was also conducted on the Landsat 4 calibration curve. The analysis consisted of breaking down the entire process into each individual piece, and calculating the error in each piece. Each process overall used Beers method of error propagation, which can be seen in Equation 9.2.

$$S_Y = \left[\left(\frac{\partial Y}{\partial X_1} S_{X_1} \right)^2 + \left(\frac{\partial Y}{\partial X_2} S_{X_2} \right)^2 + ... + \left(\frac{\partial Y}{\partial X_N} S_{X_N} \right)^2 + \sum 2\rho_{ij} \frac{\partial Y}{\partial X_i} \frac{\partial Y}{\partial X_j} S_{X_i} S_{X_j} \right]^{\frac{1}{2}} \qquad (9.2)$$

Where S_Y is the total process error, S_{Xi} is the error in the individual input variables and ρ_{ij} is the correlation coefficient between variables X_i and X_j summed over all combinations of correlated variables (Padula, 2008).

9.5.1   Bulk to skin Temperature Error

The first error analysis to perform was the error in predicting the bulk to skin temperature of the water target. By applying Equation 5.1 to the skin temperature equation derived by Zeng (Equation 2.3) results in Equation 9.3:

86

$$S_{T_s} = \left[\left(\frac{\partial T_s}{\partial T_z} S_{T_z} \right)^2 + \left(\frac{\partial T_s}{\partial a} S_a \right)^2 + \left(\frac{\partial T_s}{\partial z} S_z \right)^2 + \left(\frac{\partial T_s}{\partial d} S_d \right)^2 \right]^{\frac{1}{2}} \tag{9.3}$$

Error Term	Value	Source
S_{Tz} – water temp at depth	0.3 K	Padula 2008
S_a – thermal gradient	0.305 K/m	empirically derived
S_z – measurment depth	0.254 m	Padula 2008
S_d – cool skin effect	0.07 K	Donlon et. Al. (2002)

Table 5: Definition of errors used in Eq. 9.3

Using equation 9.3 the overall error in bulk to skin temperature was 0.39 K. This error was found using the inputs in Table 5 along with: depth of thermistor (z) = 0.6 m (3m discus buoys used in this research), thermal gradient (a) = 0.010769 (using the average wind speed of the data and Eq. 6.4) and cool skin effect (d) = 0.17 K according to (Donlon, 2002).

9.5.2   Atmospheric Error

The second error analysis applied to the process of calibrating Landsat 4 data was to calculate the error in the predicted column of atmosphere above the buoy. The Beers method would again be applied this time to the big equation used for this study (Equation 7.10) resulting in Equation 9.4:

$$S_{Leff} = \left[\begin{array}{l} \left(\dfrac{\partial L_{eff}}{\partial \varepsilon} S_\varepsilon \right)^2 + \left(\dfrac{\partial L_{eff}}{\partial L_{BB}} S_{L_{BB}} \right)^2 + \left(\dfrac{\partial L_{eff}}{\partial L_d} S_{L_d} \right)^2 + \left(\dfrac{\partial L_{eff}}{\partial \tau} S_\tau \right)^2 + \left(\dfrac{\partial L_{eff}}{\partial L_u} S_{L_u} \right)^2 + 2\rho_{\tau,L_u} \dfrac{\partial L_{eff}}{\partial \tau} \dfrac{\partial L_{eff}}{\partial L_u} S_\tau S_{L_u} \\[2mm] + 2\rho_{\tau,L_d} \dfrac{\partial L_{eff}}{\partial \tau} \dfrac{\partial L_{eff}}{\partial L_d} S_\tau S_{L_d} + 2\rho_{L_u,L_d} \dfrac{\partial L_{eff}}{\partial L_u} \dfrac{\partial L_{eff}}{\partial L_d} S_{L_u} S_{L_d} \end{array} \right]^{\frac{1}{2}} \qquad (9.4)$$

$$\frac{\partial L_{eff}}{\partial \varepsilon} = L_{BB}\tau - L_d\tau \qquad \frac{\partial L_{eff}}{\partial L_d} = \tau - \varepsilon\tau$$

$$\frac{\partial L_{eff}}{\partial L_u} = 1$$

$$\frac{\partial L_{eff}}{\partial L_{BB}} = \varepsilon\tau \qquad \frac{\partial L_{eff}}{\partial \tau} = \varepsilon L_{BB} + L_d - \varepsilon L_d$$

S_ε – Error in emissivity of water
S_{LBB} – Error associated with bulk-skin target temperature model
S_τ, S_{Ld}, S_{Lu} – Atmospheric correction terms
$\rho_{\tau,Lu}$, $\rho_{\tau,Ld}$, $\rho_{Lu,Ld}$ – Correlation Values

Table 6: Definition of variables used in Eq. 9.4

    The errors in atmospheric terms in the above equation were calculated by running a Monte Carlo approach. To find the overall process error (S_{Leff}) seven atmospheric cases were chosen (ranging from a cold dry day to a warm moist day) and three target temperatures per atmospheric condition were tested. Using the error terms and Equation 9.4 the overall process error was on average 0.41 K. (Padula, 2008)

9.5.3 Observed Radiance Error

The final calculation to determine the observed radiance error includes adding one last term to the error calculation, which is the instrument induced noise, and can be expressed as:

$$S_m = \left(S_p^2 + S_i^2\right)^{\frac{1}{2}} \tag{9.5}$$

This expression includes S_p, which is the precision of the instrument, and S_i representing the accuracy of the instrument or approach (Schott, 2007). In the case of Landsat 4 this equation can be written as:

$$S_{L_{obs}} = \left[\left(S_{L_{eff}}\right)^2 + \left(S_{L_{ins}}\right)^2\right]^{\frac{1}{2}} \tag{9.6}$$

According to (Barsi J., 2003) the instrument noise (S_{Lins}) expressed in apparent temperature for Landsat 5 ranged from 0.17 K to 0.3 K. Unfortunately the instrument noise for Landsat 4 has not been determined. Because the sensor aboard Landsat 4 is identical to the sensor on Landsat 5, and the same gain and bias have been applied to the historic data for Landsat 4 and Landsat 5, it is safe to assume that the instrument noise on Landsat 4 will be the same (0.17 K to 0.30 K). Using the same conservative number of 0.25 K as (Padula, 2008), the observed radiance error is calculated to be 0.48 K.

Although different buoys were used in the Landsat 4 study, and some were not under ideal wind conditions, a higher error in atmospheric terms would be expected. After the results of Landsat 4, and in particular the low RMSE value, the atmospheric error of 0.41 K and the overall process error of 0.48 K have been accepted as the error in the Landsat 4 data.

9.6 Summary

The physics based approach to calibrating the TM sensor band 6 was applied to both the Landsat 4 and Landsat 5 data sets. The Landsat 5 data was targeted toward a window of

data from 1996-1999. This timeframe was selected based on previous results suggesting an apparent shift in bias. After processing 21 scenes from buoys that are in the water year round, no exact shift in bias can be found. The data appears to be well calibrated ranging in a temperature difference between derived top of atmosphere temperature and image derived temperature of ~ -1 K to ~ 1 K. This data agrees with previous results produced by (Padula, 2008).

The TM sensor band 6 on Landsat 4 was also evaluated using the Physics based approach. This sensor has never been calibrated and because of on orbit issues the spacecraft did not have as much available data. A more extensive search of NOAA buoys resulted in 30 viable scenes to process. The Landsat 4 analysis used 17 different NOAA buoys to gather the 30 ground truth data points needed to complete the calibration, unlike the 5-6 buoys used to calibrate Landsat 5. The overall result produced a calibration curve that suggests the sensor was well calibrated before a 3-year hibernation period starting in 1984, with a significant shift in calibration after returning to operation in 1987. This shift in data can be attributed to a shift in operating temperature of the optics and shutter of the spacecraft. The post 1987 data can be corrected by adding a bias of 0.4533 [W/m^2 sr μm] in Radiance with an error of less than 0.5 K.

9.7   Recommendations/Future Work

9.7.1   Future Landsat 4 Calibration

Results indicate that the Landsat 4 data is steady around the -3.3 K range and with a bias shift can be considered calibrated. The use of multiple buoys has expanded the data points of the curve by three times as much data. Although the NOAA buoys around the

US have been exhausted, the search for international buoys is still incomplete. Future

work in finding viable ocean temperature measurements from either moored buoys or

ships in international water could expand the Landsat 4 calibration curve by hundreds of

data points. As shown in Figure 44 Landsat 4 took many images after the hibernation

period, and as can be seen in Appendix B, most of those images are in international

locations.
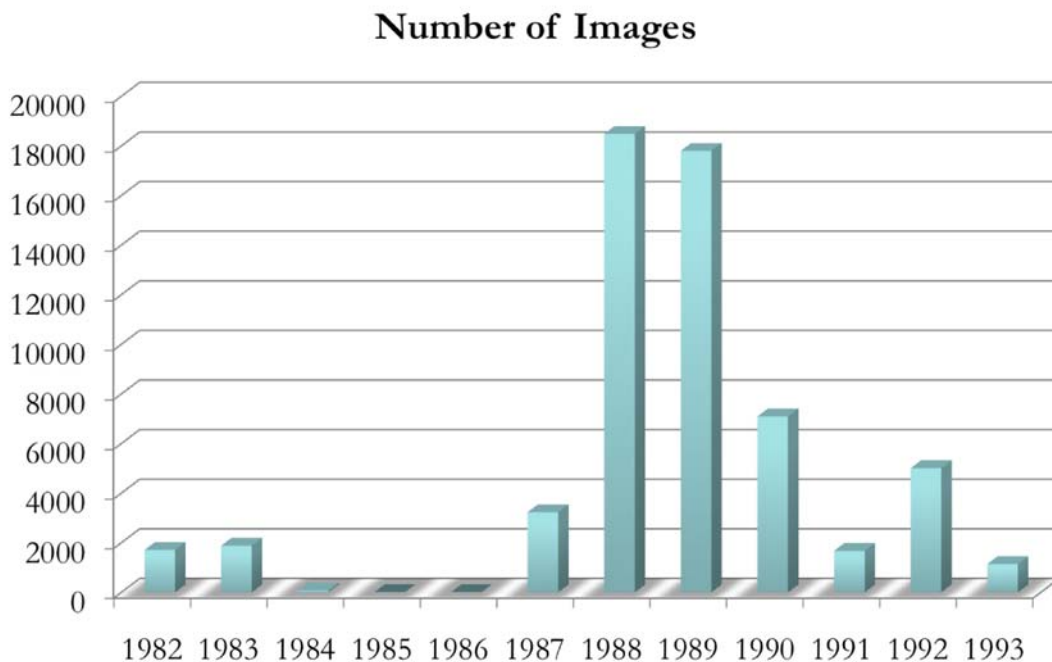
Number of Images

Figure 44. Number of images per year captured by Landsat 4 during the lifetime of the spacecraft

9.7.2 Automated Calibration Process

Calibrating Landsat 4 has further validated the physics based approach to a vicarious

calibration of a spacecraft sensor. This work has tested the limits on how accurate input

parameters are needed to attain a reasonable data point. This research has proven that

multiple locations can be used, Radiosonde data from further distances to the buoy are

still accurate enough, and also prevailing winds that do not carry the Radiosonde device directly over the ground truth buoy will still provide valid data points.

The next step in expanding the physics based approach is to automate the system. This task should be possible based on the fact that all of the supporting data, including the Landsat images, are readily available data on the Internet. With the proper computer coding, a Landsat image could be deemed good (no cloud cover) over a specific location. Once the scene is deemed useable, the program could then go to the NDBC site and download the historic buoy data for that date and location. The next program could then go to the global surface weather site and download the weather data for the specific day from the nearest weather station. Lastly the Radiosonde data would also be collected from the closest launch site.

Once all of the data are automatically collected from the Internet it would be fed into an IDL program that would then run the programs already created to calculate the Image Derived radiance, and the top of atmosphere derived radiance from the ground truth buoy measurement.

The convenience of an automated process, along with using multiple buoys from multiple locations allows the calibration of the sensor to occur in a matter of days rather than months. Just using the buoys around the US and a sixteen-day revisit time, the automated system could collect multiple images per month, resulting in a calibration curve of 30-40 points being created within the first few years of a satellite being launched. Also the automatic process allows near real time additions to the calibration curve allowing operators to discover bias or gain issues the data may encounter.

Calibrating a sensor directly after launch, and having the ability to update the calibration near real time using the automated process would provide a better calibration record than the methods used in the past.

10   Bibliography

Barsi J., S. J. (2003). Landsat TM and ETM+ thermal band calibration. *Canada Journal of Remote Sensing , 29*, 141-153.

Barsi, J. A. (2000). *MISI and Landsat ETM+: Thermal Calibration and Atmospheric Correction.* Rochester Institute of Technology, Imaging Science. Rochester: CIS.

Berk A., A. G.-G. (1999). Modtran4 Radiative Transfer Modeling for Atmospheric Correction. *Optical Spectroscopic Techniques and Instrumentation for Atmospheric and Space Research III , 3756*, 348-353.

Donlon, C. e. (2002). Toward Improved Validation of Satellite Sea Surface Skin Temperature Measurements for Climate Research. *Journal of Climate , 15*, 353-369.

ENWS. (2001, 05 15). *Radiosonde Observations-Factsheet*. Retrieved 8 9, 2009 from Radiosonde Observations-Factsheet: http://www.erh.noaa.gov/er/gyx/weather_balloons.htm

EOI. (2009, 12 17). *Electro Optical Industries, Inc*. Retrieved 11 20, 209 from Electro Optical Industries, Inc: http://www.electro-optical.com/

NCDC. (2009, 12 15). *National Climatic Data Center*. Retrieved 10 2, 2009 from National Climatic Data Center: http://gis.ncdc.noaa.gov/website/ims-cdo/sod/viewer.htm

NDBC, N. O. (2008, 11 24). *National Data Buoy Center (NDBC)*. Retrieved 12 17, 2009 from NDBC: http://www.ndbc.noaa.gov/rmd.shtml

NWS. (2009, 1 13). *Maps of the NWS Rawinsonde network*. Retrieved 8 5, 2009 from Maps of the NWS Rawinsonde network: http://www.ua.nws.noaa.gov/nws_upper.htm

Padula, F. P. (2008). *Historic Thermal Calibration of Landsat 5 TM through an Improved Physics Based Approach.* Rochester Institute of Technology, Imaging Science. Rochester: CIS.

Planck, M. (1901). *Annalen der Physik* (Vol. 4).

Radiosonde. (2009, 12 17). *Radiosonde*. Retrieved 8 1, 2009 from Radiosonde: http://web.mit.edu/~jonmosk/www/wx/radiosonde.jpg

Radiosonde2. (2009, 12 17). *Radiosonde 2*. Retrieved 8 1, 2009 from Radiosonde 2: http://www.me.upenn.edu/undergrad/images/RadiosondeRecovery_001.jpg

Schott, J. R. (2007). *Remote Sensing: An Image Chain Approach.* Rochester, Ny: Oxford.

Schott, J. R. (1985). Thematic mapper thermal infrared calibration. *Photogrammetric Engineering and Remote Sensing , 51*.

Sospedra, F. C. (1998). Effective wavenumber for thermal infrared bands-Application to Landsat-TM. *International Journal of Remote Sensing , 19* (11), 2105-2117.

Tonooka, H. e. (2005). Vicarious Calibration of ASTER Thermal Infrared Bands. *IEEE Transactions on Geoscience and Remote Sensing , 43* (12), 2733-2746.

USGS. (2007, 10 27). *Earth Explorer*. Retrieved 09 01, 2009 from Earth Explorer: http://edcsns17.cr.usgs.gov/EarthExplorer/

USGS. (2009, 11 18). *Global Visualization Viewer*. Retrieved 9 5, 2009 from Global Visualization Viewer: http://glovis.usgs.gov/

USGS. (2009, 12 17). *Landsat Mission*. Retrieved 8 1, 2009 from Landsat Mission: http://landsat.usgs.gov/about_landsat4.php

USGS. (2009, 12 09). *The Landsat Program-History*. (L. Rocchio, Producer) Retrieved 8 1, 2009 from USGS: http://landsat.gsfc.nasa.gov/about/timeline.html

Wallace, J. a. (1977). *Atmospheric Science An Introductory Survey.* New York: Academic Press.

Zeng, X. e. (1999). A multiyear hourly sea surface skin temperature data set derived from the TOGA TAO bulk temperature and wind speed over the tropical Pacific. *Journal of Geophysical Research , 104* (C1), 1525-1536.

11 Appendix A – Landsat 4 Scenes/Radiosonde profiles

20 Nov 82
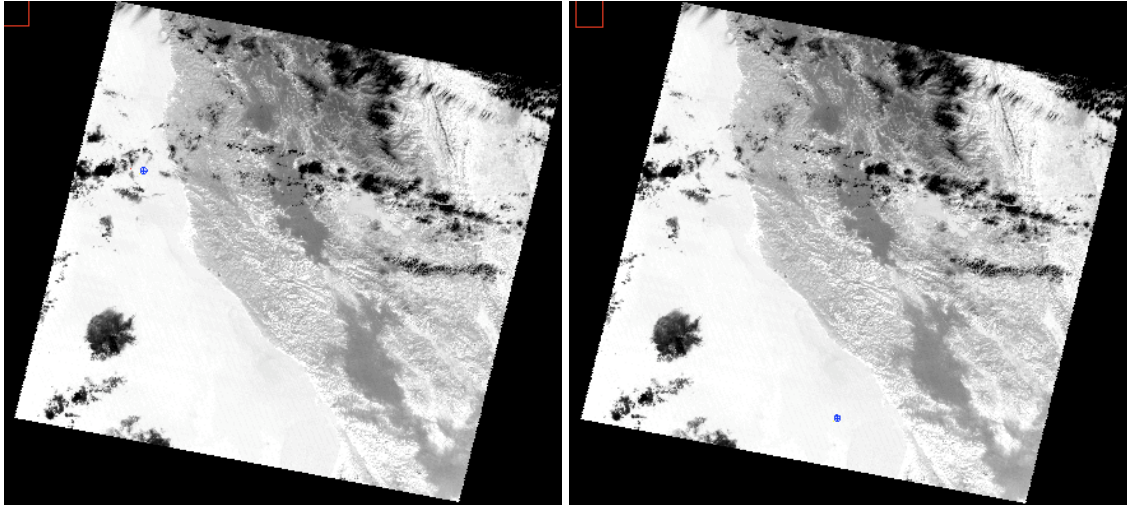
Thermal Image for Buoy 46014 (left) and Buoy 46013 (right)
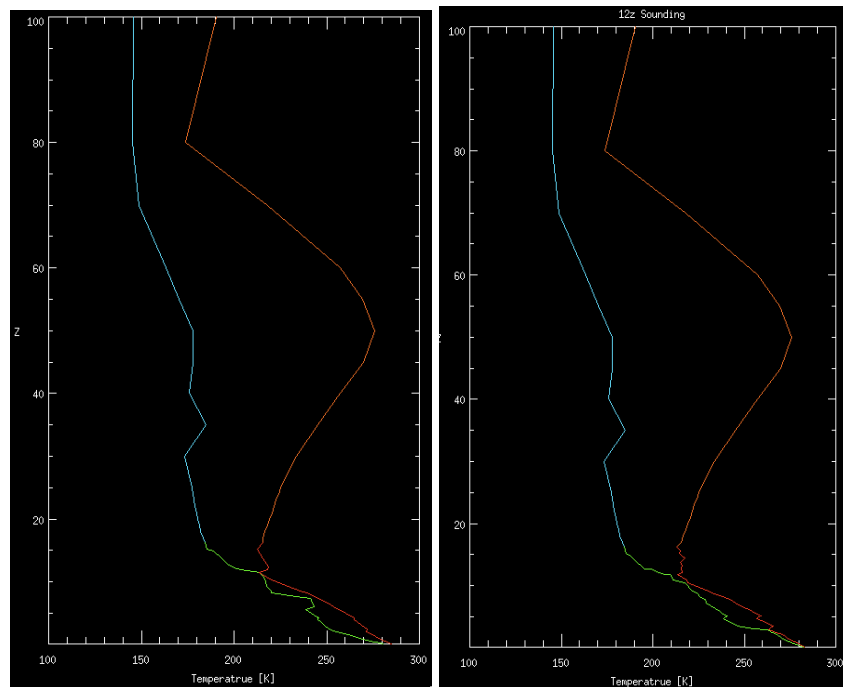
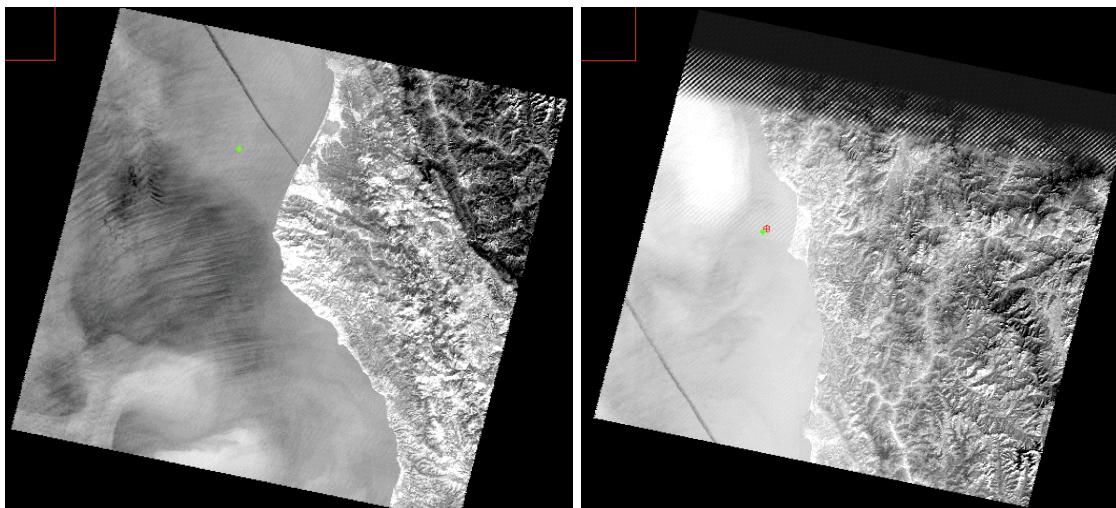Radiosonde Profile for Buoy 46014 (left) and Buoy 46013 (right)
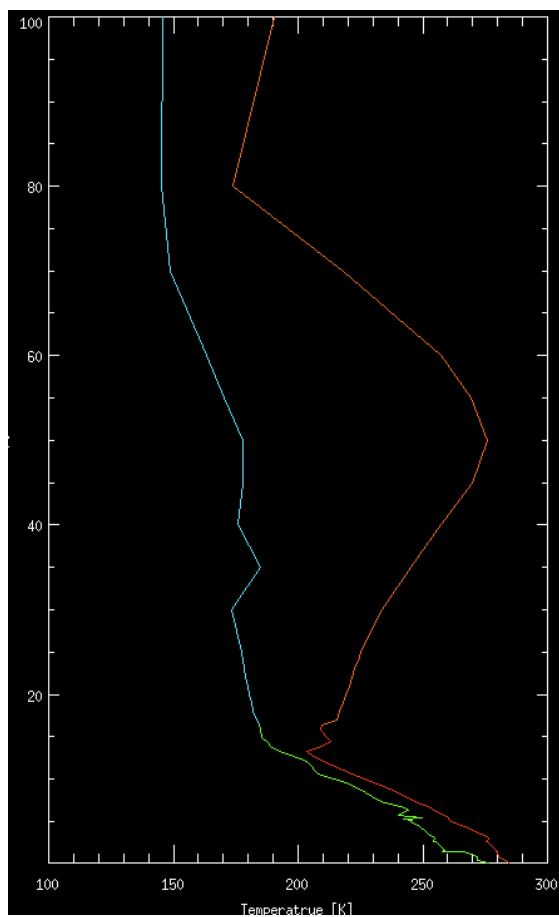
24 Nov 82
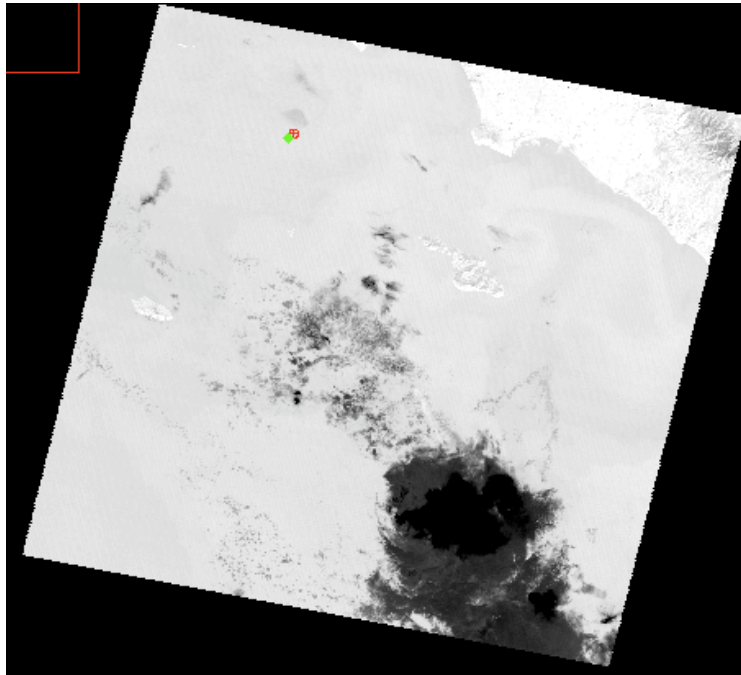
Thermal Image for Buoy 46025
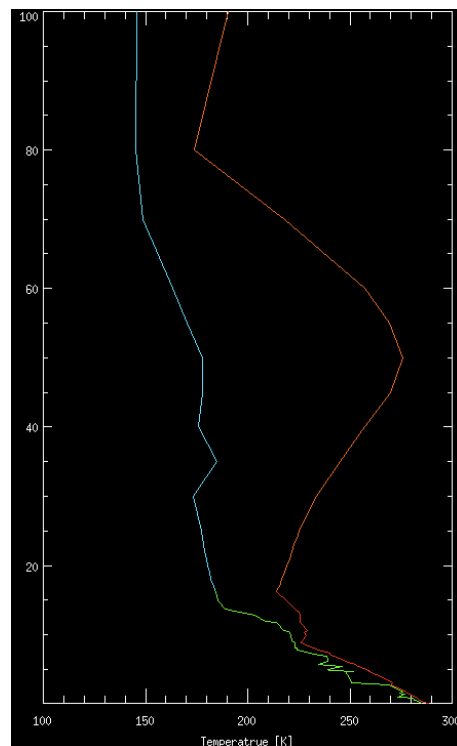
Radiosonde Profile

8 Dec 82
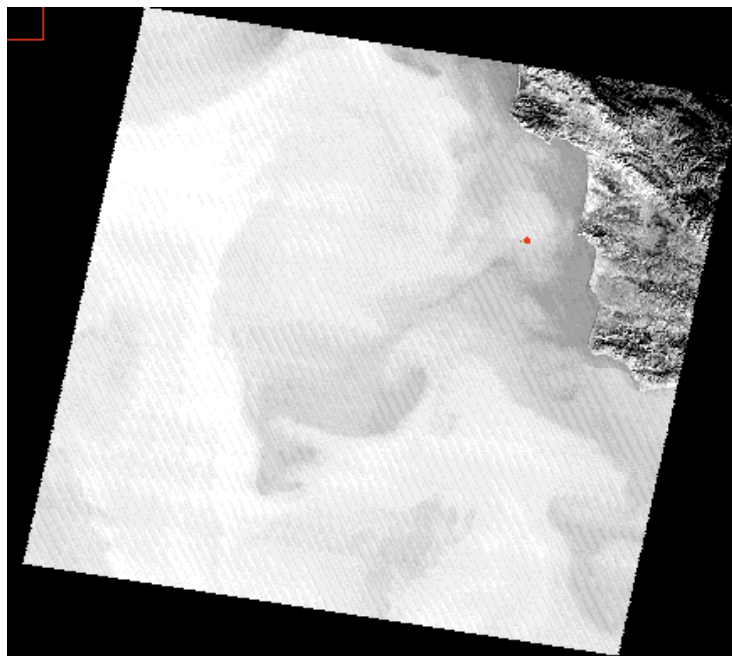
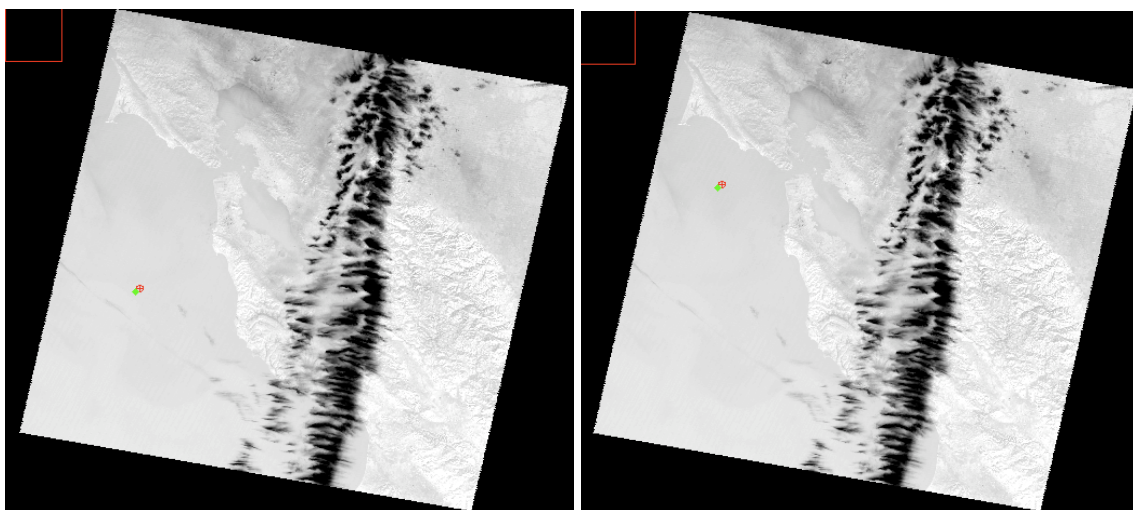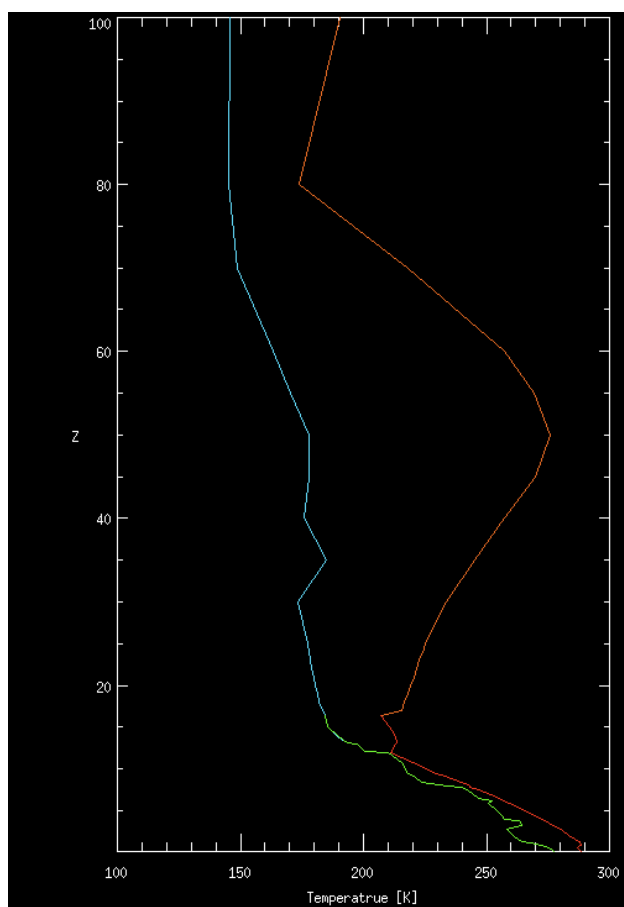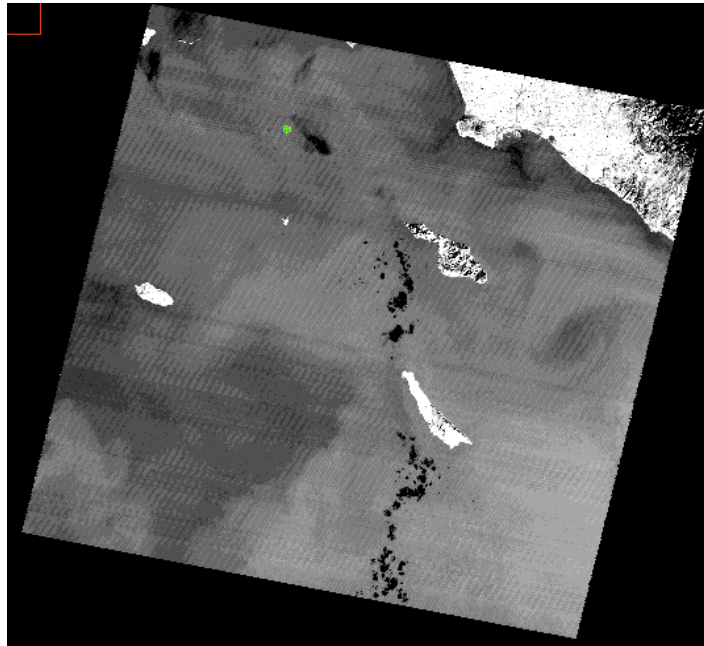Thermal Image
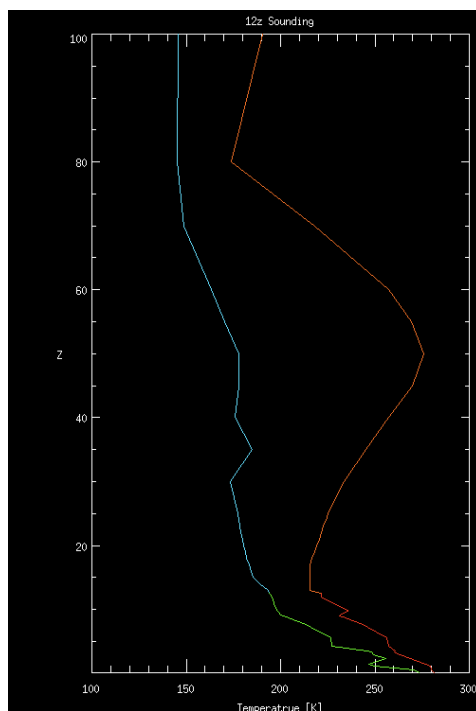
Radiosonde Profile

31 Dec 82
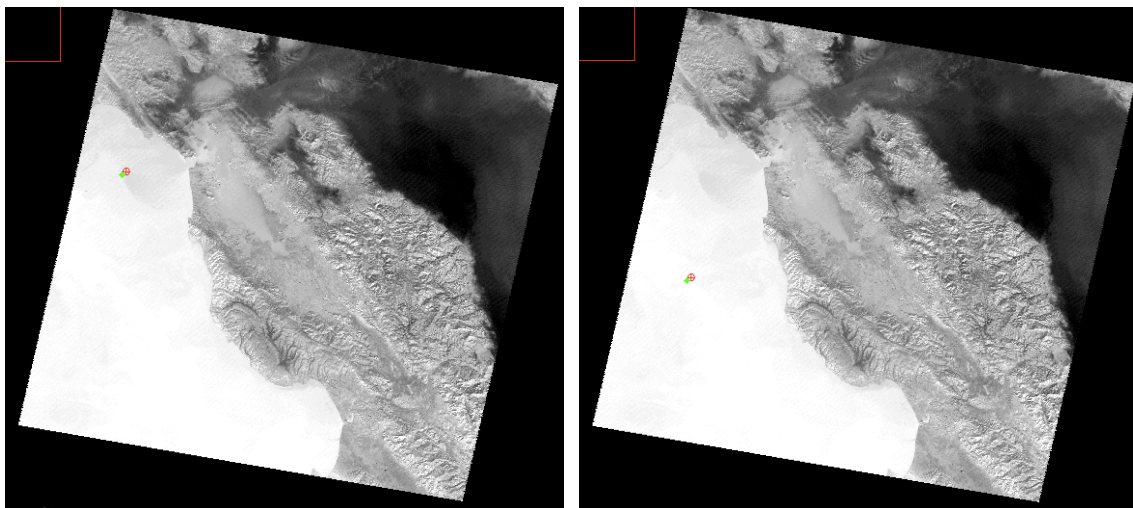
Thermal Images for Buoy 46026 (left) and Buoy 46012 (right)
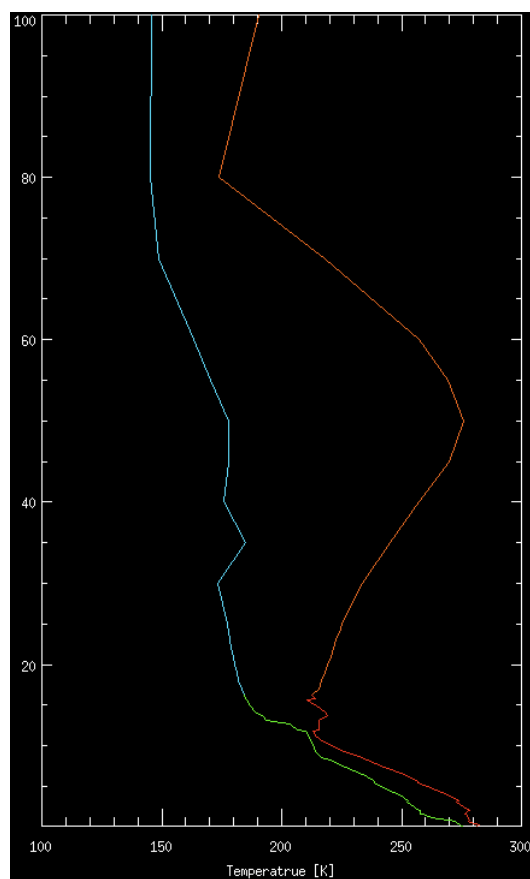
Radiosonde Profile

9 Jan 83
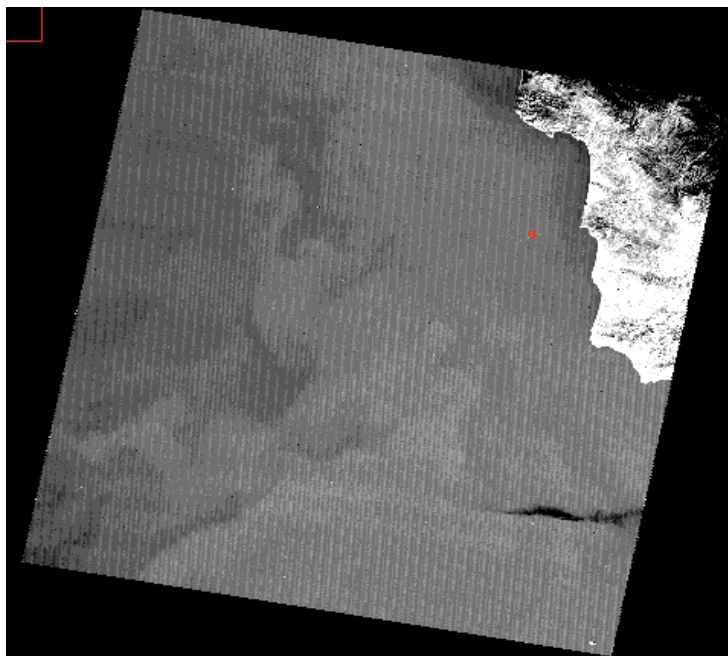
Thermal Image for Buoy 46011
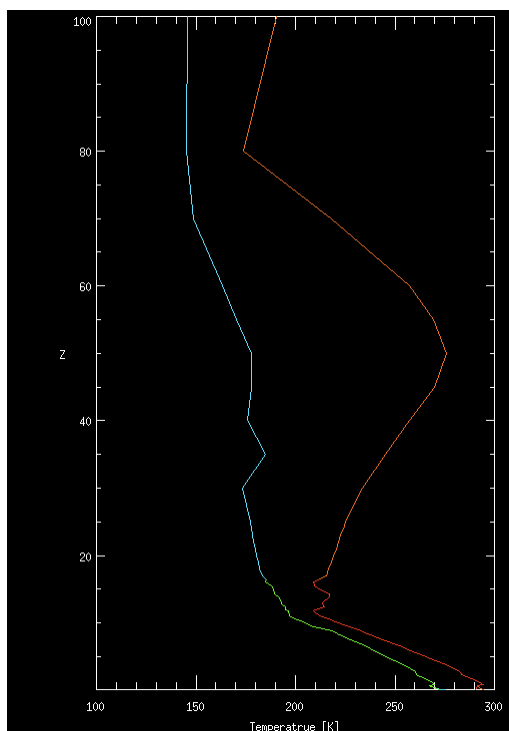
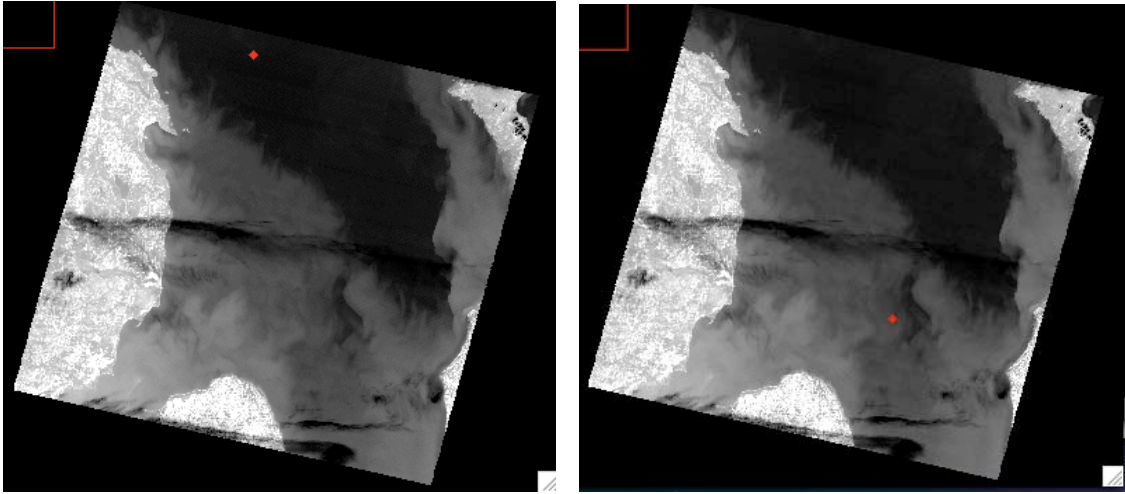Radiosonde Profile

15 Jan 83
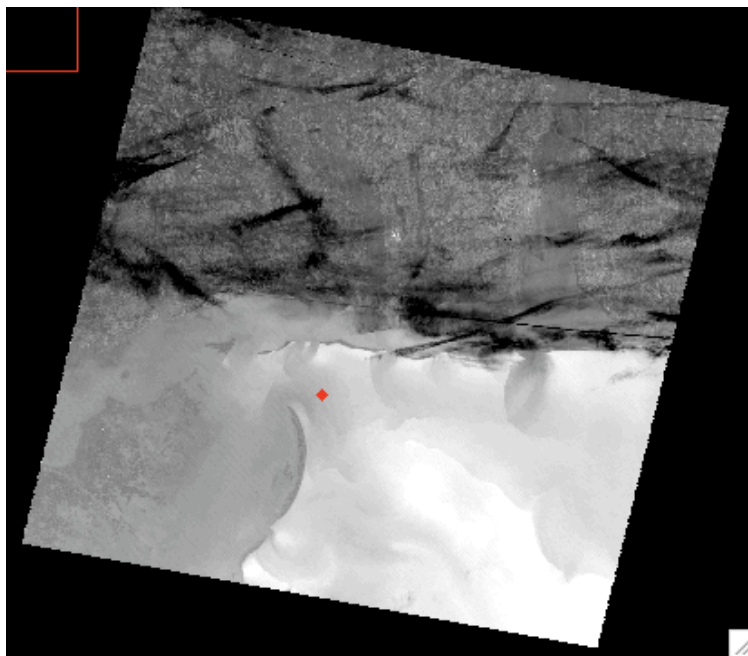
Thermal Image for Buoy 42007
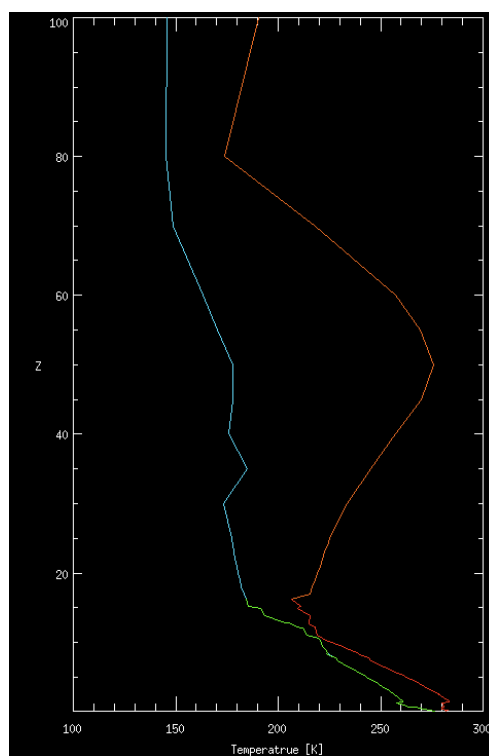
Radiosonde Profile

31 Dec 87
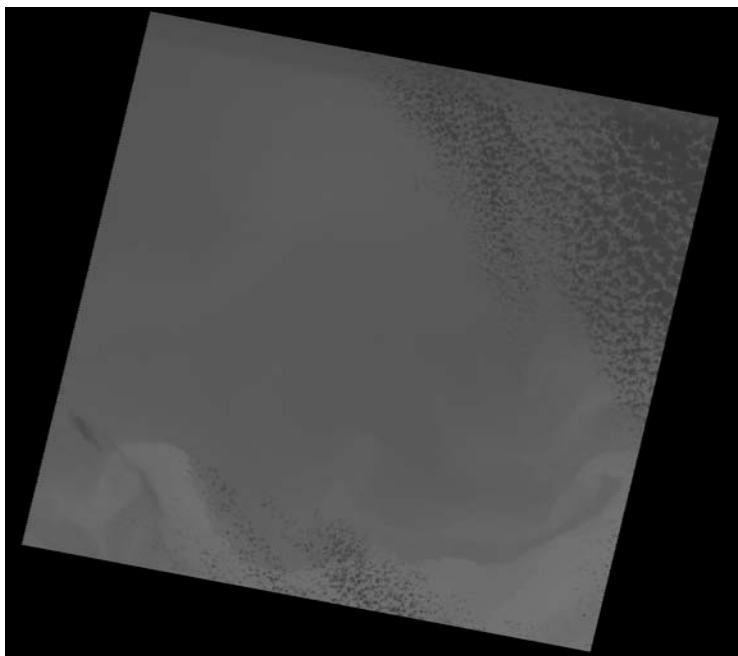
Thermal Image for Buoy 44008
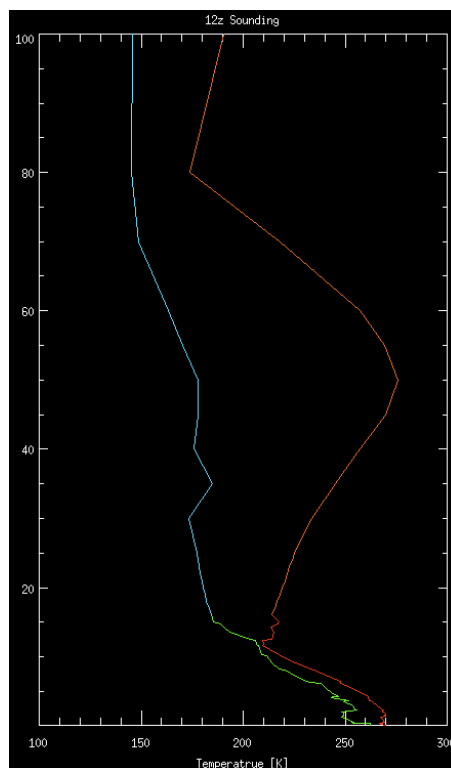
Radiosonde Profile

17 Feb 88
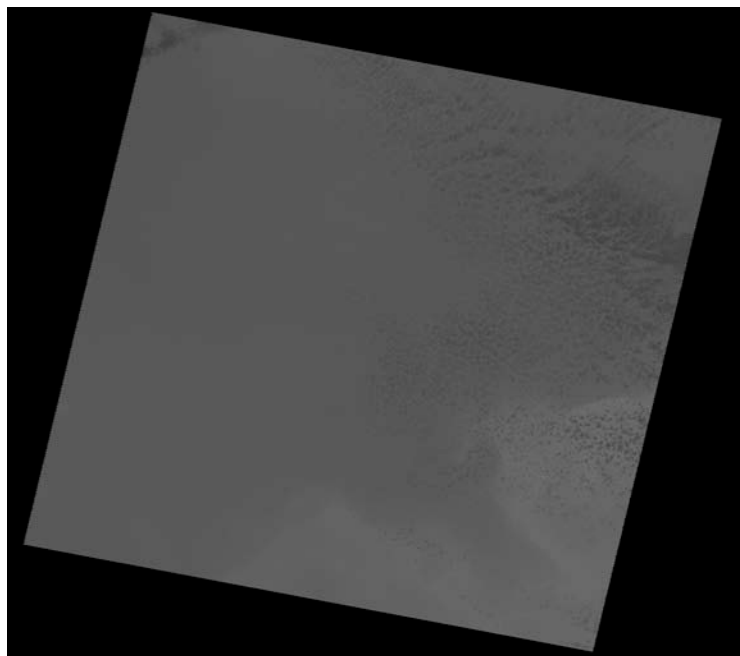
Thermal Image for Buoy 44008
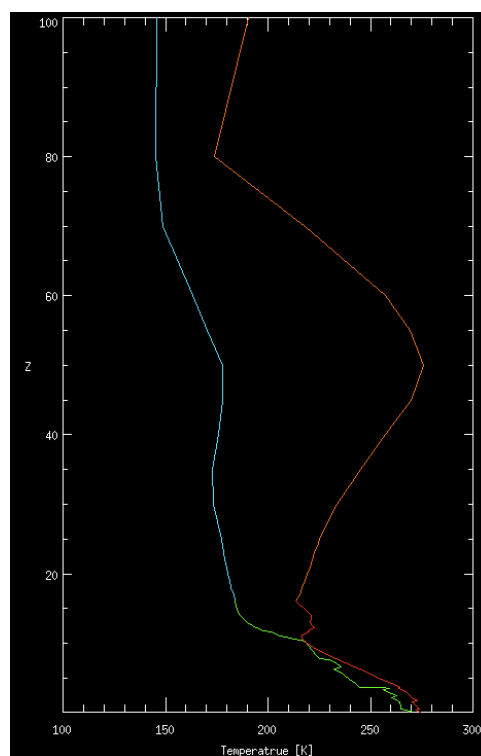
Radiosonde Profile

27 Jul 89
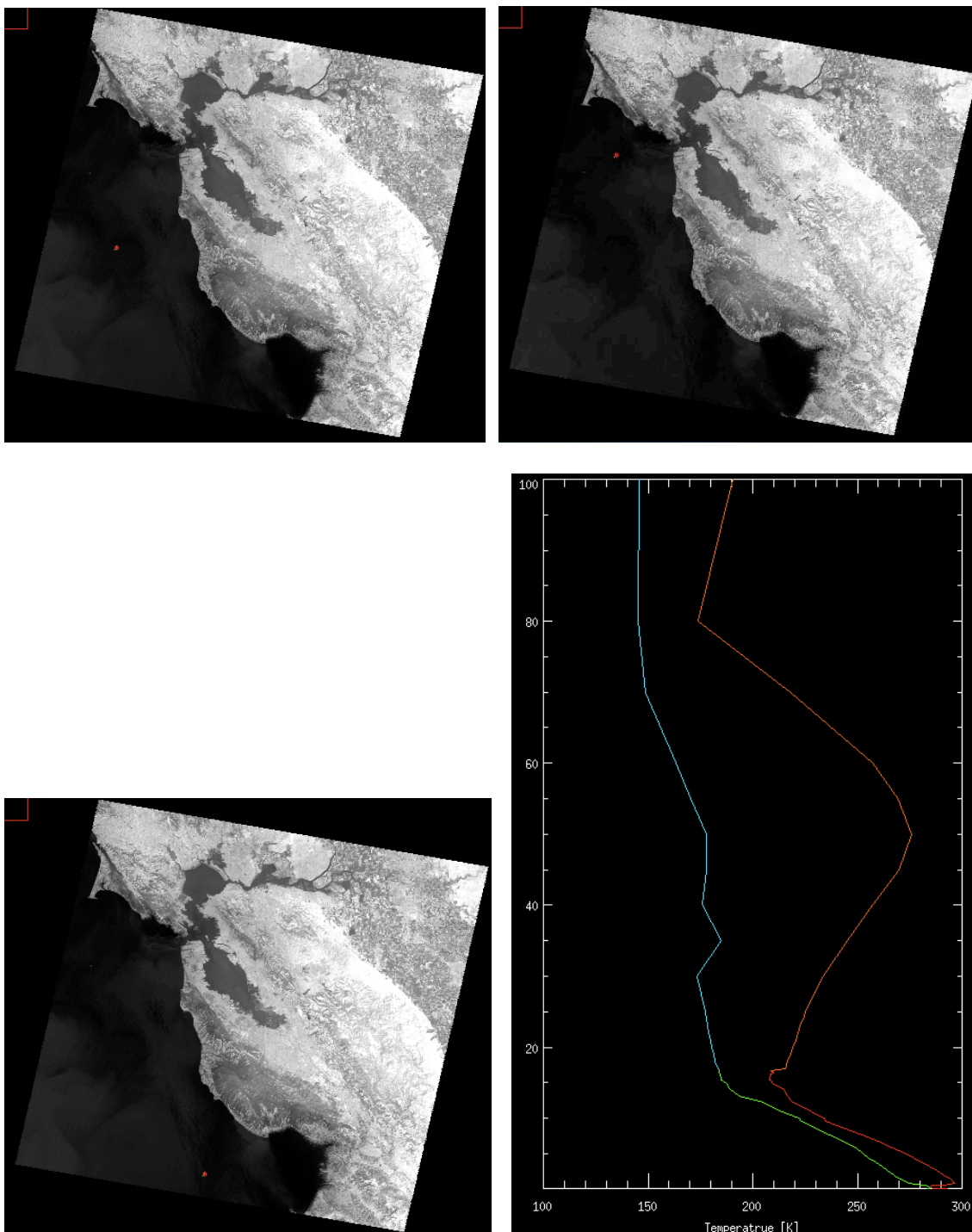
Thermal Image for Buoy 46012 (top left), Buoy 46026 (top right), Buoy 46042 (bottom
left) and Radiosonde Profile (bottom right)

7 Nov 89
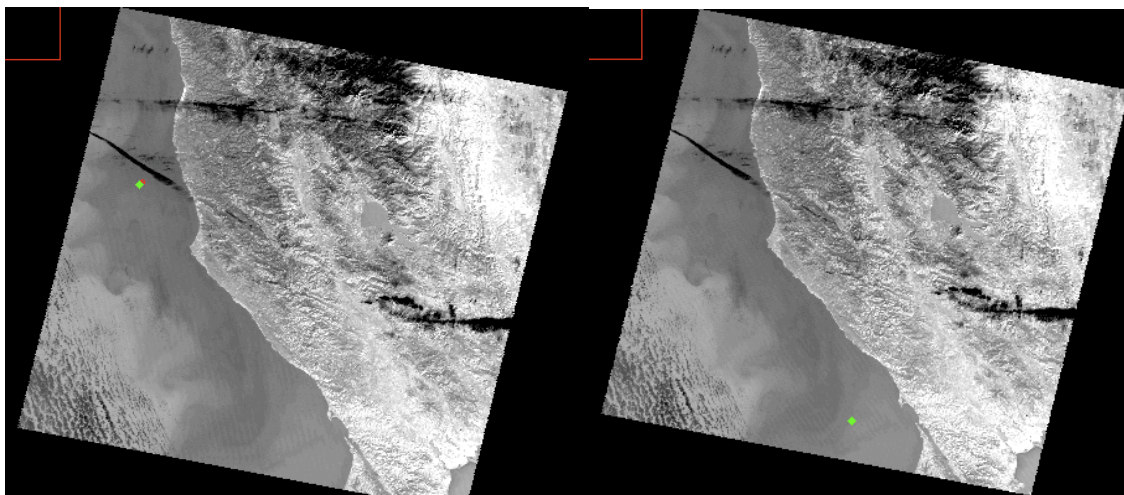

Thermal Image for Buoy 46014 (left) and Buoy 46013 (right)
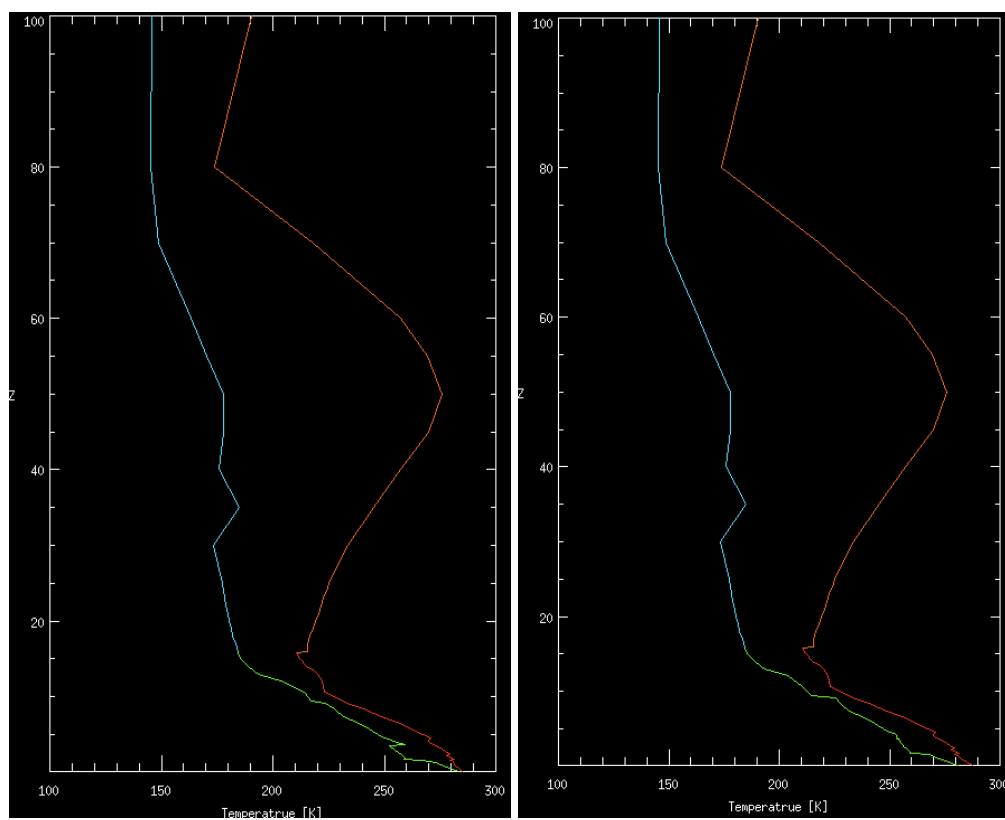
Radiosonde Profile for Buoy 46014(left) and Buoy 46013 (right)

9 Nov 89
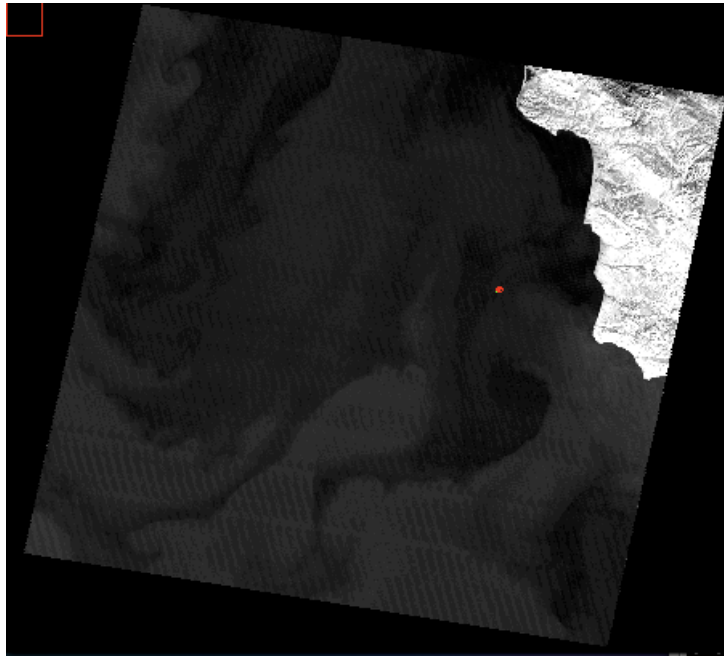
Thermal Image for Buoy 46023
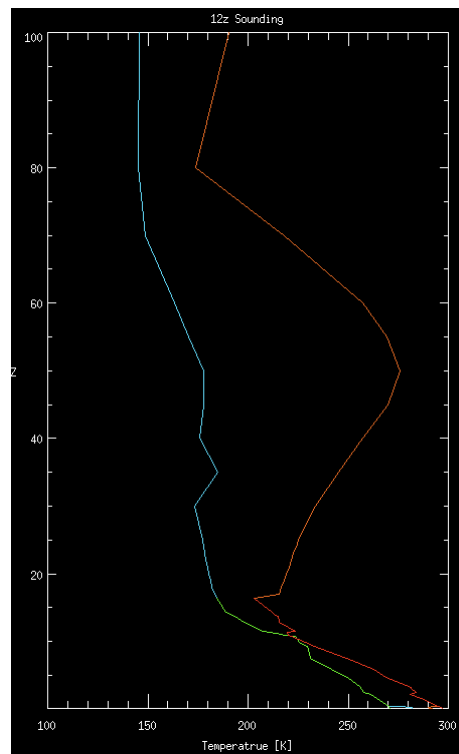
Radiosonde Profile

14 Nov 89

Thermal Image for Buoy 46022 (left) and Buoy 46027 (right)

Radiodsonde Profile

2 Dec 89

Thermal Image for Buoy 46012 (left) and Buoy 46026 (right)

Radiosonde Profile

15 Feb 90

Thermal Image for Buoy 46025
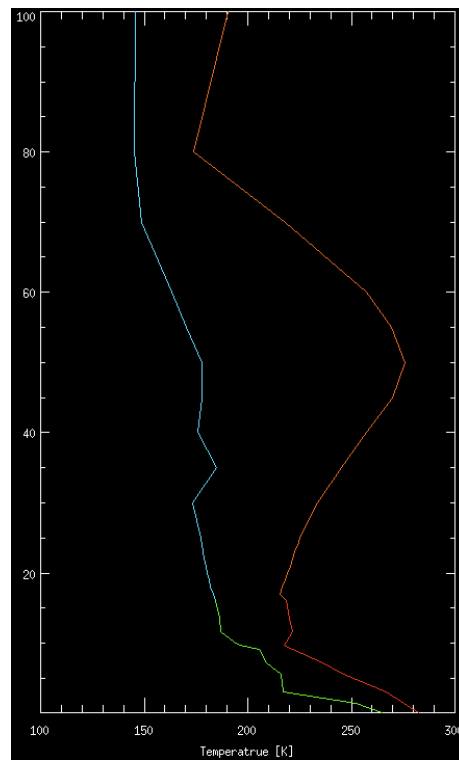
Radiosonde Profile

31 May 90
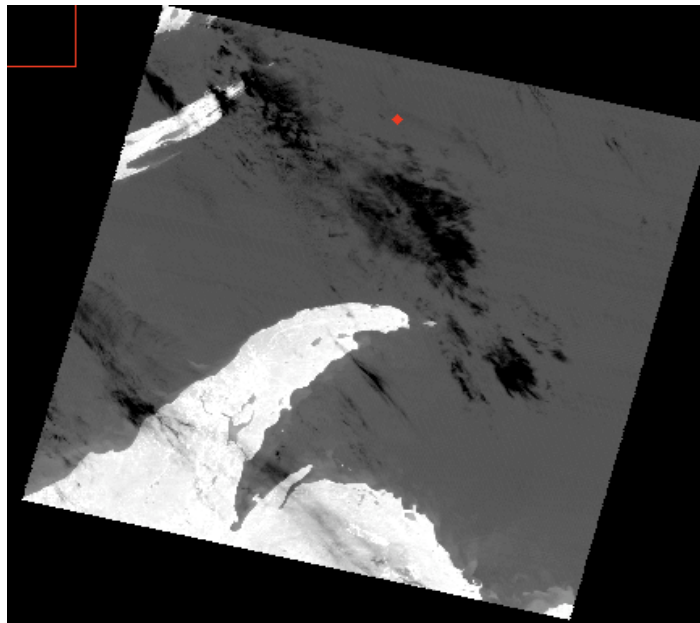
Thermal Image for Buoy 45001
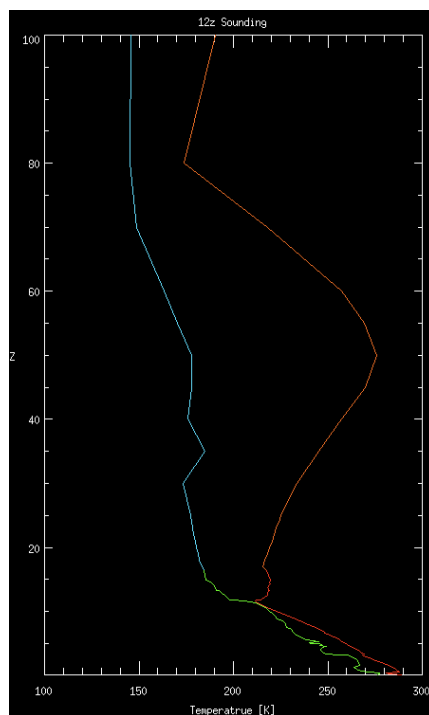
Radiosonde Profile

22 Nov 91
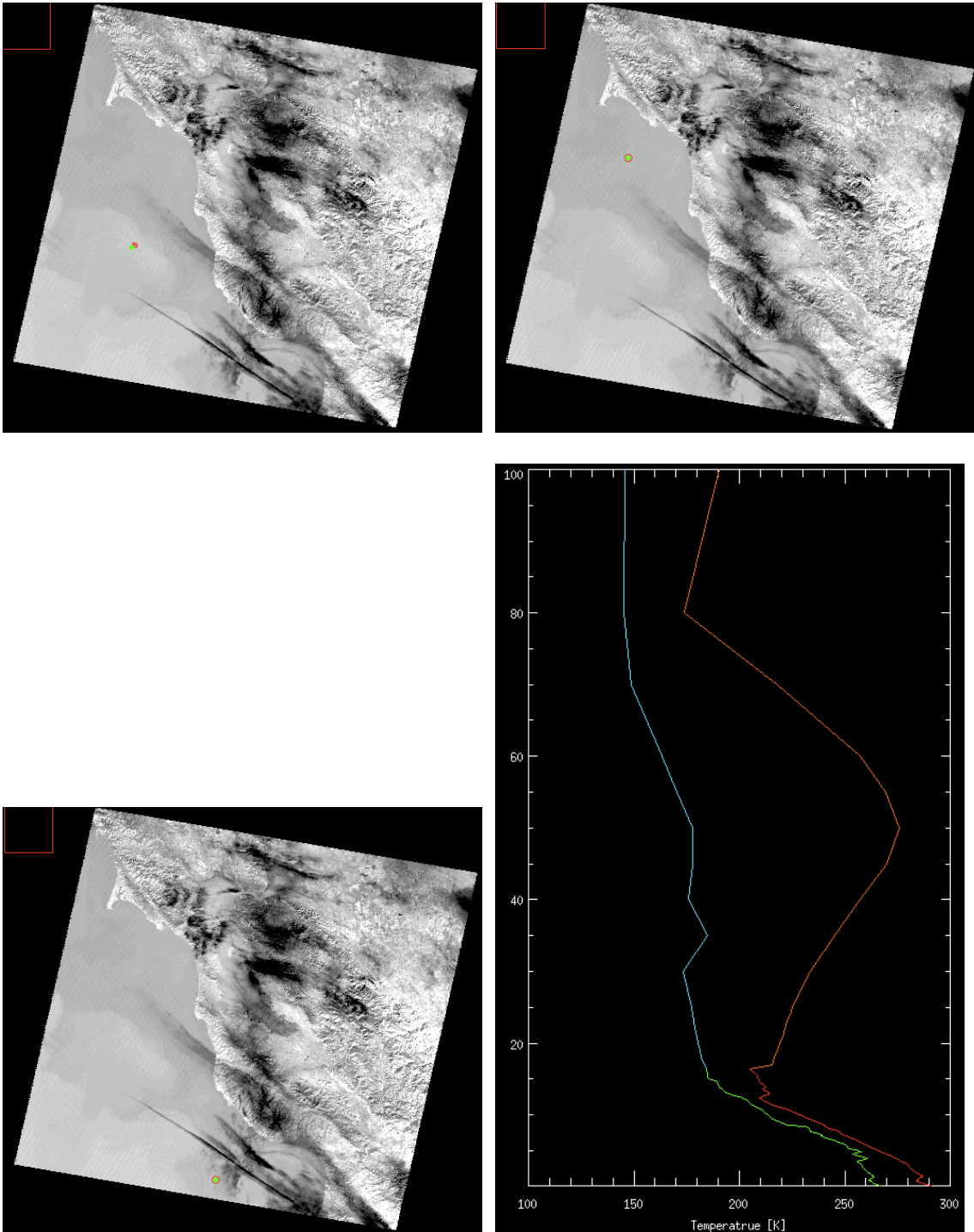
Thermal Images for Buoy 46012 (top left), Buoy 46026 (top right), Buoy 46042 (bottom left) and Radiosonde Profile (bottom right)

9 Jun 92

Thermal Image for Buoy 45003 (left) and Buoy 45008 (right)
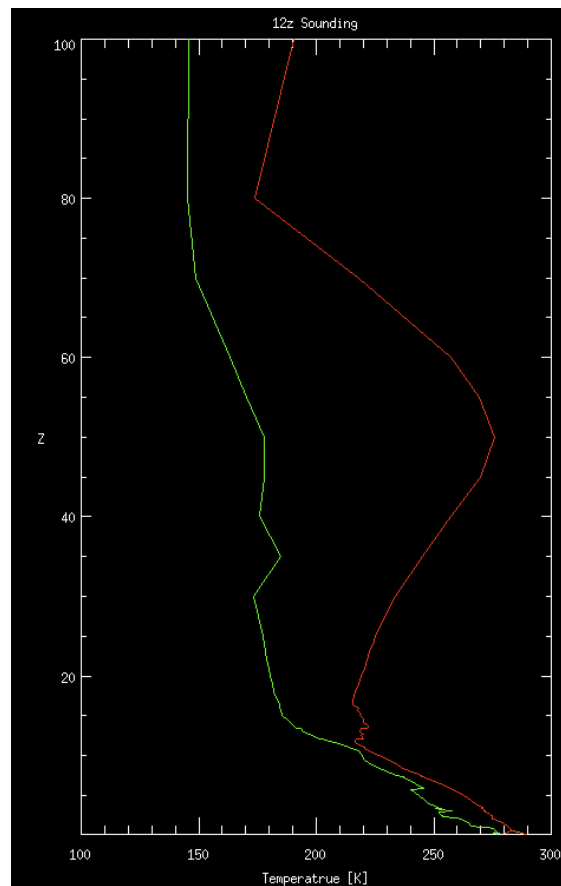
Radiosonde Profile

12 Appendix B – Landsat 4 Land coverage by year
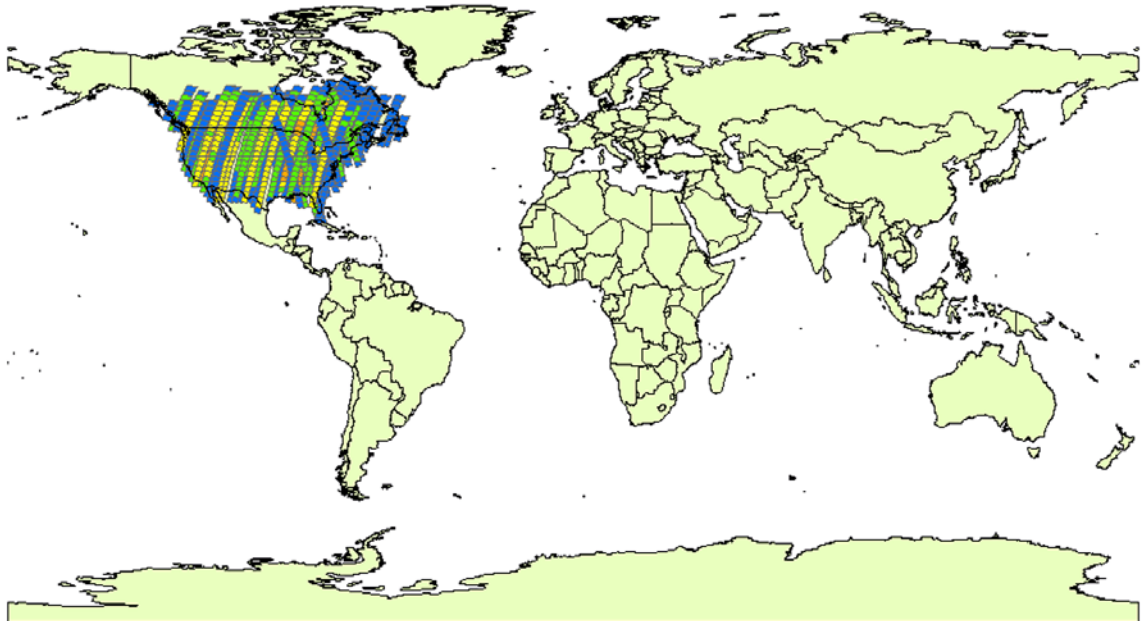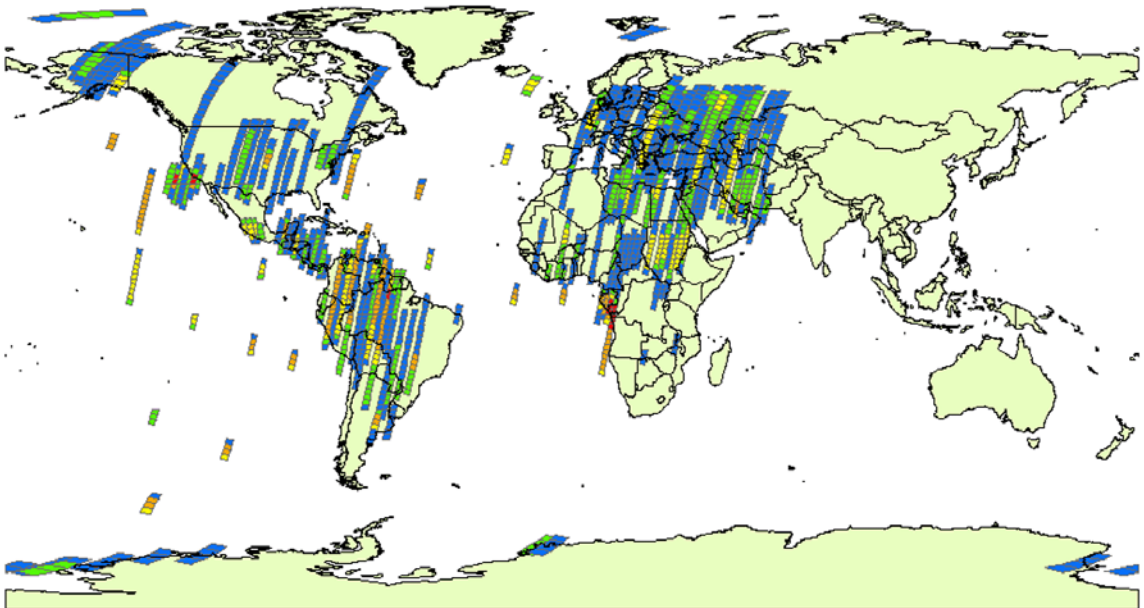

TM L4 1982
Total Marketable Scenes: 1,704
Unique Marketable Locations: 990

■ 1 ■ 2 □ 3 ■ 4
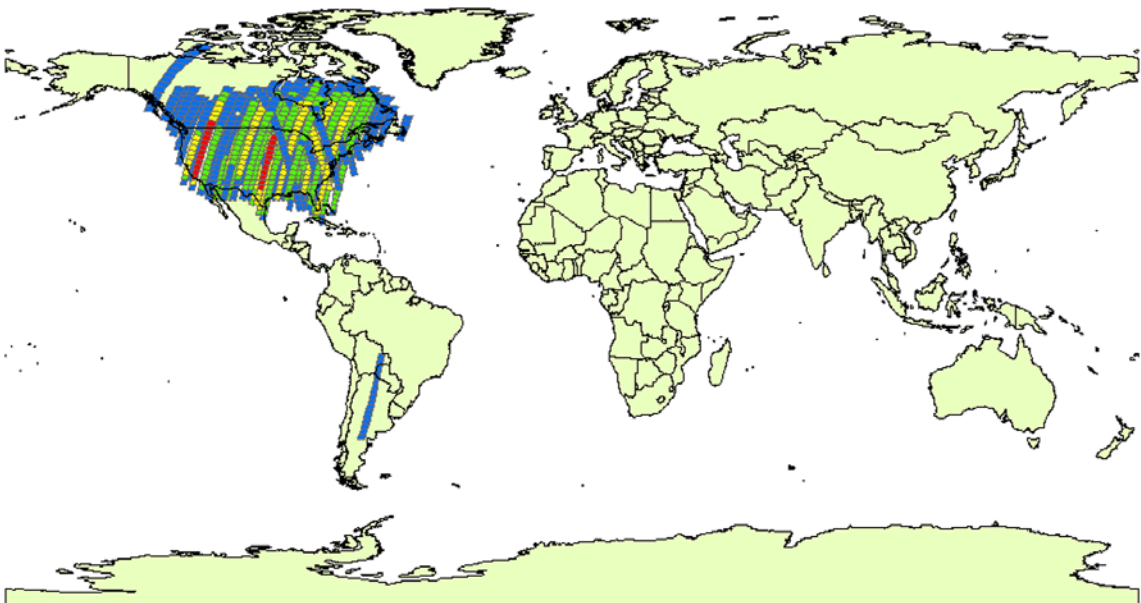
TM L4 1983
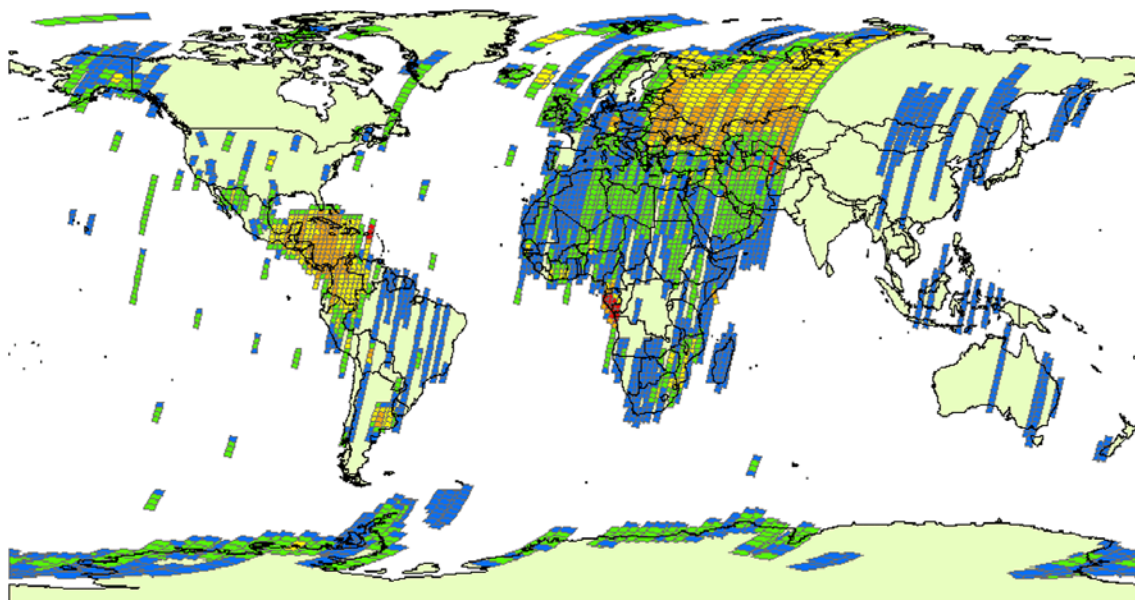Total Marketable Scenes: 1,875
Unique Marketable Locations: 1,126

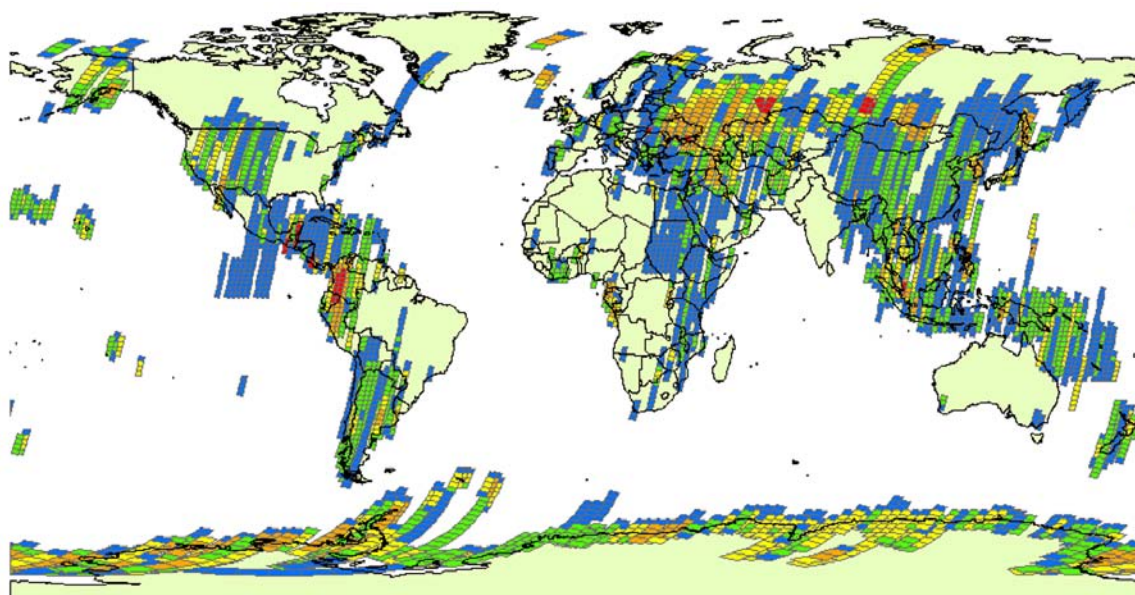■ 1 ■ 2 □ 3 ■ 4

TM L4 1984
Total Marketable Scenes: 69
Unique Marketable Locations: 69

█ 1

TM L4 1987
Total Marketable Scenes: 3,228
Unique Marketable Locations: 1,942
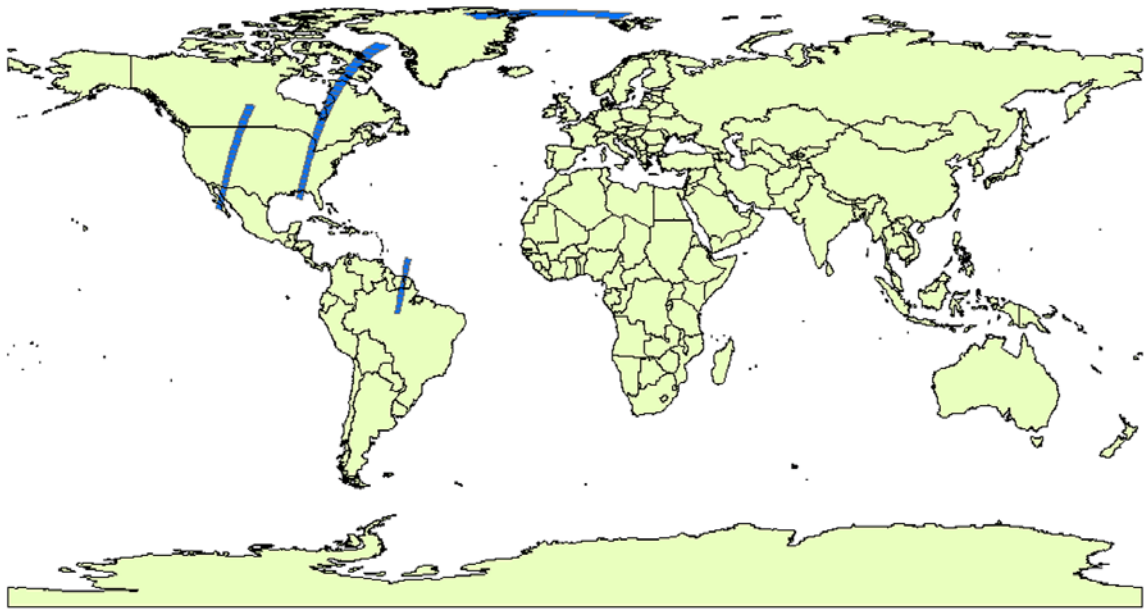
█ 1 █ 2 █ 3 █ 4 █ 5

TM L4 1988
Total Marketable Scenes: 18,479
Unique Marketable Locations: 4,380

1 - 2	3 - 6	7 - 10	11 - 16	17 - 23

TM L4 1989
Total Marketable Scenes: 17,796
Unique Marketable Locations: 5,129

1 - 2	3 - 4	5 - 7	8 - 12	13 - 20
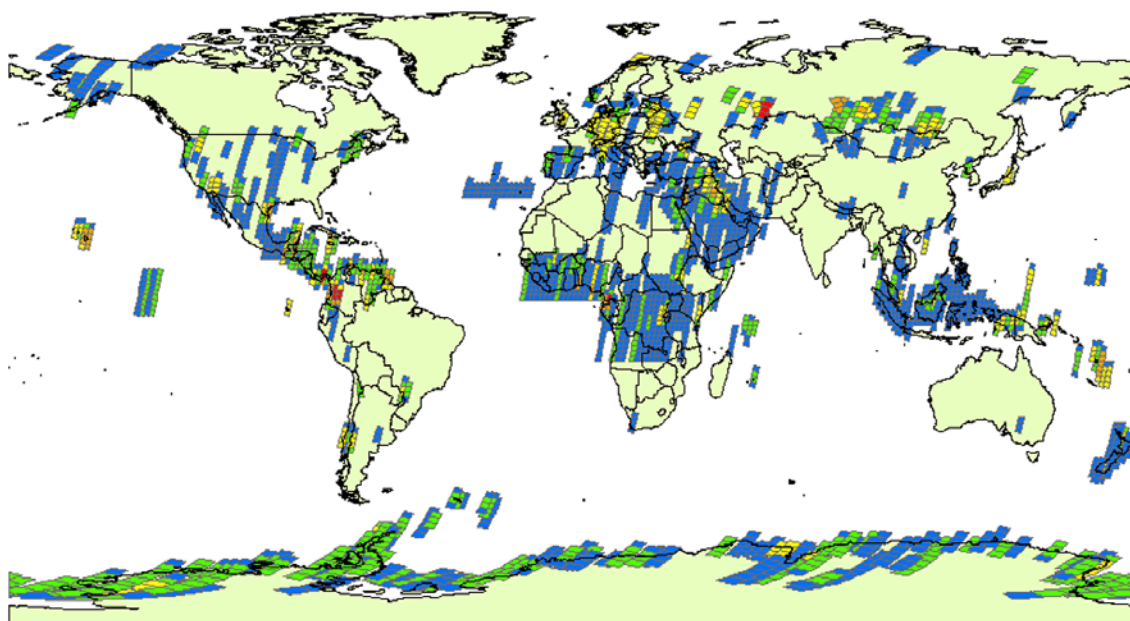
TM L4 1990
Total Marketable Scenes: 7,087
Unique Marketable Locations: 2,602

| | 1 - 2 | | 3 - 4 | | 5 - 8 | | 9 - 13 | | 14 - 20 |
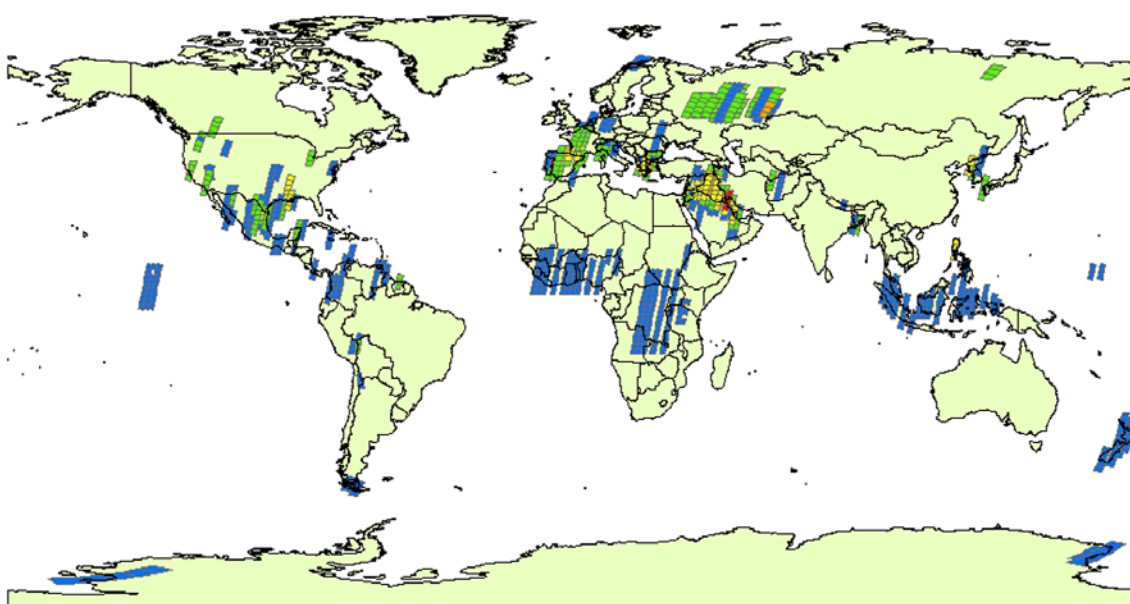
TM L4 1991
Total Marketable Scenes: 1,667
Unique Marketable Locations: 922

| | 1 | | 2 - 3 | | 4 - 6 | | 7 - 10 | | 11 - 15 |
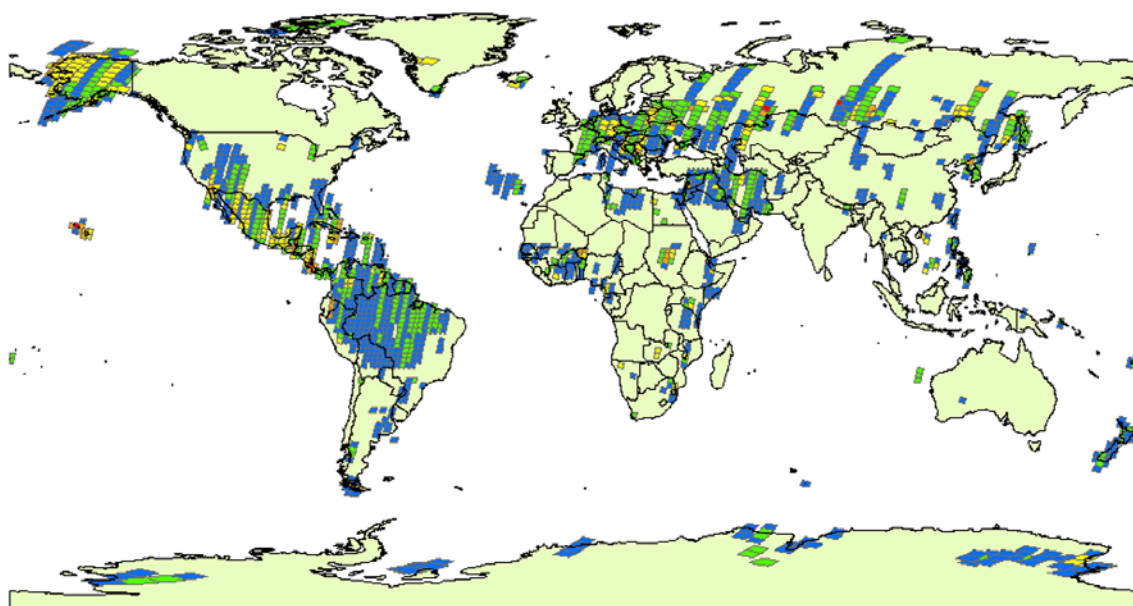
TM L4 1992
Total Marketable Scenes: 4,999
Unique Marketable Locations: 1,833

	1 - 2		3 - 4		5 - 6		7 - 10		11 - 15
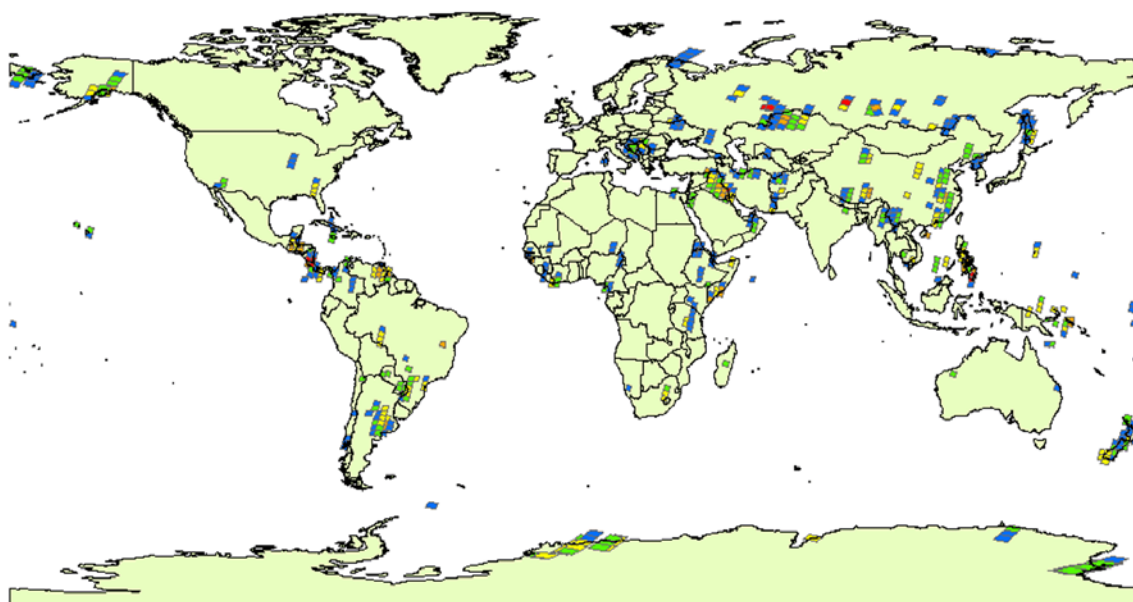
TM L4 1993
Total Marketable Scenes: 1,136
Unique Marketable Locations: 525

	1		2		3 - 4		5 - 6		7 - 8

13 Appendix C – Landsat 5 Seasonal Variation Study

Bias Temperature vs Date
[Filtered data & Volcano Corrected, 1999 Correction Applied]
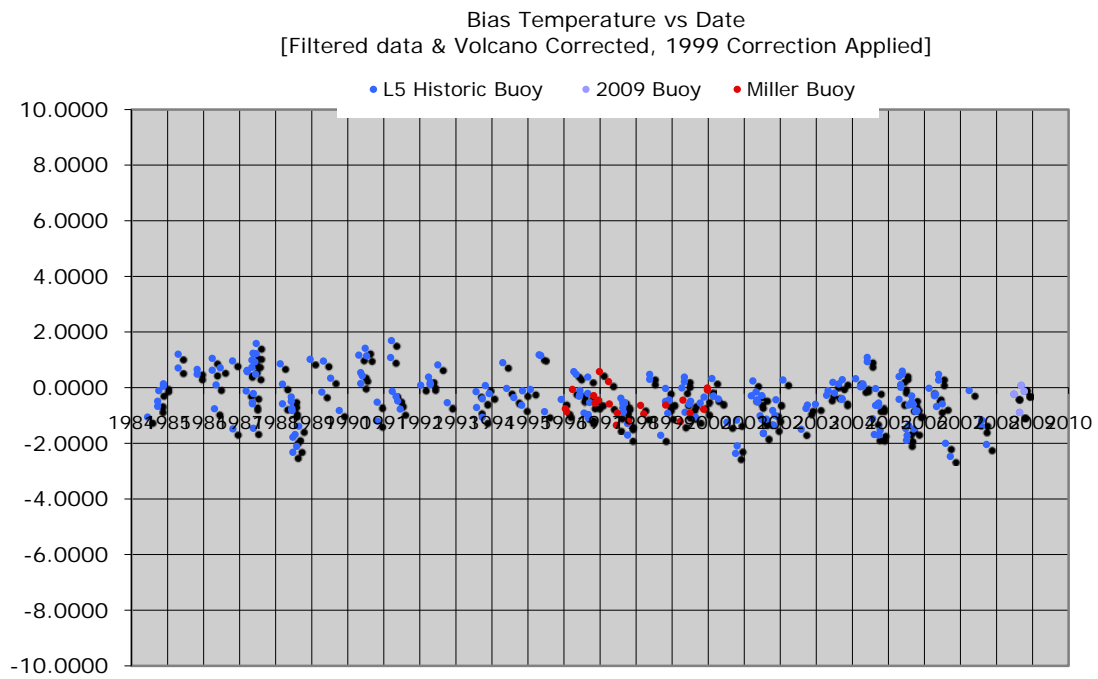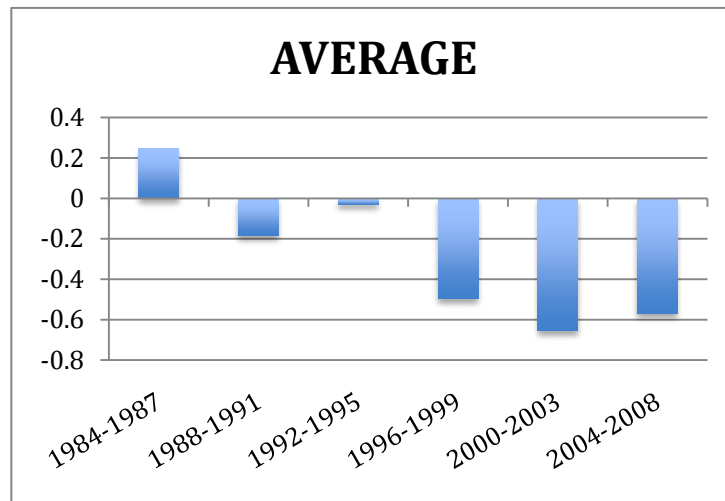

Landsat 5 bias temperature from ranging from 1984-2007
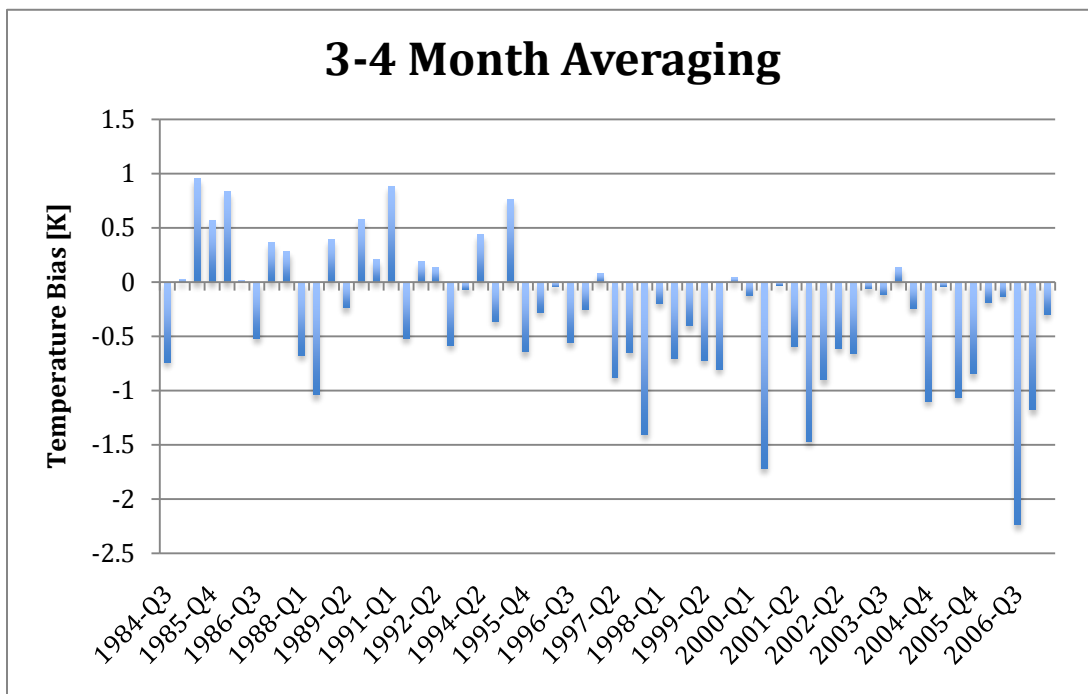
Averaging the Landsat 5data in 3-4 month timeframes
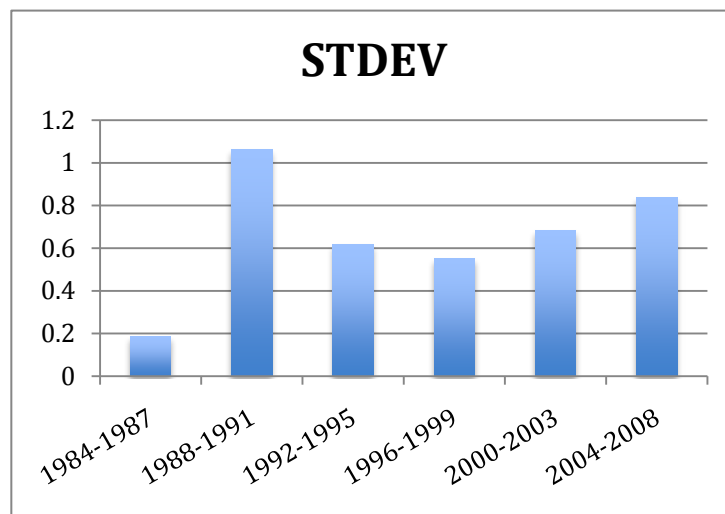
AVERAGE

STDEV

	AVERAGE	STDEV	# OF POINTS
1984-1987	0.2458	0.18635	30
1988-1991	-0.1844	1.0648	30
1992-1995	-0.0305	0.6183	21
1996-1999	-0.4934	0.5511	55
2000-2003	-0.6522	0.6847	34
2004-2008	-0.5673	0.83986	47

Four Year Averages and Standard Deviation of Landsat 5 bias data

14 Appendix D – Correlation of Air Temperature and Water Temperature Study
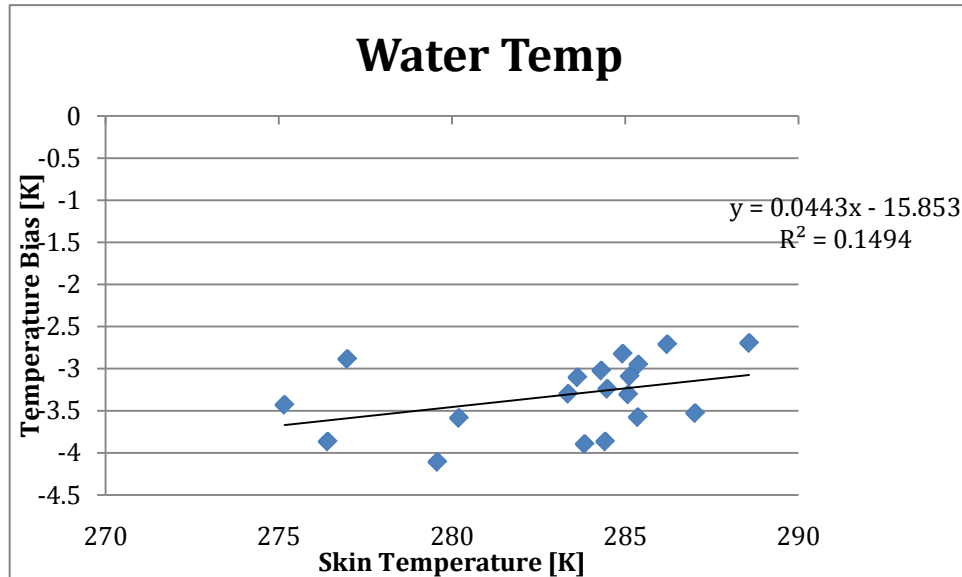
Water Temp

$y = 0.0443x - 15.853$
$R^2 = 0.1494$

Correlation between bias (difference between sensor reaching radiance and image derived radiance) and water temperature
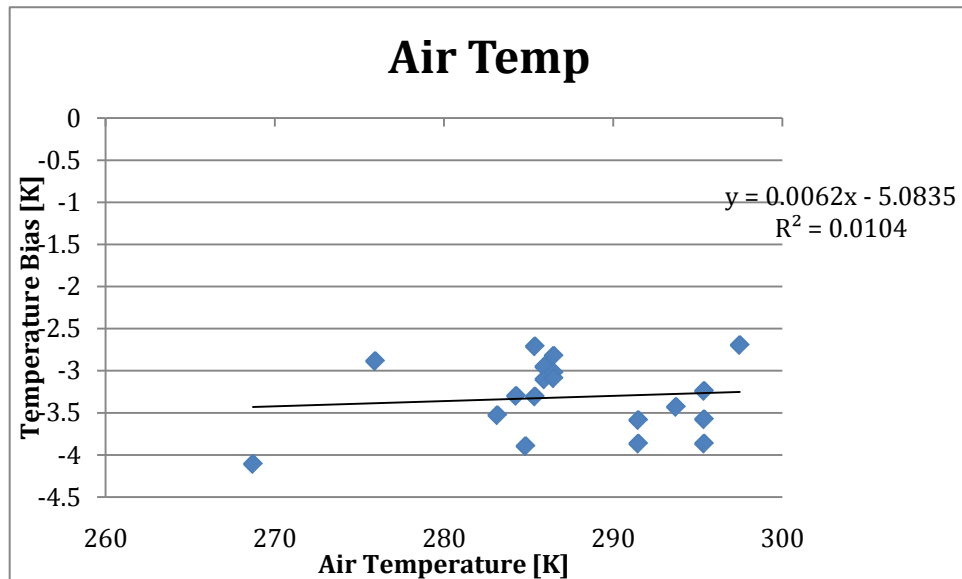
Air Temp

$y = 0.0062x - 5.0835$
$R^2 = 0.0104$

Correlation between bias (difference between sensor reaching radiance and image derived radiance) and air temperature